

# EarthNets: Empowering AI in Earth Observation

Zhitong Xiong, *Member, IEEE*, Fahong Zhang, Yi Wang, Yilei Shi, *Member, IEEE*,  
and Xiao Xiang Zhu, *Fellow, IEEE*.

**Abstract**—Earth observation (EO), aiming at monitoring the state of planet Earth using remote sensing data, is critical for improving our daily lives and living environment. With a growing number of satellites in orbit, an increasing number of datasets with diverse sensors and research domains are being published to facilitate the research of the remote sensing community. This paper presents a comprehensive review of more than 500 publicly published datasets, including research domains like agriculture, land use and land cover, disaster monitoring, scene understanding, vision-language models, foundation models, climate change, and weather forecasting. We systematically analyze these EO datasets from four aspects: volume, resolution distributions, research domains, and the correlation between datasets. Based on the dataset attributes, we propose to measure, rank, and select datasets to build a new benchmark for model evaluation. Furthermore, a new platform for EO, termed EarthNets, is released to achieve a fair and consistent evaluation of deep learning methods on remote sensing data. EarthNets supports standard dataset libraries and cutting-edge deep learning models to bridge the gap between the remote sensing and machine learning communities. Based on this platform, extensive deep-learning methods are evaluated on the new benchmark. The insightful results are beneficial to future research. The platform and dataset collections are publicly available at <https://earthnets.github.io/>.

**Index Terms**—Dataset review, deep learning, Earth observation, foundation models, remote sensing

## I. INTRODUCTION

Earth Observation (EO) aims to monitor and assess the status of the Earth’s surface using various Remote Sensing (RS) technologies [1], [2]. EO can significantly contribute to our ability to better understand and analyze the planet Earth using RS data. The research in EO has been successfully applied to urban planning[3], natural resources management[4], agriculture[5], food security [6] and disaster monitoring [7], [8]. All these applications are important for the sustainable development of human society.

With the development of EO technology, more and more satellites with diverse imaging sensors have been launched for different missions. A huge amount of RS data with global coverage and high resolution is received every day for automatic processing and analysis. To deal with large-scale data, deep learning techniques [9] have been proven effective for different research areas. In this context, recent RS datasets are constructed with larger and larger volumes

Zhitong Xiong, Fahong Zhang, and Yi Wang are with the Chair of Data Science in Earth Observation, Technical University of Munich, Munich 80333, Germany (email: zhitong.xiong@tum.de; fahong.zhang@tum.de; yi4.wang@tum.de).

Y. Shi is with the Chair of Remote Sensing Technology, Technical University of Munich (TUM), 80333 Munich, Germany (e-mail: yilei.shi@tum.de).

X. X. Zhu is with the Chair of Data Science in Earth Observation, Technical University of Munich, 80333 Munich, Germany, and also with the Munich Center for Machine Learning, 80333 Munich, Germany (e-mail: xiaoxiang.zhu@tum.de).

of data. In Fig. 1, we show a chronological overview of the volumes of more than 500 existing datasets. This figure shows that more numerous and larger datasets have been constructed and published during the past decade. Although considerable progress has been made with the overwhelming success of deep learning techniques [10], [11], there are still problems requiring more research efforts to handle.

There is a lack of comprehensive dataset review for EO tasks. Owing to the efforts made by EO researchers, there are numerous datasets in the RS community with different modalities, resolutions, and application domains. Some of these RS data modalities include optical (RGB), Synthetic Aperture Radar (SAR), multispectral, hyperspectral, and point cloud data. Regarding the application domains, the published datasets may be designed for Land Use and Land Cover (LULC) [12], change monitoring[13], disaster monitoring[14], scene recognition, semantic segmentation, ground object detection, object tracking, agriculture, climate change, and weather forecasting. A comprehensive review of the RS datasets can provide researchers with a holistic view of the status of the research community. Bakula et al. [15] review benchmarking in photogrammetry and remote sensing related to geodata. They provide dataset collections and a bibliographic analysis, which are useful for future research. Schmitt et al. [16], [17] provide a historic review of RS datasets. They discuss dataset features based on a few examples and present some important criteria for the establishment of a standard database. Although a few works [18], [19], [20] attempt to review existing RS datasets, they are not sufficient and comprehensive to cover a large range of research domains, like datasets for vision-language models and RS foundation models.

There is no systematic summary and analysis of RS datasets. The ever-growing quantity of RS datasets makes it difficult to find the proper one for a specific application in the jungle of remote sensing datasets. For example, there are more than 20 datasets related to building extraction [21]. Finding, assessing, and selecting the one most suitable for a given application can be laborious and time-consuming. Thus, it is vitally important to summarize and categorize RS datasets to provide valuable guidance and reference for researchers. Both the EOD\* [22] and the AiTLAS Semantic Data Catalog<sup>†</sup> have been designed as search engines for RS datasets, and are valuable and helpful for the RS community. However, the information about RS datasets collected in these existing databases is still limited. Beyond summarization and categorization, insightful analysis of existing datasets can help researchers understand

\*<https://eod-grss-ieee.com/dataset-search>

<sup>†</sup><http://eodata.bvlabs.ai/#/>

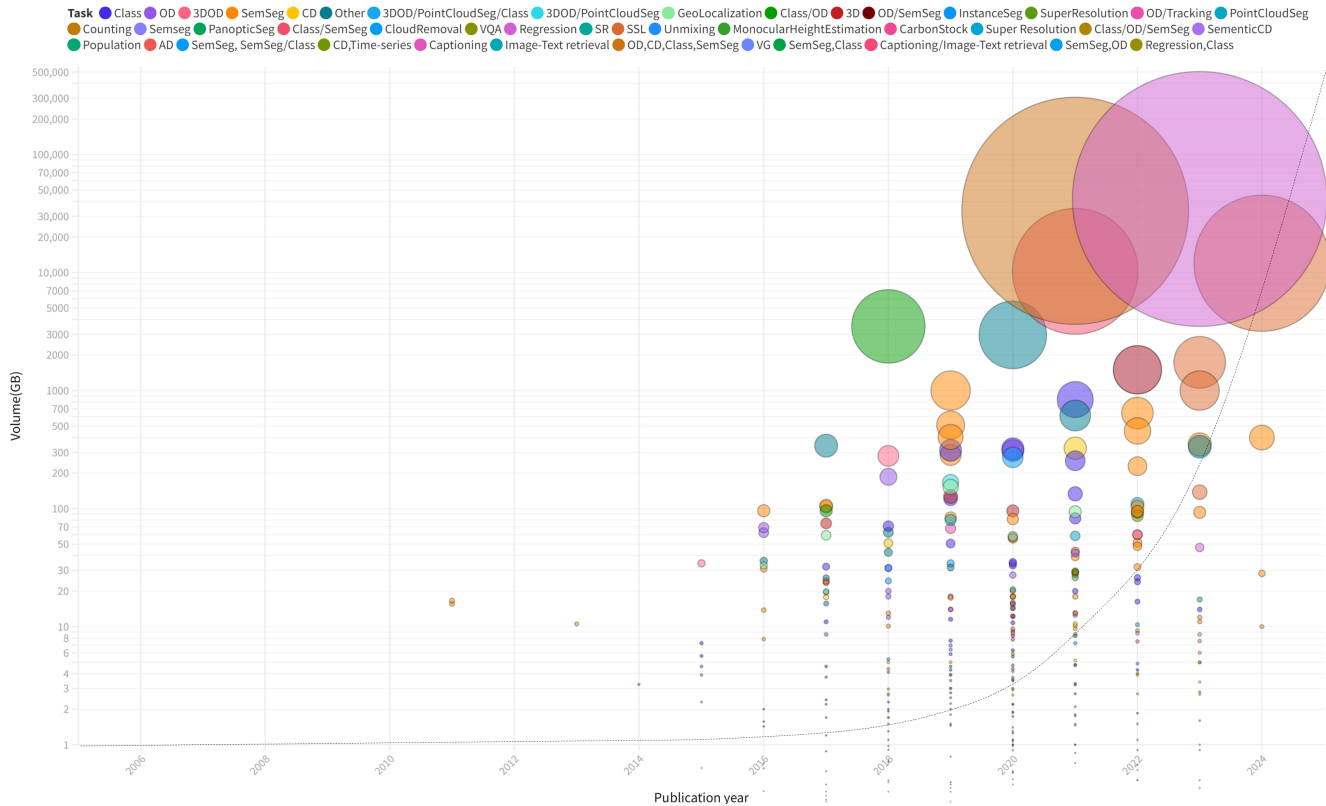


Fig. 1. Chronological overview of the volumes (in logarithmic scale) of over 500 existing datasets. As can be seen, increasingly numerous and larger datasets have been constructed and published over time. (Best viewed by zooming in.)

the current research state and trends of the whole community. Systematic analysis of RS datasets is thus crucial to the future development of different research fields.

There is no unified benchmark for fair comparisons of remote sensing methods. In the Computer Vision (CV) community, a large-scale dataset like ImageNet [23] is usually used to evaluate newly developed deep learning models. Compared with small-scale datasets, large-scale datasets with rich semantic annotations align better with complex real-world scenarios [18]. Thus they can be more reliable for performance validation and comparison of deep learning algorithms. Although several large-volume RS datasets have been published [24], [25], [26], many of the currently developed methods are still evaluated on small-scale datasets. However, datasets with a small scale or limited geographic coverage may be biased to a specific data distribution that is not representative of real-world scenarios. Moreover, many RS datasets are published with no standard train/validation/test splits. This increases uncertainty during the evaluation of algorithms. Thus, it is urgent to build new RS benchmarks to enable a fair comparison of different methods.

Recently, foundation models in RS have demonstrated significant achievements across various EO applications [27]. The key to further enhancing these models involves a thorough investigation of the relationships between existing RS datasets. Such an investigation is important for assembling similar datasets to form a more comprehensive large-scale data archive. This amalgamation of analogous datasets is crucial for

effectively pre-training and evaluating large-scale RS foundation models. Despite its importance, the relationships among various RS datasets remain insufficiently explored in current studies.

Currently, there is a lack of an open platform for different EO tasks. For deep learning methods, backbone networks, hyper-parameters, and training tricks are influential factors that should be considered for fair performance comparison. However, existing works usually evaluate the performance with different dataset splits, which makes it difficult to fairly and reliably compare different algorithms. Due to the large variance in data collection sensors and pre-processing pipelines, it is non-trivial to adapt modern deep learning models to RS datasets [28]. As a result, many cutting-edge and off-the-shelf deep learning methods from the machine learning community are not evaluated and compared on RS data.

To tackle the previously mentioned issues, in this study, we first make an exhaustive and comprehensive review of the publicly accessible RS datasets. Next, a systematic analysis is undertaken based on the information about these datasets. Based on the attribute information, we filter, rank, and select five large-scale datasets designed for general purposes to build a new benchmark for model evaluation. To further enable a fair and reproducible comparison of different algorithms, we construct a new deep learning platform, EarthNets, as a foundation for future work. Our main contributions are summarized below.

1) We review over 500 RS datasets and summarize them into

different research tasks and domains. Beyond summarization and categorization, EarthNets provides insightful analysis of existing datasets that can help researchers understand the current research state and trends of the whole community.

- 2) Systematic analyses are made concerning four aspects of these datasets to provide insights for future research within the RS community. Specifically, the volume, resolution distributions, research domains, and dataset relationship are considered for a comprehensive dataset analysis.
- 3) To our knowledge, we are the first to measure and rank existing RS datasets using the dataset attributes provided in this study. In addition, we provide the affinity relationships between existing datasets, which is useful in assembling similar datasets to support the training of large-scale RS foundation models.
- 4) We release an open platform, EarthNets, for EO tasks. EarthNets aims to enable fair comparisons, efficient development of methods, and the greater availability of the RS data to a larger research community.

The rest of this paper is organized as follows. Section II reviews existing RS datasets for different tasks. Section III presents the analyses of the reviewed datasets from four different perspectives. Section IV introduces the proposed dataset ranking, selection method, and the benchmark-building process. Section V describes the newly released EarthNets platform. Section VI presents the benchmarking results and analysis on the five selected RS datasets. Section VII concludes the paper.

## II. REMOTE SENSING DATASET REVIEW

In this section, we review and organize over 500 existing public RS datasets into five parts concerning their tasks: image classification, object detection, semantic segmentation, change detection, vision-language understanding, and foundation models. For an in-depth analysis of these datasets, we collect as much detailed information as possible for each dataset. Compared with existing review articles, our work provides richer information on the attributes of the datasets. Specifically, the following 9 aspects are considered.

**1) Research domain.** To present these reviewed datasets clearly, we organize them according to the specific domains in which they are created. Some typical research domains include agriculture, building, road, cloud, LULC, general scenes or objects, etc.

**2) Publication year.** We provide the year of publication of the dataset, which is useful for the chronological analysis of these datasets.

**3) Number of samples:** To measure the dataset scale, we list the number of samples for each dataset. Note that it could be the number of images (for image-based datasets), the number of video clips (for video-based datasets), the number of points (for point cloud datasets), or the number of image pairs (for change detection datasets).

**4) Size of sample:** The size of each sample in the dataset is also an important factor for measuring the dataset scale. For

images, the size is the height and width. For datasets designed for 3D understanding, the sample size could be the covered area. For vision-language datasets, the size could be the image-text pairs.

**5) Number of Classes:** For image classification, object detection, semantic segmentation, and vision-language tasks, we provide the number of classes annotated in each dataset.

**6) Data modality:** A wide range of imaging sensors can be used to build datasets for different EO tasks. For example, some of the data sources of RS datasets may include optical images, multispectral images, hyperspectral images [31], SAR[42], point cloud [109], and Digital Surface Model (DSM) [110], [111].

**7) Resolution range:** The spatial resolutions of RS images are highly correlated with the image content. The resolution range is also highly relevant to specific EO tasks to which it can be applied.

**8) Volume:** The volume of each RS dataset is also factored in as a measurement of the dataset scale.

**9) Dataset link:** To facilitate the research, we provide the download link of each dataset. More detailed information can be found at <https://earthnets.github.io/>.

### A. RS Image Classification Datasets

Image classification is a fundamental task in both the CV and RS communities. With image- or patch-level annotations, RS image classification has been employed in different real-world applications. Table I presents some representative RS image classification datasets. To facilitate researchers to search and index, we organize them into different research domains alphabetically. To be specific, Table I contains 13 agriculture-related datasets [29], [38], [41], [39] that are constructed from the year 2015 to 2022. For agriculture-related applications, the images or patches in the datasets are labeled with different granularity levels, from binary labels (crop/non-crop) to fine-grained crop-type labels (up to 348 granular labels). For general scene classification, 16 datasets are presented in the table. Million-AID, the largest of these, contains a million instances for training and evaluating scene classification methods. MLRSNet [64], RSD46-WHU [61], and NWPU-RESISC45 [58] are annotated with more than 40 class labels. These datasets are also widely used for evaluating RS foundation models. There are 19 datasets for LULC applications in the table. Among these datasets, multiple types of data sources are used, including hyperspectral [31], multispectral [76], [24], [83], [84], SAR [75] and RGB data [79], [80].

There are 5 ship-related [94], [95], [96], [97] and 5 flood-related [49], [50], [51] datasets for RS image classification task. For the cloud-related research domain, 4 datasets are reviewed in this table. Some specific domains with fewer datasets are also presented, like smoke [98], sea lion [93], solar power plants [99] and wind datasets [108]. It is worth noting that species classification datasets are annotated with the most semantic labels.

Compared with object detection (with object-level annotation) and pixel-level segmentation tasks, agriculture-related applications are mainly modeled as image classification tasks.

TABLE I

DETAILED INFORMATION FOR SOME REPRESENTATIVE RS IMAGE CLASSIFICATION DATASETS. THESE DATASETS ARE GROUPED INTO 27 DIFFERENT RESEARCH DOMAINS IN ALPHABETICAL ORDER. NOTE THAT / DENOTES THE MISSING INFORMATION AND MS DENOTES THE MULTISPECTRAL DATA. THE COMPLETE INFORMATION FOR THESE DATASETS CAN BE FOUND AT [HTTPS://EARTHNETS.GITHUB.IO](https://earthnets.github.io).

| Domain                   | Name                                | Year                        | #Samples   | Sample Size         | #Classes | Modality                       | Resolution    | Vol.(GB) |
|--------------------------|-------------------------------------|-----------------------------|------------|---------------------|----------|--------------------------------|---------------|----------|
| Agriculture              | Brazilian Coffee Scene [29]         | 2015                        | 2876       | 64                  | 2        | RGB                            | 20m           | 0.004    |
|                          | Indian Pines [30]                   | 2015                        | 1          | 145                 | 16       | Hyperspectral                  | 20m           | 0.0059   |
|                          | Salinas [31]                        | 2015                        | 1          | 365                 | 16       | Hyperspectral                  | 3.7m          | 0.026    |
|                          | Crop Type Mapping Ghana [32]        | 2019                        | /          | /                   | 18       | Sentinel-1,Sentinel-2,Planet   | 3~10m         | 312.54   |
|                          | CV4A Kenya [33]                     | 2020                        | 4688       | 2016x3035           | 7        | Sentinel-2                     | 10m           | 3.5      |
|                          | BreizhCrops [34]                    | 2020                        | 610000     | /                   | 9        | Sentinel-2,MT                  | 10~60m        | /        |
|                          | CaneSat [35]                        | 2020                        | 1627       | 10                  | 2        | Sentinel-2,MT                  | 10m           | 0.006    |
|                          | CropHarvest [36]                    | 2021                        | 90,480     | 12 ts               | 343      | Sentinel-1,Sentinel-2,ERA5,DEM | 10~60m        | 20       |
|                          | South Africa Crop Type [37]         | 2021                        | 122736     | /                   | 9        | Sentinel-1,Sentinel-2          | /             | 82.77    |
|                          | DENETHOR [38]                       | 2021                        | /          | /                   | 9        | Sentinel-1,Sentinel-2          | 3m            | 254.5    |
|                          | The Canadian Cropland[39]           | 2022                        | 78536      | 64                  | 10       | Sentinel-2                     | 10m           | 26       |
| Aircraft                 | Space2Ground[40]                    | 2022                        | 10102      | 260                 | 2        | Sentinel-1,Sentinel-2,RGB      | 10~60m        | 0.501    |
|                          | Sen4AgriNet[41]                     | 2021                        | 225000     | 366                 | 158      | Sentinel-2                     | 10~60m        | 10240    |
| Cloud                    | SAR-ACD[42]                         | 2022                        | 4322       | 64                  | 20       | SAR                            | /             | /        |
|                          | MAR20 [43]                          | 2023                        | 3842       | 800x800             | 20       | RGB                            | 1m            | 1.1      |
| Event                    | SPARCS [44]                         | 2016                        | 80         | 1000                | 7        | MS,Landsat                     | 30m           | 1.43     |
|                          | Kaggle Cloud Detection[45]          | 2019                        | 9244       | 1750                | 4        | RGB                            | /             | 5.86     |
|                          | CloudCast[46]                       | 2020                        | 70080      | 1229                | 10       | NWP                            | 3km           | 320.31   |
|                          | Sentinel-2 Cloud Mask Catalogue[47] | 2020                        | 513        | 1022                | 3        | Sentinel-2                     | 20m           | 15.38    |
| Flood                    | ERA[48]                             | 2020                        | 343680     | 640                 | 25       | RGB Video                      | /             | 6.3      |
|                          | Hurricane Damage[49]                | 2019                        | 16000      | 128                 | 2        | RGB                            | 1m            | 0.064    |
|                          | SEN-12-FLOOD[50]                    | 2020                        | 336        | 512                 | 2        | RGB,SAR,MS                     | 10m           | 12.2     |
|                          | Sen1Floods11[51]                    | 2020                        | 4831       | 512                 | 1        | Sentinel-1                     | 10m           | 14.3     |
|                          | OMBRIA [52]                         | 2022                        | 3376       | 256                 | 2        | Sentinel-1,Sentinel-2          | 10m~20m       | 0.19     |
|                          | FloodNet[14]                        | 2021                        | 2343       | 4000                | 9        | RGB                            | 0.015m        | 2.1      |
| General Scenes           | Kaggle Planet Forest[53]            | 2017                        | 150000     | 256                 | 17       | RGB-NIR                        | 5m            | 32.23    |
|                          | OVERHEAD MNIST[54]                  | 2020                        | 1000       | 28                  | 9        | Grayscale                      | /             | 0.017    |
|                          | fMoW[25]                            | 2018                        | 523846     | /                   | 63       | RGB,MS                         | 0.3m          | 3500     |
|                          | UC Merced[55]                       | 2010                        | 2100       | 256                 | 21       | RGB                            | 0.3m          | 0.3      |
|                          | WHU-RS19[56]                        | 2012                        | 1013       | 600                 | 19       | RGB                            | 0.5m          | 0.1      |
|                          | RSSCN7[57]                          | 2015                        | 2800       | 400                 | 7        | RGB                            | /             | 0.086    |
|                          | NWPU-RESISC45[58]                   | 2016                        | 31500      | 256                 | 45       | RGB                            | 0.2~30m       | 0.404    |
|                          | RSC11 [59]                          | 2016                        | 1232       | 512                 | 11       | RGB                            | /             | 0.63     |
|                          | AID [60]                            | 2017                        | 10000      | 600                 | 30       | RGB                            | 3m            | 2.4      |
|                          | RSD46-WHU [61]                      | 2017                        | 117000     | 256                 | 46       | RGB                            | 0.5~2m        | 11       |
|                          | PatternNet [62]                     | 2018                        | 30,400     | 256                 | 38       | RGB                            | 0.062~4.693m  | 1.3      |
|                          | OPTIMAL-31 [63]                     | 2019                        | 1860       | 256                 | 31       | RGB                            | /             | 0.024    |
|                          | MLRSNet[64]                         | 2020                        | 109,161    | 256                 | 46       | RGB                            | 0.1~10m       | 1.254    |
|                          | CLRSI[65]                           | 2020                        | 15000      | 256                 | 25       | RGB                            | 0.26~8.85m    | 1.735    |
|                          | Million AID[18]                     | 2021                        | 1,000,000  | 150~550             | 28       | RGB                            | 0.5~153m      | 133.5    |
|                          | NaSC-TG2[66]                        | 2021                        | 20000      | 256                 | 10       | RGB-NIR                        | 100m          | /        |
|                          | Satellite Image Classification [67] | 2021                        | 5631       | 256                 | 4        | RGB                            | /             | 0.023    |
| Multi-label Scenes       | MultiScene[68]                      | 2021                        | 100,000    | 512                 | 36       | RGB                            | 0.3~0.6m      | 0.85     |
| Geophysical              | Hephaestus[69]                      | 2022                        | 216106     | 224                 | 6        | InSAR                          | /             | 93.71    |
| Golf Course              | MUSIC4GC (Golf Course)[70]          | 2017                        | 83431      | 16                  | 2        | MS,Landsat                     | 30m           | 0.37     |
| Hot Area                 | MUSIC4HA (Hot Area)[70]             | 2022                        | 2511       | 16                  | 6        | Sentinel-2                     | 10m           | 0.01     |
| Iceberg                  | Iceberg Detection[71]               | 2018                        | 10028      | 75                  | 2        | SAR                            | /             | 0.295    |
| Land Cover               | SAT-4[72]                           | 2015                        | 500000     | 28                  | 4        | RGB-NIR                        | 1~6m          | 7.25     |
|                          | SAT-6[72]                           | 2015                        | 405000     | 28                  | 6        | RGB-NIR                        | 1m            | 5.65     |
|                          | Botswana [31]                       | 2015                        | 1          | 875                 | 14       | Hyperspectral                  | 30m           | 0.077    |
|                          | TiSeLaC [73]                        | 2017                        | 23         | 2866x2633           | 9        | RGB-NIR,MT                     | 30m           | /        |
|                          | Gaofen Image Dataset (GID) [74]     | 2018                        | 150        | 7200                | 15       | RGB-NIR                        | 4m            | 71.1     |
|                          | MSLCC [75]                          | 2018                        | 2          | 5596x6031,8149x5957 | 4        | SAR,MS                         | 10m           | 0.5      |
|                          | BigEarthNet [76]                    | 2019                        | 590326     | 120                 | 43       | Sentinel-1,Sentinel-2          | 10m, 20m, 60m | 121      |
|                          | Slovenia Land Cover [77]            | 2019                        | 940        | 500                 | 10       | Sentinel-2                     | 10m           | 11.55    |
|                          | So2Sat LCZ42 [24]                   | 2019                        | 400673     | 32                  | 17       | Sentinel-1,Sentinel-2          | 10m           | 50.59    |
|                          | TG1HRSSC [78]                       | 2021                        | 204        | 512                 | 9        | Hyperspectral                  | 5m, 10m, 20m  | 0.277    |
|                          | Land Use                            | SIRI-WHU (Google+USGS) [79] | 2016       | 2400                | 200      | 12                             | RGB           | 2m       |
| RSI-CB256 [80]           |                                     | 2017                        | 24000      | 256                 | 35       | RGB                            | 0.3~3m        | 2.2      |
| RSI-CB128 [80]           |                                     | 2017                        | 36000      | 128                 | 45       | RGB                            | 0.3~3m        | 0.88     |
| Austin Zoning [81]       |                                     | 2017                        | 3,666      | 773x961             | 5        | RGB                            | /             | 0.596    |
| HistAerial [82]          |                                     | 2019                        | 42000      | 25,50,100           | 7        | Grayscale                      | /             | 7.6      |
| AiRound [83]             |                                     | 2020                        | 11753      | 300                 | 11       | RGB,Sentinel-2,Ground,Aerial   | /             | 33       |
| CV-BrCT [83]             |                                     | 2020                        | 24000      | 500                 | 9        | RGB                            | /             | 9.2      |
| EuroSAT [84]             |                                     | 2018                        | 27000      | 64                  | 10       | Sentinel-2                     | 10m           | 1.92     |
| SenseEarth classify [85] |                                     | 2020                        | 70000      | 100~12655           | 51       | RGB                            | 0.2~153m      | 10.8     |
| Landslide                | Bijie Landslide[86]                 | 2020                        | 2773       | 200                 | 2        | RGB                            | 0.68m         | 0.51     |
| Military                 | MSTAR-8class[87]                    | 1996                        | 9466       | 368                 | 8        | SAR                            | 0.3m          | 0.444    |
| Plant/Tree               | Tallos [88]                         | 2024                        | 190,481    | /                   | 1160     | SAR,MS                         | 10m           | /        |
|                          | WiDS Datathon 2019[89]              | 2019                        | 11000      | 256                 | 2        | RGB                            | 3m            | 0.46     |
|                          | The Auto Arborist Dataset[90]       | 2022                        | 2,637,208  | 1,024               | 344      | RGB,MS                         | /             | 24       |
|                          | TreeSatAI[91]                       | 2022                        | 50381      | 304x304,6x6         | 47       | Sentinel-1,Sentinel-2,RGB      | 10m,0.2m      | 16.3     |
|                          | Forest Damages Larch Casebearer[92] | 2021                        | 1543       | 1500                | 5        | RGB                            | UAV           | 3.3      |
| Sea Lion                 | NOAA Sea Lion Population Count[93]  | 2017                        | 950        | 4900                | 4        | RGB                            | /             | 96       |
| Ship                     | Ships in Satellite Imagery[94]      | 2017                        | 4000       | 80                  | 2        | RGB                            | 3m            | 0.343    |
|                          | MASATI[95]                          | 2018                        | 7389       | 512                 | 7        | RGB                            | 0.08~2m       | 2.3      |
|                          | DSCR[96]                            | 2019                        | 20,675     | 150~800             | 7        | RGB                            | /             | /        |
|                          | FGSCR-42[96]                        | 2021                        | 9320       | 140~800             | 42       | RGB                            | /             | 4.76     |
|                          | SynthWakeSAR[97]                    | 2022                        | 46080      | 96000               | 10       | SAR                            | 3.3m          | 4.3      |
| Smoke                    | USTC_SmokeRS [98]                   | 2019                        | 6225       | 256                 | 6        | RGB                            | 1000m         | 0.79     |
| Solar Power Plants       | MUSIC4P3[99]                        | 2017                        | 1280000    | 16                  | 2        | MS,Landsat                     | 30m           | 4.6      |
| Species                  | GeoLifeCLEF 2021[100]               | 2021                        | 19,000,000 | 256                 | 31,435   | RGB-IR,MS,LC,DEM               | 1m,0.3m,0.1m  | 840      |
| Tailings Dam             | BrazilDAM[101]                      | 2020                        | 769        | 384                 | 2        | RGB                            | 10~60m        | 57       |
| Urban Village            | S2UC [102]                          | 2021                        | 1714       | 224                 | 2        | RGB                            | 2m            | 1.8      |
| Vegetation               | Kennedy Space Center[103]           | 2015                        | 1          | 550                 | 13       | Hyperspectral                  | 0.18m         | 0.055    |
|                          | Brazilian Cerrado-Savanna [104]     | 2016                        | 1311       | 64                  | 4        | MS                             | 5m            | 0.011    |
|                          | WAMI DIRSIG [105]                   | 2017                        | 55226      | 64                  | 2        | Hyperspectral                  | 0.3m          | 0.33     |
| Vehicles                 | Kaggle Find a Car Park[106]         | 2019                        | 3262       | 1296                | 2        | RGB                            | /             | 2.75     |
|                          | MAFAT-Fine-Grained [107]            | 2021                        | 4216       | /                   | 37       | RGB                            | 0.05~0.15m    | /        |
| Wind                     | Airbus Wind Turbine Patches[108]    | 2021                        | 155,000    | 128                 | 2        | RGB,MS                         | 1.5m          | 1        |

In contrast, aircraft [42] and ship-related datasets are built primarily for object detection tasks. For agriculture-related datasets, data from the Sentinel satellites is mostly used with a lower spatial resolution to cover larger crop areas. General scene classification and LULC are dominant domains in RS image classification datasets.

### B. RS Object Detection Datasets

Object detection is closely related to real-world applications like autonomous driving, video surveillance, and many other high-level scene understanding tasks. Thus, several widely-read works have been published in the CV community, like Faster RCNN [112], SSD [113], YOLO [114], and Transformer-based detectors [115]. For the RS object detection task, more and larger datasets are also being published for different EO applications, including aircraft detection [116], building detection [117], [118], [119], [120], ship detection [121], [122], [123], [124], vehicle detection [125], [126], [127], [128], [129], general ground object detection [130], [131], [132], [133], [134], [135] and other research domains [136], [137], [138].

Object detection from satellite and Unmanned Aerial Vehicles (UAV) perspectives is crucial for applications such as traffic analysis, wildlife protection, and search and rescue operations. Consequently, numerous datasets have been developed for tasks like object counting, person detection, ship detection, and vehicle detection. Table II presents some representative RS object detection datasets organized into 18 different research domains. Some popular research domains for RS object detection tasks are general object detection with 12 datasets, building detection with 13 datasets, aircraft detection with 7 datasets, ship detection with 14 datasets, and vehicle-related object detection with 20 datasets. Since object detection is a task with object-level annotations, the spatial resolutions of these datasets are usually higher than those of image classification datasets. However, for objects with large sizes, like ships, the data from Sentinel-1 and Sentinel-2 satellites are also used [139], [140]. For the detection of traffic objects [141] or other small objects [142], images captured from UAV are usually used.

### C. RS Semantic Segmentation Datasets

Pixel-level semantic segmentation aims to assign semantic labels to each image pixel. Compared with image-level and object-level tasks, interpreting the image data with semantic maps can provide a more complete understanding of the scene at a fine-grained level. Table III presents some representative datasets for RS semantic segmentation tasks. Given the close association of agriculture, buildings, roads, LULC, and urban scenes with essential applications such as urban growth, urban planning, and city living, these areas emerge as primary domains for semantic segmentation tasks.

Among them, 21 datasets are built for LULC segmentation tasks [143], [144], [145], [146], [147], [148], [110], [111], [26]. There are 17 additional datasets constructed for the segmentation of general scenes. There are 13 datasets [157], [158], [159], [160], [118], [161], [162] that are designed

for building extraction with pixel-level annotations. Note that some of them are constructed for building instance segmentation tasks. In those cases, the buildings are annotated with both the object-level and pixel-level labels. For road extraction, 10 datasets [206], [207], [20], [208], [209], [210], [211] are constructed. Datasets designed for LULC, general scenes, buildings, and road segmentation dominate the RS semantic segmentation tasks. We present 10 datasets built with lower spatial resolution RS images than other domains [212], [213], [214], [215], [216] for cloud-related applications. Furthermore, 9 agriculture datasets are annotated with pixel-level labels towards a fine-grained understanding of the crops [217], [218], [219], [149], [220].

### D. RS Change Detection Datasets

RS change detection focuses on quantitatively analyzing surface alterations using data obtained from remote sensors. This research is vital for practical applications, including damage monitoring and urban planning. Table IV presents some representative datasets built for RS change detection tasks. Flood events and other natural disasters can inflict damage on structures. In these scenarios, change detection plays a crucial role in assessing the extent of the damage and supplying data for analysis and rescue operations. Therefore, datasets related to buildings [282] and floods [283] have been developed to facilitate these applications. The majority of change detection datasets primarily concentrate on changes in land cover or land use. Detecting these changes is crucial for analyzing urban development, as well as for urban growth and planning. In addition, the time-series data can aid in monitoring crops to ensure food security [284].

Several other datasets are constructed for 3D change detection [285]. Many different data modalities are used for constructing these datasets, including optical (RGB), point cloud, multispectral, hyperspectral, and SAR data. Note that some datasets like SECOND [286] and Dynamic World [287] are annotated with pixel-wise semantic labels, not only the change/non-change binary label.

### E. Datasets for RS Foundation Models

As we reviewed, extensive annotated RS datasets have been constructed to train task-specific algorithms [313]. However, these traditional deep learning models require significant human labor for data collection and annotation, as well as considerable computational costs for model development and evaluation. In contrast, foundation models [314], trained on a wide array of data, can be fine-tuned for specific downstream tasks using far fewer annotated examples. This efficiency stems from their capacity to leverage general feature representations learned from vast amounts of unlabeled data. To foster research on foundation models, many RS datasets have been built for pre-training and evaluating them, as presented in Table V. Among them, SatlasPretrain [315] is a large-scale RS dataset containing data from different sensors with 302,222,000 annotated labels, which is useful for training RS foundation models. Metadataset is a collection of existing datasets, which can be used for pre-training or evaluating RS foundation models. For instance, DOFA-data [316],

TABLE II  
 DETAILED INFORMATION FOR SOME REPRESENTATIVE RS OBJECT DETECTION DATASETS. THESE DATASETS ARE GROUPED INTO 18 DIFFERENT RESEARCH DOMAINS IN ALPHABETICAL ORDER. NOTE THAT / DENOTES THE MISSING INFORMATION AND MS DENOTES THE MULTISPECTRAL DATA. THE DOWNLOAD LINKS FOR ALL THESE DATASETS CAN BE FOUND AT [HTTPS://EARTHNETS.GITHUB.IO](https://earthnets.github.io).

| Domain            | Name                                       | Year                         | # samples   | Size              | # classes | Modality            | Resolution     | Volume (GB) |      |
|-------------------|--|------------------------------|-------------|-------------------|-----------|---------------------|----------------|-------------|------|
| Agriculture       | PASTIS [149]                               | 2021                         | 2433        | 128               | 18        | Sentinel-2          | 10m            | 29          |      |
| Aircraft          | MAR20 [43]                                 | 2023                         | 3842        | 800×800           | 20        | RGB                 | 1m             | 1.1         |      |
|                   | MTARSI (Aircraft) [150]                    | 2019                         | 9385        | 256               | 2         | RGB                 | /              | 0.48        |      |
|                   | RarePlanes [151]                           | 2020                         | 713348      | 512               | 110       | MS,WorldView3       | 0.3~1.5m       | 310.55      |      |
|                   | CGI Planes [152]                           | 2021                         | 500         | /                 | 2         | RGB                 | /              | 0.7         |      |
|                   | CASIA-aircraft [116]                       | 2021                         | 58,121      | 399               | 2         | RGB                 | /              | /           |      |
|                   | Airbus Aircraft Detection [153]            | 2021                         | 109         | 2560              | 2         | RGB                 | 0.5m           | 0.092       |      |
|                   | SAR Aircraft [154]                         | 2022                         | 2966        | 224               | 2         | SAR                 | 0.5m~3m        | 0.18        |      |
| Bridge            | Bridges Dataset [155]                      | 2019                         | 500         | 4800x2843         | 2         | RGB                 | 0.5m           | 1.45        |      |
| Building          | SpaceNet-4 (Multi-View) [120]              | 2018                         | 60000       | 900               | 1         | MS,WorldView2       | 0.3m           | 186         |      |
|                   | DeepGlobe (Building) [117]                 | 2018                         | 24586       | 650               | 2         | Panchromatic,RGB,MS | 0.5m           | /           |      |
|                   | WHU Building [156]                         | 2018                         | 25577       | 512               | 2         | RGB                 | 0.3m           | 24.41       |      |
|                   | CrowdAI Mapping [157]                      | 2018                         | 401,755     | 300               | 1         | RGB                 | /              | 5.3         |      |
|                   | Map Challenge [157]                        | 2018                         | 341,058     | 300               | 2         | RGB                 | /              | /           |      |
|                   | TBF [158]                                  | 2018                         | 13          | 40,000            | 2         | RGB                 | /              | /           |      |
|                   | Microsoft Building (Australia) [159]       | 2019                         | 11,334,866  | /                 | 2         | /                   | /              | 6.4         |      |
|                   | Microsoft Building (Uganda/Tanzania) [160] | 2019                         | 17,942,345  | /                 | 2         | /                   | /              | 3.5         |      |
|                   | Microsoft Building (USA) [118]             | 2019                         | 129,591,852 | /                 | 2         | /                   | /              | 34.4        |      |
|                   | Microsoft Building (Canada) [161]          | 2019                         | 11,842,186  | /                 | 2         | /                   | /              | 2.5         |      |
|                   | Urban Building Classification [162]        | 2022                         | 800         | 600               | 61        | RGB                 | 0.5~0.8m       | 0.675       |      |
| General           | BONAI [163]                                | 2022                         | 3,300       | 1,024             | 1         | RGB                 | 0.3m~0.6m      | 4.86        |      |
|                   | MSNet [164]                                | 2020                         | 1030        | /                 | 3         | RGB                 | /              | 0.43        |      |
|                   | NWPU-VHR10 [130]                           | 2014                         | 800         | 1000              | 10        | RGB,IRRG            | 0.08~2m        | 0.07        |      |
| General           | RSOD [131]                                 | 2017                         | 976         | 1000              | 4         | RGB                 | 0.3~3m         | 0.077       |      |
|                   | TGRS HRRSD [132]                           | 2017                         | 21761       | 10569             | 13        | RGB                 | 0.15~1.2 m     | 8.6         |      |
|                   | xView [133]                                | 2018                         | 1,413       | 3,000             | 60        | RGB,MS              | 0.3m           | 20          |      |
|                   | fMoW [134]                                 | 2018                         | 523846      | /                 | 63        | RGB,MS              | 0.3m           | 3500        |      |
|                   | DOTA v1.0 [135]                            | 2018                         | 2806        | 4000              | 15        | RGB                 | /              | 18          |      |
|                   | DOTA v1.5 [165]                            | 2019                         | 2806        | 4000              | 16        | RGB                 | /              | 18          |      |
|                   | DIOR [19]                                  | 2019                         | 23463       | 800               | 20        | RGB                 | 0.5~30 m       | 6.93        |      |
|                   | DOTA v2.0 [166]                            | 2020                         | 11268       | 4000              | 18        | RGB                 | 0.1~0.81       | 34.3        |      |
|                   | iSAID [167]                                | 2020                         | 2806        | 4000              | 15        | RGB                 | /              | 18          |      |
|                   | VALID [168]                                | 2020                         | 6690        | 1024              | 30        | RGBD                | /              | 15.7        |      |
|                   | UAVOD10 [136]                              | 2022                         | 844         | 1000~4800         | 10        | RGB                 | 0.15m          | 0.9         |      |
|                   | Human/Animals                              | BIRDSAI [169]                | 2020        | 162000            | 640       | 10                  | Thermal        | UAV@60-120m | 3.7  |
|                   | Land Covers                                | Dstl Satellite Imagery [137] | 2017        | 57                | 3,348     | 10                  | RGB,MS         | 0.3m~7.5m   | 21.7 |
| Object Counting   | RSOC (Object Counting) [170]               | 2020                         | 3057        | 2500              | 4         | RGB                 | /              | 0.082       |      |
| Oil Storage Tanks | Oil and Gas Tank (OGST) [171]              | 2020                         | 10000       | 512               | 2         | RGB                 | 0.3m           | 1.87        |      |
|                   | Airbus Oil Storage Detection [138]         | 2021                         | 103         | 2560              | 2         | MS                  | 1.2m           | 0.102       |      |
|                   | Oil Storage Tanks [172]                    | 2019                         | 10000       | 512               | 2         | RGB                 | 0.5m           | 3           |      |
| Volcanoes         | Hephaestus [173]                           | 2022                         | 216106      | 224               | 6         | InSAR               | /              | 93.71       |      |
| Person            | Semantic Drone-OD [174]                    | 2019                         | 400         | 5000              | 2         | RGB                 | /              | 3.91        |      |
|                   | Stanford Drone [175]                       | 2016                         | 100         | 1400x1904         | 6         | RGB Video           | 0.025m         | 69          |      |
| Sea               | NOAA Sea Lion Count [93]                   | 2017                         | 950         | 4,900             | 4         | RGB                 | /              | 96          |      |
|                   | Aerial Maritime Drone [176]                | 2020                         | 508         | 800x600           | 5         | RGB                 | /              | 0.038       |      |
|                   | SeaDronesSee [177]                         | 2022                         | 5630        | 3,840~5,456       | 6         | RGB                 | /              | 60.3        |      |
|                   | AFO-Floating objects [178]                 | 2020                         | 3647        | 720~3840          | 6         | RGB                 | /              | 4.7         |      |
| Search/Rescue     | Search And Rescue [179]                    | 2021                         | 2552        | 1000              | 1         | RGB                 | 0.5m           | /           |      |
| Ship              | OpenSARShip [121]                          | 2017                         | 11346       | 900               | 1         | Sentinel-1          | 10m            | 1.7         |      |
|                   | SSDD [122]                                 | 2017                         | 1160        | 500               | 2         | SAR                 | 1~15m          | /           |      |
|                   | HRSC2016 (Ship) [180]                      | 2017                         | 1061        | 300x300~1500x900  | 26        | RGB                 | 0.4~2m         | 3.74        |      |
|                   | Kaggle Airbus Ship [123]                   | 2018                         | 192556      | 768               | 2         | /                   | 1.5m           | 31.41       |      |
|                   | Airbus Ship Detection [123]                | 2018                         | 40,000      | 768               | 2         | RGB                 | /              | 31.4        |      |
|                   | Ships in Google Earth [124]                | 2018                         | 794         | 2000              | 2         | RGB                 | /              | 2           |      |
|                   | SAR Ship Detection [181]                   | 2019                         | 43819       | 256               | 2         | SAR                 | 3m, 5m, 8m,10m | 0.4         |      |
|                   | AIR-SARShip-1.0 [182]                      | 2019                         | 31          | 3000              | 2         | SAR                 | 1~3m           | 0.24        |      |
|                   | AIR-SARShip-2.0 (GF-3) [148]               | 2020                         | 300         | 1,000             | 2         | SAR                 | 1~3m           | 0.22        |      |
|                   | LS-SSDD (Large Scale) [139]                | 2020                         | 15          | 20,000            | 2         | Sentinel-1,SAR      | 0.5,1,3m       | 7.8         |      |
|                   | HRSID (Ship) [140]                         | 2020                         | 5,604       | 800               | 2         | Sentinel-1,SAR      | 0.5~3m         | 0.58        |      |
|                   | SWIM-Ship [183]                            | 2021                         | 14610       | 768               | 2         | RGB                 | 0.5~2.5m       | 12.5        |      |
|                   | CASIA-Ship [184]                           | 2021                         | 1,118       | 1,680             | 2         | RGB                 | /              | /           |      |
|                   | xView3-SAR [185]                           | 2022                         | 1000        | ~29400x24400      | 2         | Sentinel-1          | 10m            | 1500        |      |
| Small Objects     | AI-TOD [141]                               | 2021                         | 28036       | 800               | 8         | RGB                 | 0.3m~30m       | 42          |      |
|                   | SODA-A [142]                               | 2022                         | 2510        | 4761x2777         | 9         | RGB                 | /              | /           |      |
| Traffic Objects   | AU-AIR [186]                               | 2020                         | 32823       | 1920              | 8         | RGB                 | UAV@30m        | 2.2         |      |
|                   | HighD [187]                                | 2018                         | 110000      | 4096x2160         | 2         | RGB                 | /              | /           |      |
|                   | Interaction Dataset [188]                  | 2019                         | 10,933      | /                 | 1         | RGB                 | /              | /           |      |
|                   | Intersection Drone [189]                   | 2020                         | 11,500      | 4096x2160         | 5         | RGB                 | /              | /           |      |
|                   | Roundabouts Drone [190]                    | 2020                         | 13,746      | 4096x2160         | 8         | RGB                 | /              | /           |      |
| Tree              | NEON Tree Crowns [191]                     | 2020                         | 11,000      | 100 million trees | 2         | RGB                 | /              | 27.4        |      |
|                   | Oil Palm Plant [192]                       | 2019                         | 20,000      | /                 | 2         | RGB                 | 3m             | 0.5         |      |
|                   | Forest Damages [193]                       | 2021                         | 1543        | 1500              | 5         | RGB                 | UAV            | 3.3         |      |
| Vehicles          | Things And Stuff (TAS) [125]               | 2008                         | 30          | 792               | 2         | RGB                 | 0.5m           | 0.01        |      |
|                   | OIRDS [194]                                | 2009                         | 900         | 256~640           | 5         | RGB                 | 0.15m          | 0.153       |      |
|                   | UCAS_AOD [195]                             | 2014                         | 976         | 1,000             | 2         | RGB                 | /              | 3.24        |      |
|                   | VEDAI (Vehicle) [126]                      | 2015                         | 1,250       | 1,024             | 9         | IRGB                | 0.125m         | 3.9         |      |
|                   | PKLot (Parking Lot) [196]                  | 2015                         | 12417       | 1280              | 2         | RGB                 | UAV            | 4.6         |      |
|                   | COWC [127]                                 | 2016                         | 388435      | 256               | 2         | RGB                 | 0.15m          | 62.5        |      |
|                   | Car Parking Lot (CARPK) [197]              | 2016                         | 1448        | 1280              | 2         | RGB                 | UAV            | 2           |      |
|                   | DLR3k/DLR-MVDA [128]                       | 2016                         | 20          | 3744              | 7         | RGB                 | 0.13m          | 0.162       |      |
|                   | ITCVD (Vehicle) [129]                      | 2016                         | 173         | 5616              | 2         | RGB                 | 0.1m           | 12          |      |
|                   | VisDrone2019-DET [198]                     | 2019                         | 10209       | 2000x1500         | 10        | RGB                 | UAV            | 2           |      |
|                   | VisDrone2019-VID [198]                     | 2019                         | 40000       | 3840x2160         | 5         | RGB                 | UAV            | 14          |      |
|                   | VisDrone2019-SOT [198]                     | 2019                         | 139300      | 3840x2160         | 3         | RGB Video           | UAV            | 68          |      |
|                   | VisDrone2019-MOT [198]                     | 2019                         | 40000       | 3840x2160         | 5         | RGB Video           | UAV            | 14          |      |
|                   | SIMD (Multi-vehicles) [199]                | 2020                         | 5000        | 1024              | 15        | RGB                 | UAV@150m       | 1           |      |
|                   | VisDrone [200]                             | 2020                         | 275,437     | 1,400             | 11        | RGB                 | UAV            | 16          |      |
|                   | EAGLE [201]                                | 2020                         | 8820        | 936               | 2         | RGB                 | 0.05~0.45m     | /           |      |
|                   | MOR-UAV [202]                              | 2020                         | 10948       | 1080              | 1         | RGB                 | UAV            | /           |      |
|                   | DroneVehicle [203]                         | 2021                         | 56,878      | 840               | 5         | RGB-Infrared        | UAV@100m       | 13.09       |      |
|                   | Swimming pool/car [204]                    | 2019                         | 3750        | 224               | 2         | RGB                 | /              | 0.12        |      |
|                   | ArtifiVe-Potsdam [205]                     | 2021                         | 4800        | 600               | 1         | MS                  | 0.05m          | 15.6        |      |

TABLE III

DETAILED INFORMATION FOR SOME REPRESENTATIVE RS SEMANTIC SEGMENTATION DATASETS. THESE DATASETS ARE GROUPED INTO 19 DIFFERENT RESEARCH DOMAINS IN ALPHABETICAL ORDER. NOTE THAT / DENOTES THE MISSING INFORMATION AND MS DENOTES THE MULTISPECTRAL DATA.

MORE INFORMATION CAN BE FOUND AT [HTTPS://EARTHNETS.GITHUB.IO](https://earthnets.github.io).

| Domain                         | Name  | Year  | #Samples | Sample Size                    | #Classes      | Modality                   | Resolution | Vol.(GB) |
|--------------------------------|---|-------|----------|--------------------------------|---------------|----------------------------|------------|----------|
| Agriculture                    | Agricultural Crop Cover[217]                  | 2018  | 40       | /                              | 2             | MS                         | 30m        | 4.4      |
|                                | GF2 Dataset for 3DFGC [218]                   | 2019  | 11       | 2,652                          | 5             | RGB-NIR                    | 4m         | 0.056    |
|                                | TimeSen2Crop [219]                            | 2020  | 1000000  | 10980                          | 16            | Sentinel-2                 | 10m        | 1.1      |
|                                | Agriculture-Vision [220]                      | 2020  | 94986    | 512                            | 9             | RGB-NIR                    | 0.1~0.2m   | 4.4      |
|                                | WHU-Hi-LongKou [221]                          | 2020  | 1        | 550x400                        | 9             | Hyperspectral              | 0.463m     | /        |
|                                | WHU-Hi-HanChuan [221]                         | 2020  | 1        | 1217x303                       | 16            | Hyperspectral              | 0.109m     | /        |
|                                | WHU-Hi-HongHu [221]                           | 2020  | 1        | 940x475                        | 22            | Hyperspectral              | 0.043m     | /        |
|                                | ZueriCrop [222]                               | 2021  | 28000    | 24                             | 48            | Sentinel-2                 | 10m        | 39       |
|                                | EuroCrops [223]                               | 2021  | 805,401  | 0.5 ha                         | 43            | Sentinel-2                 | 10m        | 8.6      |
| Arctic                         | Arctic Sea Ice Image Masking [224]            | 2021  | 3392     | 357x306                        | 8             | RG-NIR                     | 10m        | 0.092    |
| Building                       | SpaceNet-1 (Building)[225]                    | 2016  | 9735     | 650                            | 2             | RGB,MS                     | 0.5~1m     | 31       |
|                                | SpaceNet-2 (Building)[225]                    | 2017  | 24586    | 650                            | 2             | RGB,MS                     | 0.3m       | 104      |
|                                | INRIA Aerial Image Labeling [207]             | 2017  | 360      | 1500                           | 1             | RGB                        | 0.3m       | 19.5     |
|                                | built-structure-count dataset[226]            | 2019  | 5364     | 512                            | 1             | RGB                        | 0.3m       | 2.23     |
|                                | SpaceNet-6 (Multi-Sensor All Weather)[227]    | 2020  | 3401     | 900                            | 2             | SAR,RGB                    | 0.5m       | 55.9     |
|                                | SpaceNet-7 (Multi-Temporal Urban)[228]        | 2020  | 1525     | 1024                           | 2             | MS,MT                      | 4m         | 20.1     |
|                                | Synthinel-1 [229]                             | 2020  | 2108     | 572                            | 2             | RGB                        | 0.3m       | 0.977    |
|                                | Kaggle buildings segmentation[119]            | 2020  | 6038     | 256                            | 2             | RGB                        | /          | 0.899    |
|                                | Kaggle Massachusetts Buildings[230]           | 2020  | 151      | 1500                           | 2             | RGB                        | 1m         | 2.93     |
|                                | Open Cities AI Challenge[231]                 | 2020  | 11,000   | 1,024                          | 2             | RGB                        | 0.03~0.2m  | 81.5     |
|                                | Mini Inria Aerial Image Labeling Dataset[207] | 2021  | 32,500   | 512                            | 2             | RGB                        | 0.3m       | /        |
|                                | High-speed Rail Line Building Dataset[232]    | 2021  | 336      | 2000                           | 2             | RGB                        | 0.5m       | /        |
|                                | ALS From Online Maps [233]                    | 2017  | 1671     | 3000                           | 2             | RGB                        | 0.5m       | 23.8     |
| Cloud                          | Biome: L8 Cloud Cover[212]                    | 2016  | 96       | /                              | 4             | RGB                        | 30m        | 96       |
|                                | 38-Cloud [213]                                | 2018  | 17601    | 384                            | 2             | RGB                        | 30m        | 13       |
|                                | Sentinel-2 Cloud Detection (ALCD)[234]        | 2019  | 38       | 1830                           | 2             | MS,Sentinel-2              | 10~60m     | 0.234    |
|                                | HRC_WHU [215]                                 | 2019  | 150      | 1280x720                       | 2             | RGB                        | 0.5~15m    | 0.17     |
|                                | WHU Cloud Dataset[235]                        | 2020  | 859      | 512                            | 2             | RGB                        | 30m        | 3.56     |
|                                | 95-Cloud [214]                                | 2020  | 34701    | 384                            | 2             | RGB                        | 30m        | 18       |
|                                | WHUS2-CD+ [216]                               | 2021  | 36       | 10980                          | 2             | Sentinel-2                 | 10m        | 27.8     |
|                                | AIR-CD [236]                                  | 2021  | 34       | 7300                           | 2             | RGB-NIR                    | 4m         | 13       |
|                                | The Azavea Cloud Dataset[237]                 | 2021  | 32       | /                              | 2             | Sentinel-2                 | 10m~60m    | /        |
|                                | Sentinel-2 Cloud Cover [238]                  | 2022  | 22728    | /                              | 2             | MS                         | 10m~60m    | 51.2     |
| General Objects                | DLRS [239]                                    | 2018  | 2100     | 256                            | 17            | RGB                        | 0.3m       | 0.004    |
|                                | Kaggle aerial segmentation [147]              | 2020  | 72       | 800                            | 6             | RGB                        | /          | 0.033    |
|                                | AIR-PolSAR-Seg [148]                          | 2022  | 2000     | 512                            | 6             | SAR                        | 8m         | 0.609    |
| General Scenes                 | ISPRS 2D - Potsdam [110]                      | 2011  | 38       | 6000                           | 6             | RGB,nDSM                   | 0.05m      | 15.625   |
|                                | ISPRS 2D - Vaihingen [111]                    | 2011  | 33       | 2200                           | 6             | RGB,nDSM                   | 0.09m      | 16.6     |
|                                | Aerial Image Segmentation [240]               | 2013  | 80       | 512                            | 2             | RGB                        | 0.3~1m     | 0.007    |
|                                | DFC2015 Zeebrugge [241]                       | 2015  | 7        | 100,000                        | 8             | RGB,DSM,LIDAR              | 0.05m      | 0.0024   |
|                                | Zurich Summer Dataset [242]                   | 2015  | 20       | 1000                           | 8             | RGB-NIR                    | 0.61m      | 0.38     |
|                                | Ticino [243]                                  | 2024  | 1502     | /                              | 10            | RGB,DTM,Pan.,Hyperspectral | 186m-30m   | /        |
|                                | EvLab-SS Dataset [244]                        | 2017  | 60       | 4500                           | 11            | RGB                        | 0.1m,0.25m | /        |
|                                | SynthAer [245]                                | 2018  | 765      | 1280                           | 8             | RGB                        | /          | 0.977    |
|                                | Aeroscapes [246]                              | 2018  | 3269     | 1280                           | 11            | RGB                        | UAV@5~50m  | 0.73     |
|                                | Urban Drone Dataset (UDD) [247]               | 2018  | 301      | 4,096                          | 6             | RGB                        | UAV        | 1.1      |
|                                | RIT-18 [144]                                  | 2018  | 3        | 9393x5642,8833x6918,12446x7654 | 18            | MS                         | 0.047m     | 1.5      |
|                                | Semantic Drone Dataset-SemSeg [174]           | 2019  | 400      | 5000                           | 20            | RGB                        | /          | 3.91     |
|                                | DroneDeploy [248]                             | 2019  | 55       | 6,000                          | 7             | RGB                        | 0.1m       | /        |
|                                | MidAir [249]                                  | 2019  | 420000   | 1024                           | 12            | RGBD,Odometry              | /          | 1000     |
|                                | AeroRIT [250]                                 | 2019  | 1        | 3975x1973                      | 6             | RGB,Hyperspectral          | 0.4m       | 1.8      |
|                                | SemCity Toulouse [251]                        | 2020  | 16       | 3500                           | 8             | MS                         | 0.5~2m     | 8.8      |
|                                | UAVid [252]                                   | 2020  | 420      | 4000                           | 8             | RGB                        | UAV        | 5.88     |
| Settlements                    | DFC21-DSE [253]                               | 2021  | 98       | 800                            | 2             | SAR,MS,Hyperspectral       | 10~750m    | 18       |
| Land Cover                     | DeepGlobe (LandCover) [254]                   | 2018  | 1146     | 2448                           | 7             | RGB                        | 0.5m       | 2.96     |
|                                | HyRANK [255]                                  | 2018  | 5        | 1,000                          | 14            | Hyperspectral              | 30m        | 0.4      |
|                                | WHDLD [239]                                   | 2018  | 4940     | 256                            | 6             | RGB                        | 2m         | 0.102    |
|                                | SEN12MS [146]                                 | 2019  | 541,986  | 256                            | 17            | MS,SAR                     | 10m        | 510      |
|                                | Urban Semantic 3D (DFC19) [256]               | 2019  | 2783     | 1024                           | 6             | MS,LIDAR                   | 0.3~1.3m   | 285      |
|                                | Chesapeake Land Cover [257]                   | 2019  | 100000   | 224                            | 6             | RGB,MS                     | 1m         | 404.95   |
|                                | DFC20 [258]                                   | 2020  | 180662   | 256                            | 10            | Sentinel-1,Sentinel-2      | 10m        | 9.6      |
|                                | BDCI2020 [259]                                | 2020  | 145,981  | 256                            | 7             | RGB                        | 2m         | 1.3      |
|                                | LandCoverAI [145]                             | 2020  | 41       | 9000                           | 3             | RGB                        | 0.25m,0.5m | 1.4      |
|                                | Luojia-HSSR [260]                             | 2023  | 6438     | 256                            | 23            | RGB                        | 0.75m      | /        |
|                                | LoveDA [261]                                  | 2021  | 5,987    | 1,024                          | 7             | RGB                        | 0.3m       | 9.6      |
|                                | MiniFrance-DFC22 [262]                        | 2022  | 2322     | 2000                           | 15            | RGB                        | 0.5m       | 93       |
|                                | GeoNRW [263]                                  | 2022  | 7783     | 1000                           | 10            | RGB,nDSM                   | 1m         | 32       |
|                                | SEASONET [26]                                 | 2022  | 1759830  | 120                            | 33            | Sentinel-2                 | 10m        | 229      |
|                                | TimeSpec4LULC [264]                           | 2022  | /        | 262 months                     | 29            | MS,MT                      | 500m       | 60       |
|                                | Five-Billion-Pixels [265]                     | 2022  | 150      | 7200x6800                      | 24            | RGB,MS                     | 4m         | 104      |
| GAMUS [266]                    | 2023  | 9340  | 1024     | 6                              | RGB,nDSM      | 0.33m                      | 48         |          |
| WHU-OHS [267]                  | 2022  | 7795  | 512      | 24                             | Hyperspectral | 10m                        | 94.9       |          |
| Land Use                       | OpenSentinelMap [268]                         | 2022  | 137045   | 192, 96                        | 15            | RGB,Sentinel-2             | 10m~60m    | 455      |
|                                | DFC18 [269]                                   | 2018  | 10,798   | 2,001                          | 20            | MS,Hyperspectral,RGB       | 0.05~1m    | 10.1     |
|                                | MultiSenGE [270]                              | 2022  | 8157     | 256                            | 14            | Sentinel-1,Sentinel-2      | 10m        | 530      |
| Parking                        | APKLOT [271]                                  | 2020  | 501      | /                              | 2             | RGB                        | /          | 3        |
| Power                          | TTPL [272]                                    | 2020  | 1100     | 3840                           | 3             | RGB                        | UAV        | 4.2      |
| Road                           | Massachusetts Roads [230]                     | 2013  | 1171     | 1500                           | 1             | RGB                        | 1m         | 10.56    |
|                                | ERM PAIW [209]                                | 2015  | 41       | 4000                           | 2             | RGB                        | 0.3m       | 0.635    |
|                                | HD-Maps [208]                                 | 2016  | 20       | 4000                           | 5             | RGB                        | 0.3m       | 0.146    |
|                                | SpaceNet-3 (Road ) [225]                      | 2017  | 3711     | 1300                           | 2             | Panchromatic,RGB,MS        | 0.3~1.24m  | 106      |
|                                | RoadNet [206]                                 | 2018  | 20       | /                              | 2             | RGB                        | 0.21m      | 0.905    |
|                                | AerialLanes18 [273]                           | 2018  | 20       | 5616                           | 1             | RGB                        | 0.125m     | 0.0014   |
|                                | SpaceNet-5 (Road Network) [225]               | 2019  | 2369     | 1300                           | 2             | Panchromatic,RGB,MS        | 0.3m       | 84       |
|                                | SpaceNet-8 (Flooded Road) [274]               | 2022  | /        | 1300                           | 4             | Panchromatic,RGB           | 0.3~0.8m   | /        |
|                                | RoadTracer [210]                              | 2019  | 3,000    | 4,096                          | 1             | RGB                        | 0.6m       | /        |
| Microsoft RoadDetections [211] | 2022  | 20000 | 1088     | 1                              | RGB           | 1m                         | 9.25       |          |
| Roof                           | AIRS [275]                                    | 2019  | 1047     | 10000                          | 1             | RGB                        | 0.075m     | 17.6     |
|                                | Open AI Challenge: Caribbean[276]             | 2019  | 7        | 52,318                         | 5             | RGB                        | 0.04m      | /        |
|                                | RID [277]                                     | 2022  | 2000     | /                              | 16            | RGB                        | 0.1m       | 1.5      |
| Salient Objects                | ORSSD [278]                                   | 2019  | 800      | 500                            | 8             | RGB                        | /          | 0.026    |
|                                | EORSSD [278]                                  | 2020  | 2,000    | 500                            | 2             | RGB                        | /          | 0.06     |
| Shadow                         | AISD [279]                                    | 2020  | 514      | 512                            | 2             | RGB                        | /          | 0.29     |
| Traffic Scenes                 | DLR-SkyScapes[280]                            | 2019  | 16       | 4680                           | 31            | RGB                        | 0.13m      | /        |
| Water Body                     | Kaggle Water Bodies[281]                      | 2020  | 2841     | 1000                           | 2             | RGB                        | /          | 0.28     |

TABLE IV  
 DETAILED INFORMATION FOR SOME REPRESENTATIVE RS CHANGE DETECTION DATASETS. THESE DATASETS ARE GROUPED INTO 5 DIFFERENT RESEARCH DOMAINS IN ALPHABETICAL ORDER. NOTE THAT / DENOTES THE MISSING INFORMATION AND MS DENOTES THE MULTISPECTRAL DATA. MORE DETAILED INFORMATION CAN BE FOUND AT [HTTPS://EARTHNETS.GITHUB.IO](https://earthnets.github.io).

| Domain      | Name                                     | Year | #Samples | Sample Size                | #Classes | Modality      | Resolution                 | Vol.(GB) |
|-------------|--|------|----------|----------------------------|----------|---------------|----------------------------|----------|
| 3D          | URB3DCD[285]                             | 2021 | 50       | /                          | 2        | PointCloud    | 0.5 pm                     | 1.5      |
|             | 3DCD [288]                               | 472  | 400×400  | 2                          | RGB,nDSM | /             | /                          | /        |
| Building    | AIST Building Change Detection [289]     | 2017 | 16950    | 160                        | 2        | RGB           | 0.4m                       | 17.77    |
|             | WHU Building change detection [156]      | 2018 | 2        | 15354×32507                | 2        | RGB           | 0.075m                     | 5        |
|             | LEVIR-CD [290]                           | 2020 | 637      | 1024                       | 2        | RGB           | 0.5m                       | 2.64     |
|             | xView2 (xBD) [291]                       | 2018 | 22068    | 1024                       | 4        | RGB           | 0.5m                       | 51       |
| CropLand    | CropLand Change Decton (CLCD) [284]      | 2022 | 600      | 512                        | 2        | RGB           | 0.5~2 m                    | 0.5      |
| Flood       | California flood dataset [283]           | 2019 | 1        | 1534×808                   | 2        | RGB,MS        | 5m,30m                     | 0.33     |
| Land Change | SZTAKI AirChange [292]                   | 2008 | 13       | 800                        | 2        | RGB           | 1.5m                       | 0.04     |
|             | Cross-sensor Bastrop [293]               | 2015 | 4        | 444×300,1534×808           | 2        | MS            | 30m,120m                   | /        |
|             | GETNET dataset [294]                     | 2018 | 1        | 463×241                    | 2        | Hyperspectral | 30m                        | 0.05     |
|             | Onera Satellite CD [295]                 | 2018 | 24       | 600                        | 2        | Sentinel-2    | 10m                        | 0.48     |
|             | CDD (season-varying)[296]                | 2018 | 16000    | 256                        | 2        | RGB           | 0.03~0.1m                  | 2.7      |
|             | Hyperspectral CD[297]                    | 2018 | 3        | 984×740,600×500,390×200    | 5        | Hyperspectral | 30m                        | 1.7      |
|             | HRSCD [295]                              | 2019 | 291      | 10000                      | 5        | RGB           | 0.5m                       | 5        |
|             | MtS-WH [298]                             | 2019 | 190      | 150                        | 2        | RGB-NIR       | 1m                         | 0.43     |
|             | SECOND [286]                             | 2020 | 4662     | 512                        | 6        | RGB           | 0.5~3m                     | 2.2      |
|             | Zhang et al. CD dataset [299]            | 2020 | 4        | 1431×1431,458×559,1154×740 | 2        | RGB,NIR       | 2m,2.4m,5.8m               | 0.1      |
|             | DSIFN [300]                              | 2020 | 3,988    | 512                        | 2        | RGB           | 10m                        | 0.46     |
|             | Hermiston City Oregon [301]              | 2018 | 1        | 390×200                    | 5        | Hyperspectral | 30m                        | /        |
|             | Hi-UCD [302]                             | 2020 | 1293     | 1024                       | 9        | RGB           | 0.1m                       | /        |
|             | Google Data Set [303]                    | 2020 | 19       | 1000~5000                  | 2        | RGB           | 0.55m                      | 0.6      |
|             | DFC21-MSD [253]                          | 2021 | 2250     | 4000                       | 15       | MS,MT         | 1~30m                      | 325      |
|             | Relative Radiometric Normalization [304] | 2021 | 7        | 300~5000                   | 2        | MS            | 0.31m,0.4m,10m,20m,30m,60m | 1        |
|             | HTCD [305]                               | 2021 | 2        | 11 K×15 K,1.38 M×1.04 M    | 2        | RGB           | 0.5971m, 0.074m            | 1.74     |
|             | S2Looking [282]                          | 2021 | 5000     | 1,024                      | 2        | RGB           | 0.5~0.8m                   | 10.21    |
|             | SYSU-CD [306]                            | 2021 | 20,000   | 256                        | 2        | RGB           | 0.5m                       | 5.17     |
|             | WH-MAVS [307]                            | 2021 | 47,134   | 200                        | 15       | RGB           | 1.2m                       | /        |
|             | S2MTC [308]                              | 2021 | 1520     | 600                        | /        | MS            | 10m                        | 10.6     |
|             | RapidAI4EO [12]                          | 2021 | 500,000  | /                          | 44       | MS,RGB        | 3m,10m                     | /        |
|             | Dynamic EarthNet Challenge [309]         | 2021 | 22500    | 1024                       | 7        | RGB           | 3m                         | /        |
|             | MSBC [310]                               | 2022 | 3,769    | 256                        | 2        | RGB,SAR,MS    | 2m                         | 3.9      |
|             | Dynamic World [287]                      | 2022 | /        | /                          | 9        | Sentinel-2    | 10m                        | /        |
|             | MSOSCD [310]                             | 2022 | 5,107    | 256                        | 2        | RGB,SAR,MS    | 10~60m                     | 2.7      |
|             | ChangeNet [311]                          | 2024 | 31000    | /                          | 6        | RGB           | 0.3m                       | /        |
|             | BANDON [312]                             | 2023 | 2283     | 2048×2048                  | 2        | RGB           | 0.6m                       | 3.4      |

GeoPile(GFM) [317], and Prithvi [27] construct large-scale dataset by assembling different sub-datasets. This concept has also been adopted by GEO-Bench [318], SATIN [319], and FoMo-Bench [88] for the evaluation of RS foundation models across various tasks.

### F. RS Vision-Language Datasets

Large Language Models (LLMs) and Vision-Language Models (VLMs) have attracted significant attention in research on Natural Language Processing (NLP) and CV. These models leverage large-scale Transformer networks to enhance natural language understanding, multi-modal learning, and reasoning ability, achieving significant performance improvements across various tasks. Compared with the reviewed image classification, object detection, semantic segmentation, and change detection tasks, research on VLMs still signifies an emerging and innovative area in the RS domain. Various vision-language datasets have been constructed to accelerate research on VLMs, as presented in Table V.

Among these datasets, image captioning [333], [341], [328] and Visual Question Answering (VQA) [330], [342] combine natural language and image data to enable a more natural interaction between end-users and artificial intelligence systems. Datasets for RS Visual Grounding (VG) [329] are constructed to enable specific object detection guided by natural language. In the era of VLMs, large-scale vision-language datasets including RS5M [332], Skyscript [337] and ChatEarthNet [338] are built for aligning natural language with RS imagery and fine-tuning VLMs.

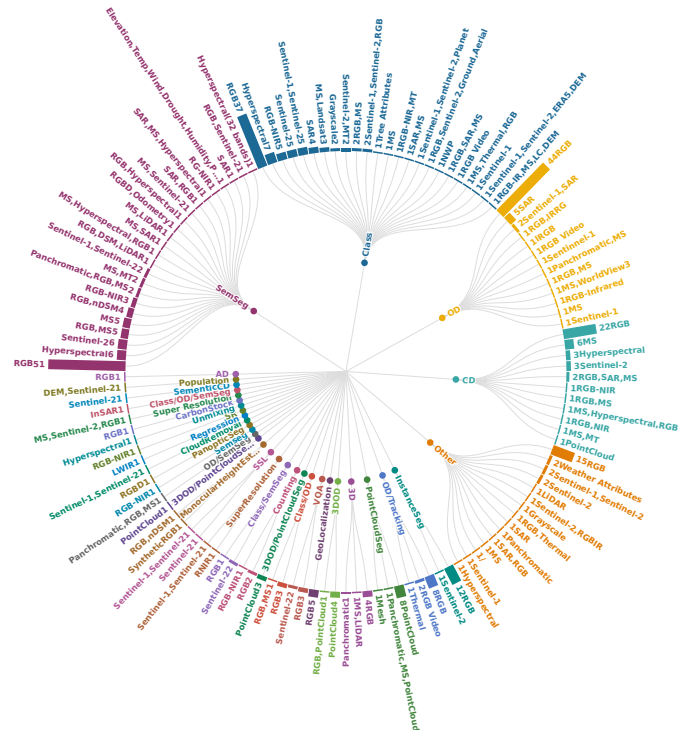


Fig. 2. Data modalities (outer perimeter) organized by EO tasks (inner labels). Although a wide range of data sources are used for EO, optical data (RGB) remains the most commonly used modality for the majority of RS tasks.



TABLE V  
DETAILED INFORMATION OF SOME REPRESENTATIVE DATASETS FOR RS FOUNDATION MODELS AND VISION-LANGUAGE MODELS. NOTE THAT / DENOTES THE MISSING INFORMATION AND MS DENOTES THE MULTISPECTRAL DATA. MORE INFORMATION CAN BE FOUND AT [HTTPS://EARTHNETS.GITHUB.IO](https://earthnets.github.io).

| Domain                         | Name                         | Publication year | # samples          | Task                 | # classes  | Modality                  | Resolution |
|--------------------------------|------------------------------|------------------|--------------------|----------------------|------------|---------------------------|------------|
| Foundation Models Evaluation   | GEO-Bench [318]              | 2023             | 12 subdatasets     | SemSeg,Class         | /          | RGB,SAR,MS,Hyperspectral  | 0.5m - 30m |
|                                | SATIN [319]                  | 2023             | 27 subdatasets     | SemSeg,Class         | 250        | RGB                       | /          |
|                                | PhilEO [320]                 | 2024             | 3 subdatasets      | SemSeg               | 11         | RGB,MS                    | 10m        |
|                                | FoMo-Bench [88]              | 2024             | 15 subdatasets     | SSL                  | /          | RGB,MS,SAR                | 0.5m - 20m |
|                                | SustainBench [321]           | 2021             | 15 subdatasets     | Regression,Class     | /          | RGB,Time-seris            | 30m        |
| Foundation Models Pre-training | SatlasPretrain [315]         | 2021             | 302,222,000 labels | OD,CD,Class,SemSeg   | 137        | NAIP,RGB,MS               | 1m,10m     |
|                                | SSL4EO-L [322]               | 2023             | 5,000,000          | SSL                  | /          | MS                        | 30m        |
|                                | CACo1M [323]                 | 2023             | 1,000,000          | SSL                  | /          | Sentinel,MS               | 10m        |
|                                | TOV-RS-Balanced [324]        | 2023             | /                  | SSL                  | /          | RGB,SAR,Hyperspectral     | /          |
|                                | GeoPile(GFM) [317]           | 2023             | 600,000            | SSL                  | /          | RGB                       | 0.1m - 30m |
|                                | DOFA-data(Metadataset) [316] | 2024             | 8,081,411          | SSL                  | /          | RGB, SAR,MS,Hyperspectral | 0.5m - 30m |
|                                | GRAFT [325]                  | 2024             | 189,000,000        | SSL                  | /          | RGB,MS                    | /          |
|                                | SAMRS(Metadataset) [326]     | 2023             | /                  | SemSeg,OD            | /          | RGB                       | /          |
|                                | Prithvi [27]                 | 2023             | /                  | SSL                  | /          | HLS-2                     | /          |
| Skysense [327]                 | 2024                         | 215,000,000      | SSL                | /                    | RGB,SAR,MS | 0.31m - 20m               |            |
| Vision-Language Datasets       | LuojiaHOG [328]              | 2024             | 565231 captions    | Captioning/Retrieval | 131        | RGB                       | 0.5m       |
|                                | RSVG [329]                   | 2023             | 38320 captions     | VG                   | /          | RGB                       | 0.5m-1m    |
|                                | RSVQA-LR [330]               | 2020             | 772                | VQA                  | 9          | MS                        | 10m        |
|                                | RSVQA-HR [331]               | 2020             | 10659              | VQA                  | 89         | RGB                       | 0.15m      |
|                                | RSVQAxBEN [330]              | 2021             | 590,326            | VQA                  | 26,875     | MS                        | 10m        |
|                                | RSIVQA [330]                 | 2021             | 37,264             | VQA                  | 864        | RGB                       | 0.1~8m     |
|                                | RS5M [332]                   | 2023             | 5,000,000          | Captioning           | /          | RGB,Text                  | 0.5m-30m   |
|                                | RSICD [333]                  | 2017             | 10921              | Captioning           | 31         | RGB,Text                  | 0.5m-30m   |
|                                | NWPU-Captions [334]          | 2022             | 31500              | Captioning           | 45         | RGB,Text                  | 0.5m-30m   |
|                                | RSITMD [335]                 | 2022             | 4743               | Retrieval            | 32         | RGB,Text                  | 0.5m-30m   |
|                                | RSICap [336]                 | 2023             | 2585               | Captioning           | 16         | RGB,Text                  | 0.5m-30m   |
|                                | SkyScript [337]              | 2023             | 2600000            | Captioning           | /          | RGB,Text                  | 0.5m-30m   |
|                                | ChatEarthNet [338]           | 2024             | 163488             | Captioning           | /          | SAR,MS,Text               | 10m-20m    |
|                                | LHRS-Align [339]             | 2024             | 1150000            | Captioning           | /          | RGB,Text                  | 0.5m-30m   |
|                                | LAION-EO [340]               | 2023             | 24933              | Captioning           | /          | RGB,Text                  | 0.5m-30m   |

Apart from these reviewed RS tasks, we list some datasets constructed for other tasks in the supplementary materials. Multi-view stereo datasets [343], [344], [345] are used for 3D reconstruction. There are also datasets used for more sporadic tasks like geo-localization [346], [347], weather forecasting [348], [349], soil parameter estimation [350], and wind speed estimation [108], [351].

### III. REMOTE SENSING DATASET ANALYSIS

In this section, we analyze the reviewed over 500 RS datasets and provide statistics related to four different aspects of these datasets.

#### A. The Volume Trend

Thanks to their powerful representation learning capabilities, deep learning networks trained with large-scale datasets have shown superior performance to classical machine learning methods. In the deep learning era, large-scale datasets are important in training deep models that yield better performance and generalizability. Another advantage of large-scale datasets is that they align better with real-world scenarios. In Fig. 1, we visualize a chronological overview of the volume of over 500 RS datasets. Note that the volume (in GBs) shown in the figure is transformed into the logarithmic scale, and larger circles indicate larger volumes. It can be seen that datasets before the year 2015 are usually smaller in volume. Similar to the CV community, after deep learning became the mainstream technique, both the number and the volume of RS datasets significantly increased. For example, the volumes of fMoW [134] and Sen4AgriNet [41] are greater than 4000 GB. Well-annotated large-scale datasets can help the RS community develop more powerful deep-learning models with better performance and generalizability.

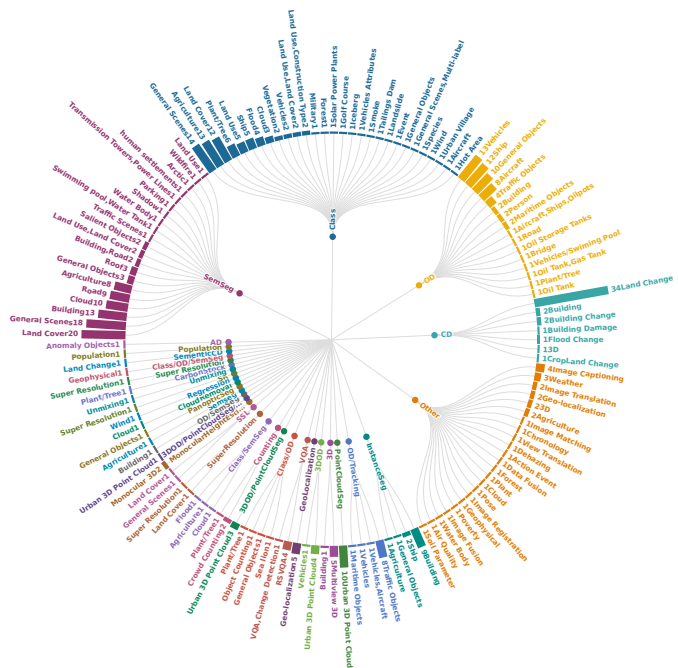


Fig. 3. Research Domains (outer perimeter) Organized by EO Tasks (inner labels). It can be seen that there are strong correlations between the research domains and EO tasks.

#### B. Analysis of Data Modalities

To analyze the image sources used in the RS community, we summarize and visualize the data modalities used for different RS tasks. The relationships between data modalities and RS tasks are shown in Fig. 2. Although there is a wide range of image sources, optical data (RGB) is still the most frequently used modality for the majority of RS tasks. In Fig. 3, we

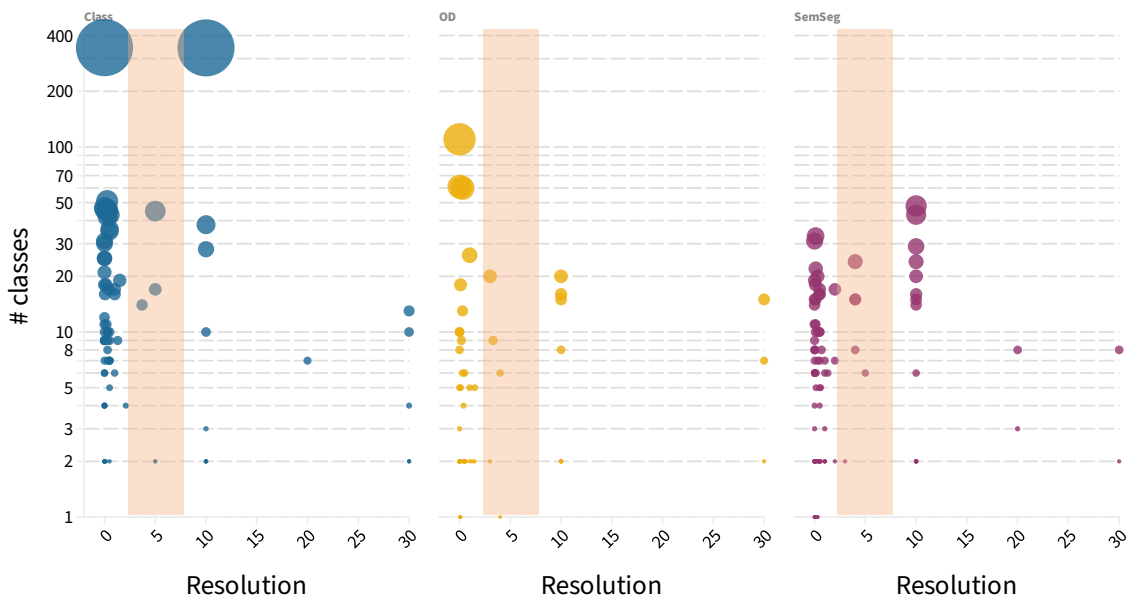


Fig. 4. Visualization of the relationships between data resolution and the number of annotated classes. An interesting finding is that most datasets have a resolution that is either smaller than 1m or larger than 10m. Datasets with a resolution range of between 1 to 10m are scarce.

display the relationships between tasks and research domains.

### C. Analysis of Spatial Resolutions

For RS images, spatial resolution has a high correlation to image content. In Fig. 4, we show the relationships between data resolution and the number of annotated classes. In general, this figure clearly shows that the number of semantic classes for RS image classification tasks is higher than those for RS object detection and segmentation tasks. The reason is that object-level and pixel-level datasets require much more annotation efforts when the number of semantic classes increases.

Another interesting finding is that most datasets have a resolution of smaller than 1m or larger than 10m. The datasets with resolution in the range between 1 to 10m are obviously scarce. The reason for this phenomenon is that many EO applications require either high-resolution ( $\leq 1m$ ) imagery or global coverage (Sentinel 1&2,  $\geq 10m$ ). However, the EO data with resolution 1~10m also has great potential in a range of applications. More research attention should be devoted to filling this gap.

### D. The correlation between different datasets

To provide a more global view of these datasets, for the first time, we propose to analyze the correlation between different datasets based on the attribute information provided in this study.

We treat the attribute information of each dataset as a data sample and measure the similarity between different datasets. Formally, let  $n$  represent the number of samples, and  $s$  represent the size of each sample in dataset  $D$ . We denote  $v$  as the volume of  $D$ . Then the scale of  $D$  can be quantitatively measured using  $n, s$ , and  $v$ . Furthermore, we quantify the annotation level of  $D$  and represent it using  $m$ .

Specifically, we assign 1 to  $m$  for image-level annotation, 2 for object-level, 3 for pixel-level, 4 for instance-level, 5 for panoptic-level, and 0 for no-label. Similarly, we also quantify the task of  $D$  to  $t$ . According to the task type,  $t$  can be 1 for RS image classification, 2 for object detection, 3 for semantic segmentation, 4 for change detection, and 0 for other tasks. Then we use  $c$  to represent the number of annotated classes in dataset  $D$ , and  $r$  to denote the max resolution of samples in  $D$ . With these definitions,  $n, s, v, m, c, r, t$  are numerical values representing the attributes of  $D$ .

Since the research domain of a dataset is provided by a word or phrase, it is non-trivial to measure the distance between them. For example, the research domain “Ship” should be closer to “Sea” than “Tree” or “Aircraft.” The research domain “Tree” should be more similar to “Forest” not “Building.” To this end, we propose to use the pre-trained word embedding [352] models to compute the real-valued vector feature  $d$  for each research domain. Here we denote  $d$  as the textual features of the domain.

Following these pre-processing pipelines, we can quantify the attributes of dataset  $D$  into two feature vectors:  $F = [n, s, v, m, c, r, t]$  and the word embeddings for the research domain  $d$ . For two datasets  $D_1$  and  $D_2$ , we use  $F_1, F_2$ , and  $d_1, d_2$  to represent the features of these two datasets. Then, we can compute the similarity using the following formula:

$$\begin{aligned} \cos(\theta_1) &= \frac{F_1 \cdot F_2}{\|F_1\|_2 \|F_2\|_2}, \\ \cos(\theta_2) &= \frac{d_1 \cdot d_2}{\|d_1\|_2 \|d_2\|_2}, \\ \text{sim}(D_1, D_2) &= \cos(\theta_1) + \cos(\theta_2). \end{aligned} \quad (1)$$

In Fig. 5, the correlation matrix between over 500 RS datasets is visualized. The lighter the color, the higher the similarity. To our knowledge, this is the first work that analyzes the correlation between existing RS datasets. The correlation

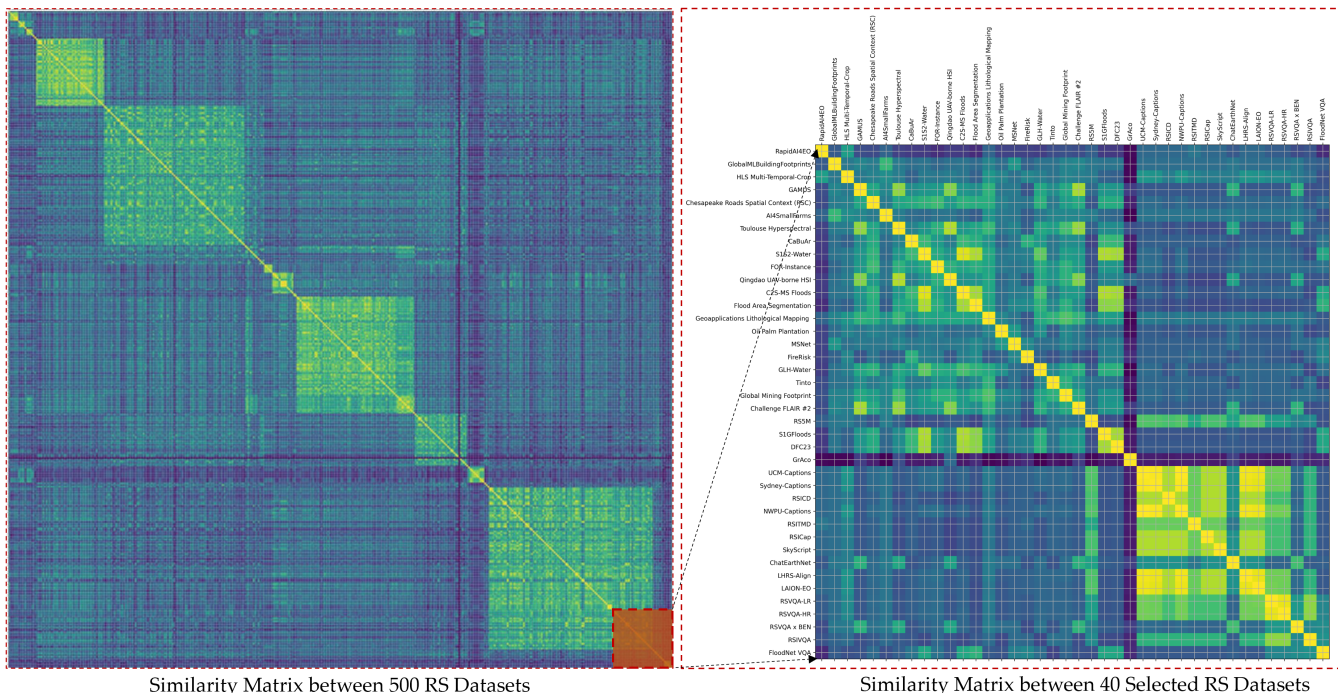


Fig. 5. Visualization of the correlation between different datasets. A lighter color means a higher correlation.

matrix reflects the distances between different pairs of the RS dataset. The distance information could be valuable for the RS community. Some possible ways to leverage the correlation between RS datasets for future research are outlined below.

- 1) **Dataset recommendation.** Similar and related datasets can be recommended based on the relationships between datasets and the given dataset. This will help researchers find desired datasets for their research tasks.
- 2) **Domain adaptation.** Domain adaptation aims to improve the performance of a model on a target domain using the knowledge learned in the source domain. With the correlation map, researchers can easily find the proper source and target datasets for developing novel domain adaptation algorithms.
- 3) **Dataset assembling.** The distance between datasets can also be used to assemble multiple small but similar datasets into a larger one (metadataset) for pre-training and evaluating large-scale RS foundation models.
- 4) **Multi-task model training.** Similarly, using the distance between datasets, we can combine datasets with similar spatial resolution, data modalities, or research domains, but different tasks into a unified dataset for training multi-task foundation models.

Furthermore, with the correlation matrix, we can visualize RS datasets using an interactive network graph. The node represents the RS dataset, and the link between nodes denotes the similarity between them. In Fig. 6, we can see that different datasets gradually cluster together when the connecting threshold decreases.

#### IV. DATASET RANKING AND BENCHMARK BUILDING

Researchers in the RS community have been publishing more and more datasets to benefit the development of new methods. However, algorithms can easily saturate their performance on these datasets [353]. Deep learning models can achieve almost perfect performance on small-scale or domain-specific datasets. However, small-scale datasets are more likely to have bias and cannot reflect the performance of methods in real-world complex scenarios [18]. Methods developed on small datasets or specific domains are difficult to generalize to other scenarios. Considering these disadvantages, it is urgent to employ new benchmarks with large-scale, general research domains, and high-quality annotations for a fair and consistent evaluation of RS methods. Although the attributes of a large number of datasets are provided, it is still not intuitive to compare the quality of different datasets. Thus, for the first time, in this study, we propose to rank these datasets based on their attributes.

##### A. Dataset Ranking Metrics

Regarding the desirable properties of benchmark datasets, Long et al. [18] propose the DiRS formula, so named for its focus on the diversity, richness, and scalability of datasets. These properties are good references for designing metrics to measure and rank the RS dataset. However, it is non-trivial to quantitatively measure the diversity and richness of existing datasets. In order to approximate the DiRS metric, we consider both data diversity and annotation diversity in this study.

To measure the data diversity, we first examine the research domain of one dataset. Some datasets constructed with specific domains will have limitations on the diversity of data sources. Hence, we first filter them and only keep datasets designed for

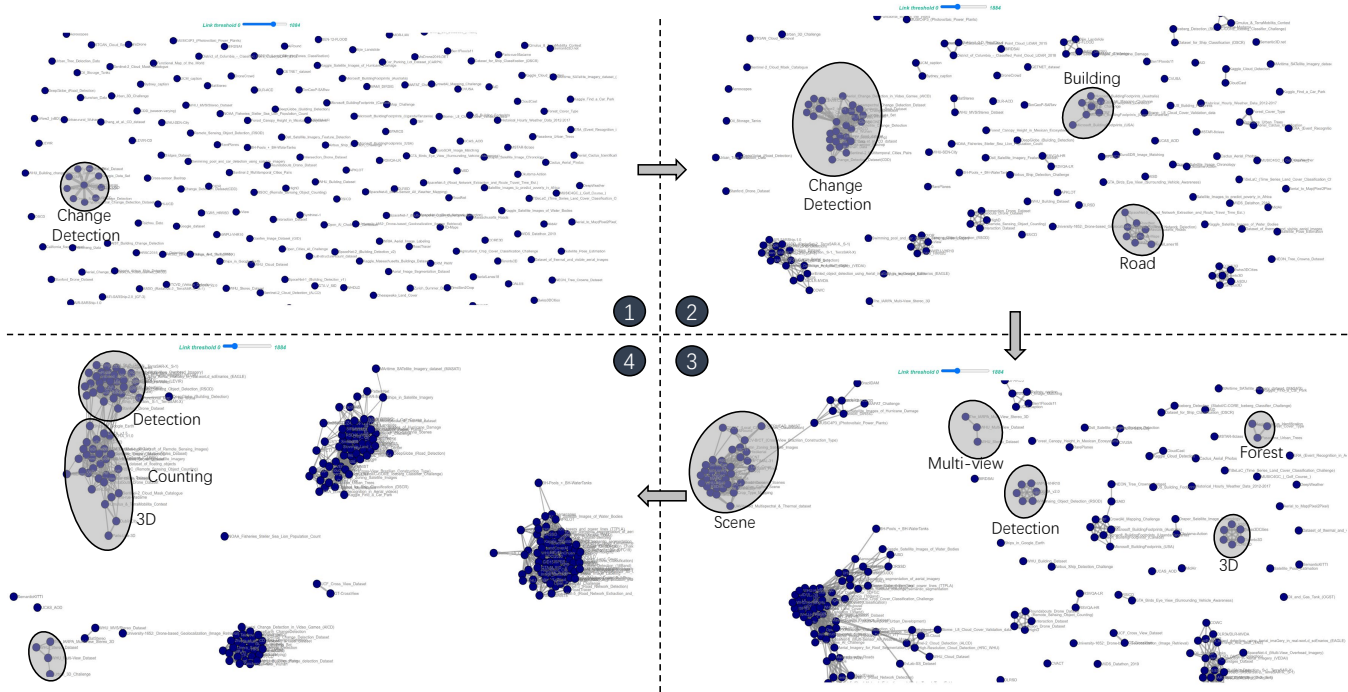


Fig. 6. With the correlation matrix, we can visualize RS datasets using network graphs. The node represents the RS dataset, and the link between nodes denotes the similarity between nodes. Datasets gradually cluster together when the connecting threshold decreases.

general purposes, like LULC or general scene understanding. Next, we choose to measure the dataset scale using the number, size of samples, and the volume of the dataset, i.e., attribute variables  $n, s, v$ . Furthermore, we take the modality diversity, that is, the number of data modalities  $k$ , into consideration. Since images with higher spatial resolution can provide richer visual content, we also factor in the resolution  $r$  as a part of the metric.

Considering the annotation richness, we use the number of annotation classes  $c$  and the quantified annotation level  $m$  to measure the richness of the labels. To start with, given 401 RS datasets, we first filter out datasets designed for specific domains. After this step, 114 datasets remain as candidates. Then, we use the aforementioned attributes to quantitatively measure the diversity and richness of each dataset. Since there exist significantly high values in the  $n, s, v$  of different datasets, we use log normalization to standardize them into the range 0 to 1. Next, we normalize each of the dataset attributes in  $r, m, c, k$  into the range 0 to 1. Finally, we add them together to form the final score for the given dataset.

Based on the measurement defined above, we can compute the scores and rank these RS datasets. Based on the rankings, we select datasets for three different tasks. Specifically, for the RS image classification task, the top five ranked datasets are: 1) fMoW [134], 2) BigEarthNet [76], 3) Million AID [18], 4) So2Sat LCZ42 [24], and 5) RSD46-WHU [61]. For the RS object detection task, the top five datasets are 1) fMoW [134], 2) DIOR [19], 3) xView [133], 4) DOTA v2.0 [166], and 5) TGRS HRRSD [132]. Finally, for the RS semantic segmentation task, the top five ranked datasets are 1) SEASONET [26], 2) OpenSentinelMap [268], 3) SEN12MS [146], 4) GeoNRW

[263], and 5) Five-Billion-Pixels [265]. A complete list of the charts is displayed on <https://earthnets.github.io>, where the radar charts are used to compare the attributes of some top-ranked datasets.

### B. Dataset Selection for Benchmarking

We aim to bridge the gap between CV and RS communities. In CV research, image classification, object detection, and semantic segmentation stand out as extensively developed tasks, with numerous state-of-the-art models proposed. Consequently, in this work, we select these three tasks for model benchmarking. Regarding datasets, we aim to select several datasets designed with general purpose, large diversity, and high richness for developing and evaluating deep learning methods. Although many large-scale RS datasets meet these standards, it is unacceptable and not environment-friendly to benchmark all of them for the evaluation of RS algorithms. Thus, in this study, we choose to select two datasets for each task, including one with high resolution and one with low resolution for larger geographical coverage.

Following this constraint, the following datasets are selected. 1) **fMoW** with high resolution ( $\sim 1m$ ) data and **BigEarthNet** with low resolution ( $>10m$ ) imagery are selected for image classification. 2) **DIOR** with high-resolution ( $\sim 1m$ ) data and **fMoW** with large objects are selected for the RS object detection task. 3) **GeoNRW** with high-resolution ( $\sim 1m$ ) images and **SEASONET** with low-resolution ( $>10m$ ) images are selected for RS semantic segmentation. In total, there are five datasets selected to build a unified benchmark for three different tasks.

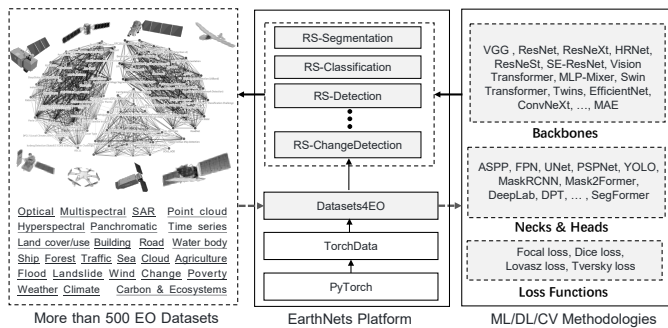


Fig. 7. The architecture design of the proposed EarthNets platform. EarthNets is based on PyTorch [354] and TorchData. It contains the Dataset4EO for a standard and easy-to-use dataset-loading library and some high-level libraries for different EO tasks.

## V. THE EARTHNETS OPEN PLATFORM

Large-scale, high-quality datasets are important for a faithful evaluation of RS algorithms, while other factors like training tricks, hyper-parameters, optimizers, and initialization methods are also critical for a fair and reliable comparison of different methods. Thus, an open platform is crucial for the fair evaluation, reproducibility, and efficient development of novel methods. However, there is still no unified deep-learning platform for different RS tasks. Torchgeo [28] mainly focuses on the data loading part. AiTLAS[353] mainly contains the codebase for the RS classification task. In contrast, we aim to build a new unified platform for the RS community that not only deals with dataset loading but also includes libraries for different RS tasks.

Fig. 7 illustrates the overall architecture design of the proposed EarthNets platform. The platform is based on PyTorch [354] and TorchData. The library Dataset4EO is designed as a standard and easy-to-use dataset-loading library. Note that Dataset4EO can be used alone or together with our high-level libraries, like RS-Classification, RS-Detection, etc.

For the design of the EarthNets platform, we consider two main factors. The first is the decoupling between dataset loading and high-level EO tasks. As shown in this study, there are over 500 RS datasets with different file formats, data modalities, research domains, and download links. Building a standard and scalable dataset-loading library can largely accelerate research for the whole RS community. Furthermore, researchers from other machine-learning communities can also benefit from the standard dataset-loading library. The second considered factor is pushing the RS data to a larger machine-learning community. There are several novel deep learning models published in the CV and machine learning community, including different backbones, models, and loss functions. The EarthNets platform is designed to easily apply these models to RS datasets and to fill in the gap between the RS and CV communities.

## VI. EXPERIMENTS

In this section, we benchmark state-of-the-art deep learning models from the CV community on five selected RS datasets.

TABLE VI  
IMAGE CLASSIFICATION RESULTS ON THE fMoW [134] DATASET. TOP-1 ACCURACY, PRECISION, RECALL, AND F1 SCORE ARE REPORTED. THE BEST RESULTS ARE IN BOLD.

| Methods         | Image Classification |              |              |              |             |
|-----------------|----------------------|--------------|--------------|--------------|-------------|
|                 | Pre-trained          | Top-1        | P            | R            | F1          |
| ViT-Small       | Random               | 54.1         | 53.45        | 51.8         | 52.03       |
| MLP-Mixer       | Random               | 43.11        | 40.33        | 41.09        | 40.18       |
| ResNet-50       | ImageNet             | 58.25        | 58.73        | 57           | 57.28       |
| EfficientNet-b4 | ImageNet             | 58.8         | 58.7         | 57.01        | 57.33       |
| ConvNext-Small  | ImageNet             | 62.05        | 63.81        | 60.34        | 61.19       |
| Swin-Tiny       | ImageNet             | <b>66.42</b> | <b>66.33</b> | <b>65.29</b> | <b>65.5</b> |

TABLE VII  
MULTI-LABEL IMAGE CLASSIFICATION RESULTS ON THE BIGEARTHNET[76] DATASET. MAP, MICRO PRECISION, MICRO RECALL AND F1 SCORE ARE REPORTED. THE BEST RESULTS ARE IN BOLD.

| Methods         | Image Classification |              |              |              |             |
|-----------------|----------------------|--------------|--------------|--------------|-------------|
|                 | Pre-trained          | mAP          | P            | R            | F1          |
| ResNet-18*[355] | Random               | 79.80        | -            | -            | -           |
| ResNet-18*[355] | ImageNet             | 85.90        | -            | -            | -           |
| ResNet-18*[355] | MoCo-v2              | 85.23        | -            | -            | -           |
| ResNet-50*[355] | ImageNet             | 86.74        | -            | -            | -           |
| ResNet-50       | ImageNet             | 85.74        | 76.87        | 75.89        | 76.38       |
| EfficientNet-b4 | ImageNet             | 84.48        | 73.84        | 77.19        | 75.48       |
| ConvNext-Small  | ImageNet             | 85.59        | 73.64        | 79.91        | 76.65       |
| Swin-Tiny       | ImageNet             | <b>87.19</b> | <b>78.01</b> | <b>80.22</b> | <b>79.1</b> |
| MLP Mixer       | ImageNet             | 82.76        | 73           | 74.36        | 73.67       |

We also compare them with the methods specifically designed for the RS datasets. The implementation details can be found in the supplementary materials.

**Metrics:** For multi-label image classification datasets, we report the following metrics: precision (P), recall (R), F1 score, and mean average precision (mAP). For precision, recall, and F1, we set the threshold value to 0.5 for all models. For object detection, mAP is used as the measurement for performance evaluation. Three metrics are used to evaluate the semantic segmentation task: overall (micro-averaged) Accuracy (aAcc), mean (macro-averaged) Accuracy(mAcc), and mean Intersection over Union (mIoU).

### A. Benchmarking Results and Comparisons

In this section, we benchmark the five selected datasets using the proposed EarthNets platform. To avoid excessive computation costs, we choose to evaluate some representative state-of-the-art (SOTA) methods from the CV community on large-scale RS datasets.

**Comparisons on the fMoW Dataset.** fMoW [134] is a large-scale dataset built to recognize the functional purpose of buildings and land use. It contains 1 million images from over 200 countries, annotated with 63 different classes. In this study, we use the fMoW-rgb version of the dataset for model evaluation. Table VI reports the benchmarking results. In general, we can see that using the ImageNet pre-trained weights can greatly improve the performance. When we compare the CNN-based methods with the Transformer-based method, we find that Swin-Tiny [357] clearly outperforms other CNN-based methods in all four metrics. Among the CNN-based methods, ConvNext [358] is the best-performing one.

TABLE VIII  
OBJECT DETECTION RESULTS ON THE DIOR[19] DATASET. THE MAP PERFORMANCE IS REPORTED. THE BEST RESULTS ARE IN BOLD.

| Method          | Object Detection |           |        |             |
|-----------------|------------------|-----------|--------|-------------|
|                 | Backbone         | Optimizer | Epochs | mAP         |
| RetinaNet* [19] | ResNet-50        | -         | -      | 65.7        |
| RetinaNet* [19] | ResNet-101       | -         | -      | 66.1        |
| PANet* [19]     | ResNet-50        | -         | -      | 63.8        |
| PANet* [19]     | ResNet-101       | -         | -      | 66.1        |
| Mask-RCNN* [19] | ResNet-50        | -         | -      | 63.5        |
| Mask-RCNN* [19] | ResNet-101       | -         | -      | 65.2        |
| YoloV3* [19]    | DarkNet53        | -         | -      | 57.1        |
| YoloV3          | DarkNet53        | SGD       | 120    | 64.0        |
| YoloV3          | Swin-Tiny        | AdamW     | 120    | 64.6        |
| YoloV3          | ConvNext-Small   | AdamW     | 120    | 67.6        |
| Mask-RCNN       | ResNet-50        | SGD       | 120    | 68.5        |
| Mask-RCNN       | Swin-Tiny        | AdamW     | 120    | 70.5        |
| Mask-RCNN       | ConvNext-Small   | AdamW     | 120    | <b>72.4</b> |

TABLE IX  
SEMANTIC SEGMENTATION RESULTS ON THE SEASONET[26] DATASET. WE REPORT THE aACC, mACC, AND mIoU METRICS. THE BEST RESULTS ARE IN BOLD.

| Method             | Semantic Segmentation |           |       |              |              |              |
|--------------------|-----------------------|-----------|-------|--------------|--------------|--------------|
|                    | Backbone              | Optimizer | Iter. | aAcc         | mAcc         | mIoU         |
| DeeplabV3* [26]    | DenseNet121           | -         | -     | -            | -            | 47.53        |
| DeeplabV3.PT* [26] | DenseNet121           | -         | -     | -            | -            | 48.69        |
| DeeplabV3          | ResNet-50             | SGD       | 80k   | 82.87        | 58.49        | 47.5         |
| DeeplabV3          | ResNet-50             | SGD       | 160k  | 83.52        | 62.65        | 50.79        |
| DeeplabV3          | ConvNext-Small        | AdamW     | 120k  | 81.36        | 56.31        | 46.39        |
| DeeplabV3          | Swin-Tiny             | AdamW     | 120k  | 82.75        | 61.5         | 50.81        |
| Upernet            | ResNet-50             | SGD       | 120k  | 83.2         | 60.36        | 49.59        |
| SegFormer          | MiT                   | AdamW     | 120k  | <b>83.75</b> | <b>64.25</b> | <b>53.87</b> |

**Comparisons on the BigEarthNet Dataset.** BigEarthNet is a large-scale multi-label Sentinel-2 benchmark dataset annotated with the CORINE Land Cover classes. There are two versions of the labels, one with 43 categories and another with 19 categories. In this study, we adopt the new class nomenclature (19 categories) introduced in [359]. Regarding the methods, we evaluate four CNN-based architectures (ResNet-18, ResNet-50, EfficientNet-b4, ConvNext). For the Transformer-based method, we evaluate the Swin-Tiny, which is usually overlooked in existing benchmarking results. Furthermore, an MLP-based method, the MLP-Mixer [360] is also compared. Additionally, we also compare the results reported by existing work [355] on the BigEarthNet dataset.

Table VII reports the benchmarking results. In general, the

TABLE X  
SEMANTIC SEGMENTATION RESULTS ON THE GEONRW[263] DATASET. WE REPORT THE aACC, mACC, AND mIoU METRICS. THE BEST RESULTS ARE IN BOLD.

| Method           | Semantic Segmentation |           |         |              |              |              |
|------------------|-----------------------|-----------|---------|--------------|--------------|--------------|
|                  | Backbone              | Optimizer | #Epochs | aAcc         | mAcc         | mIoU         |
| MultiTask* [356] | Transformer           | AdamW     | 100k    | 76.75        | 71.89        | 57.3         |
| Lu et al.* [356] | Transformer           | AdamW     | 100k    | 76.53        | 70.12        | 56.2         |
| FCN              | UNet                  | SGD       | 40k     | 78.8         | 66.86        | 55.6         |
| PSPNet           | ResNet-50             | SGD       | 40k     | 81.56        | 74.92        | 62.73        |
| Deeplabv3+       | ResNet-50             | SGD       | 40k     | 81.91        | 75.26        | 63.01        |
| Deeplabv3+       | ConvNext-Tiny         | AdamW     | 40k     | 80.89        | 73.61        | 61.63        |
| Deeplabv3+       | Swin-Tiny             | SGD       | 40k     | 78.09        | 70.01        | 56.78        |
| Deeplabv3+       | Swin-Tiny             | AdamW     | 40k     | 81.11        | 74.28        | 62.18        |
| Upernet          | ResNet-50             | SGD       | 40k     | 81.87        | 75.7         | 63.1         |
| Upernet          | ConvNext-Tiny         | AdamW     | 40k     | 82.08        | 74.9         | 63.48        |
| Upernet          | ViT-Small             | AdamW     | 40k     | 78.65        | 71.13        | 59.43        |
| Upernet          | Swin-Tiny             | AdamW     | 40k     | 82.31        | <b>75.68</b> | <b>64.48</b> |
| SegFormer        | MiT                   | AdamW     | 40k     | <b>82.55</b> | 75.63        | 64.38        |

results indicate that Swin-Tiny performs best on this multi-label classification dataset. However, there is no significant advantage compared with other CNN-based methods. Another conclusion we can make is that ResNet-50 is a strong baseline method. From the results, it can be seen that ResNet-50, pre-trained on ImageNet or using self-supervised MoCo-V2 [361], can perform better than MLP-Mixer, EfficientNet-b4 on this dataset. The performance of ConvNext is competitive to ResNet-50, but lower than the transformer-based method Swin-Tiny. Note that \* indicates that the results of the method are reported in existing work. Generally speaking, the results benchmarked using the EarthNets platform are higher than or comparable to existing reported results.

**Comparisons on the DIOR Dataset.** Table VIII presents the benchmarking results on the DIOR dataset built for the object detection task. We chose two representative and widely-used object detection methods designed by the CV community. To be specific, YoloV3[114] and Mask-RCNN[362] are evaluated on the DIOR dataset. YoloV3 is designed for lightweight and real-time object detection. Mask-RCNN is an extension of Faster-RCNN [112] with ROI alignment and a third segmentation branch. The experimental results reveal that Mask-RCNN performs better than YoloV3 on this dataset. Concerning different backbones, the results clearly show that Swin-Tiny and ConvNext can outperform other compared methods. The Mask-RCNN method with ConvNext backbone achieves an mAP of 72.4%, which is 6.3 percentage points higher than the best results reported in [19]. Notably, we observe that our benchmarked results can greatly outperform the same method reported in existing work. This comparison reveals that the choice of the optimizer, hyper-parameters, or other training tricks can greatly affect the final results, even when the same method is used.

**Comparisons on the SEASONET Dataset.** SEASONET is a large-scale multi-label LULC scene understanding dataset. It includes 1,759,830 images from Sentinel-2 tiles, and can be used for scene classification, segmentation, and retrieval tasks. In this study, we evaluate segmentation performance on this dataset. On this dataset, we evaluate the widely-used semantic segmentation method DeeplabV3 [363] with three different backbones: ResNet-50, ConvNext, and Swin-Tiny. Upernet and SegFormer [364] with mixed-Transformer encoders (MiT) are also compared. Table IX reports the benchmarking results. It can be seen that ResNet-50 and Swin-Tiny obtain comparable results and clearly surpass other backbones. SegFormer with MiT encoder clearly outperforms other models. We also find that the results obtained using EarthNets significantly outperform performance reported in existing work [26].

**Comparisons on the GeoNRW Dataset.** The benchmarking results on the GeoNRW dataset are displayed in Table X. Five segmentation methods, FCN [365], DeeplabV3+ [366], PSPNet [367], Upernet [368] and SegFormer [364] with mixed-Transformer encoders (MiT), are evaluated on this dataset. We observe that Transformer-based models like SegFormer and Swin Transformer perform better than other methods. However, the performance of ViT-Small is worse than ResNet-50. In comparison to the reported results in existing work, we can find that using the EarthNets platform

can obtain clearly better performance.

## VII. CONCLUSION

In this study, we present a comprehensive review and build a taxonomy for more than 500 publicly published datasets in the remote sensing community. Based on the attribute information of these datasets, we systemically analyze them concerning four aspects: volumes, resolution distributions, research domains, and the correlation between datasets. Next, a new benchmark including five selected large-scale datasets is built for model evaluation. A deep learning platform termed EarthNets is released to support a consistent evaluation of deep learning methods on remote sensing data. We further use the EarthNets platform to benchmark state-of-the-art methods on the new benchmark. The performance comparisons are insightful for future research.

## APPENDIX

In this supplementary material, we present the datasets constructed for Earth observation that are not included in the image classification, object detection, semantic segmentation, and change detection tasks. Next, the implementation details of the proposed EarthNets platform and the benchmarking experiments are introduced. Finally, more visualization results and detailed benchmarking results are provided.

## VIII. OTHER EARTH OBSERVATION TASKS

Image classification, object detection, semantic segmentation, and time-series modeling (change detection) are four fundamental tasks in both the computer vision and remote sensing research community. Although many real-world applications can be framed as one or more of these four tasks, there are still some important Earth observation tasks that do not fall into these categories. To provide a comprehensive review of these datasets, in this study, we arrange them into 30 different research domains, as presented in Table XI. A detailed list of the datasets can be retrieved via the website page<sup>‡</sup>.

**Image enhancement** aims to convert an input image to an enhanced one that has richer information and better details. For instance, super resolution [399], [400], [401], [402], image dehazing [381], and cloud removal [376], [377], [235] are research tasks that are useful for improving the image quality for many downstream applications.

**Multi-modal learning** attempts to combine the strengths of different modalities of data to enhance the representations for different tasks. There are some remote sensing datasets designed for multi-modal data fusion [379], [380] and cross-view geo-localization [346], [347], [383] tasks.

**3D understanding** is crucial for many real-world applications like urban planning, disaster monitoring, flood management, and autonomous driving. Hence, many datasets have been designed for different tasks, including 3D reconstruction, point cloud analysis [407], [408], [409], [412], and multi-view stereo [343], [344], [392].

**Earth system modeling** seeks to study physical, chemical, and biological processes in order to understand the Earth planet with complex integration of environmental variables. To this end, datasets are designed for plant/tree [393], [394], [395] analysis, forest monitoring [382], soil parameter estimation [350], geophysical [386], air quality monitoring [372], and population estimation [396]. There are also Earth observation datasets constructed for climate variable estimation [348] and weather forecasting [349].

## IX. IMPLEMENTATION OF EARTHNETS PLATFORM

In this section, we will detail the implementation of the main libraries in the EarthNets platform **Dataset4EO**. At present, there are some difficulties in loading RS datasets, especially for researchers in other communities. 1) The datasets have different downloading links, folder structures, file formats, data modalities, research domains, and annotation levels. It

would be helpful if it were possible to download, decompress, and split the dataset automatically. 2) Images in RS datasets usually contain multiple modalities and bands. To accelerate the training speed, it is better to move the data augmentation to GPU. 3) For datasets with very large volumes or time-series streaming data, support iterable-style data pipes would be useful to handle the dataset loading process.

**Remote Sensing Tasks** Based on the Dataset4EO library, we build the RS Classification, RS Detection, and RS Segmentation libraries. All these libraries share the same dataset loading module. To establish a deep connection with the CV community, we base these libraries for RS tasks on the libraries from OpenMMLab [427]. EarthNets enables an easy adaptation of modern deep learning models from the CV community to the RS community. For example, backbone models like ResNet [428], EfficientNet [429], ConvNext[358], Vision Transformers [430], MLP-Mixer [360], Swin Transformer [357], and so forth can be used. Numerous state-of-the-art architectures designed for CV tasks like RetinaNet [431], UNet [432], Deeplab [363], YOLO [114], Upernet [368], and SegFormer [364] can be applied to RS data. By this means, EarthNets can serve as a bridge between the CV and RS communities.

## X. IMPLEMENTATION DETAILS FOR BENCHMARKING EXPERIMENTS

**Optimizer:** For convolution-based models, SGD is used as the optimizer. The AdamW [433] is used for optimizing the Transformer-based models. **Initialization:** By default, we use the ImageNet pre-trained weights for initializing the models. For some architectures with no ImageNet [23] pre-trained weights, we train them from scratch. Other hyper-parameters including batch size and learning rate are set differently for each dataset. More implementation details are provided in the public codes at <https://github.com/EarthNets>.

## XI. VISUALIZATION RESULTS OF BENCHMARKING EXPERIMENTS

In Fig. 8, we use radar charts to compare the attributes of some top-ranked datasets. We compare six different attributes of the datasets: the modality, the resolution, the annotation level, the number of classes, the number of samples, and the volume. Using radar charts makes it easy to compare and rank different datasets. A complete set of the charts is displayed on <https://earthnets.github.io>.

For object detection and semantic segmentation tasks, we provide the visualization results to directly compare the results of different network architectures on large-scale datasets in Fig. 9. The first two rows present the object detection results on the DIOR dataset. The second two rows show the semantic segmentation results on the SEASONET dataset. The final two rows are the semantic segmentation results on the GeoNRW dataset. From the visualization results we can further verify that Transformer-based networks work well on large-scale remote sensing datasets. This is consistent with the conclusions on the computer vision datasets. However, it is worth mentioning that in some local regions of the image, the

<sup>‡</sup><https://earthnets.retool.com/embedded/public/676aa812-0dca-4e3b-a596-b043d852571d>



TABLE XI

DETAILED INFORMATION OF SOME OTHER RS DATASETS. THESE DATASETS ARE GROUPED INTO 30 DIFFERENT RESEARCH DOMAINS IN ALPHABETICAL ORDER. THE DOWNLOAD LINKS FOR ALL THESE DATASETS CAN BE FOUND AT [HTTPS://EARTHNETS.GITHUB.IO](https://earthnets.github.io).

| Domain                 | Name                                       | Year | #Samples | Sample Size   | #Classes   | Modality                   | Resolution       | Vol.(GB) |
|------------------------|--|------|----------|---------------|------------|----------------------------|------------------|----------|
| Action Event           | Okutama-Action [369]                       | 2017 | 77000    | 3840x2160     | 12         | RGB                        | UAV@10~45m       | 25.9     |
| Agriculture            | Paddy Rice Maps South Korea [370]          | 2022 | 12942    | 256           | /          | Sentinel-1                 | 10m              | 0.198    |
|                        | Paddy Rice Labeling South Korea [371]      | 2022 | /        | /             | /          | Sentinel-2                 | /                | 0.0016   |
| Air Quality            | Air Quality e-Reporting [372]              | 2021 | /        | /             | /          | /                          | /                | /        |
| Anomaly Objects        | Aerial Anomaly Detection [373]             | 2022 | /        | /             | 2          | RGB                        | UAV              | /        |
| Building               | Urban 3D Challenge [374]                   | 2017 | 157,000  | /             | 2          | RGB                        | 0.5m             | /        |
| Chronology             | Draper Satellite Image Chronology [375]    | 2016 | 1,000    | 3100x2329     | /          | RGB                        | /                | 36       |
| Cloud                  | STGAN Cloud Removal [376]                  | 2019 | 217190   | 256           | 2          | Sentinel-2,RGBIR           | 10m              | 1.5      |
|                        | SEN12MS-CR [377]                           | 2020 | 122218   | 256           | /          | Sentinel-1,Sentinel-2      | 10~60m           | 272      |
| Counting               | DLR-ACD [378]                              | 2019 | 33       | 4458          | 2          | RGB                        | 0.045~0.15m      | /        |
|                        | DroneCrowd [198]                           | 2020 | 3360     | 1920x1080     | 2          | RGB                        | UAV              | 1        |
|                        | RSOC [170]                                 | 2020 | 3057     | 2500          | 4          | RGB                        | /                | 0.082    |
| Data Fusion            | SENI-2 [379]                               | 2018 | 282384   | 256           | /          | Sentinel-1,Sentinel-2      | 10m              | 42.68    |
|                        | QXS-SAROPT [380]                           | 2021 | 40000    | 256           | /          | SAR,RGB                    | 1m               | 2.7      |
| Dehazing               | SateHaze1k [381]                           | 2017 | 1,200    | 512           | /          | RGB                        | 3m               | 1.2      |
| Forest                 | Forest Canopy Height [382]                 | 2018 | 1105     | /             | /          | LiDAR                      | 1m               | 62.9     |
|                        | CVUSA [346]                                | 2017 | 44,416   | 750x750       | 0          | RGB                        | 0.3m             | 15.7     |
| Geo-localization       | University-1652 [347]                      | 2020 | 146,580  | /             | /          | RGB                        | /                | /        |
|                        | UCF Cross View Dataset [383]               | 2017 | 35404    | 1200x1200     | 0          | RGB                        | /                | 59.5     |
|                        | CVACT [384]                                | 2019 | 128334   | 1200x1200     | 0          | RGB                        | 0.5m             | 152.8    |
|                        | University-1652 [347]                      | 2020 | 50220    | 1024x1024     | 0          | RGB                        | /                | 58.4     |
|                        | VIGOR [385]                                | 2021 | 90618    | 640x640       | 0          | RGB                        | 0.114m           | 94.2     |
| Geophysical            | TenGeoP-SARwv [386]                        | 2019 | 37000    | /             | 10         | SAR                        | 5m               | 31.7     |
| Image Matching         | EuroSDR Image Matching [387]               | 2014 | /        | /             | /          | RGB                        | 6~13m            | /        |
| Image Registration     | Dataset of thermal and visible [388]       | 2019 | 110      | 336, 4000     | 0          | RGB,Thermal                | /                | 0.31     |
| Image Translation      | Aerial to Map(Pixel2Pixel) [389]           | 2017 | 2,194    | 600           | /          | RGB                        | /                | 0.239    |
|                        | WHU-SEN-City [390]                         | 2019 | 18542    | 256           | /          | Sentinel-1,Sentinel-2      | 10m              | 4.3      |
| Multiview 3D           | The IARPA Multi-View Stereo 3D [391]       | 2017 | /        | /             | /          | MS,LiDAR                   | 0.3m             | 75       |
|                        | SatStereo [343]                            | 2019 | 144      | /             | /          | Panchromatic               | 0.5m             | 127      |
|                        | WHU MVS/Stereo Dataset [344]               | 2020 | 1776     | 5376          | /          | RGB                        | 0.1m             | 95.7     |
|                        | WHU TCL SatMVS [392]                       | 2021 | 300      | 5,120         | /          | Panchromatic               | 2.1~2.5m         | 29       |
|                        | WHU Multi-View Dataset [392]               | 2020 | 28400    | 768           | /          | RGB                        | 0.1m             | 12.3     |
|                        | WHU Stereo Dataset [392]                   | 2020 | 21868    | 768           | /          | RGB                        | 0.1m             | 8.4      |
| Plant/Tree             | Cactus Aerial Photos [393]                 | 2018 | 24,000   | 32            | 2          | RGB                        | /                | 0.053    |
|                        | ReforesTree [394]                          | 2022 | 105      | 4000          | /          | RGB                        | 0.02m            | 7.5      |
|                        | Urban Tree Detection Data [395]            | 2020 | 60       | 256           | 2          | RGB-NIR                    | 0.6m             | 0.114    |
| Population             | So2Sat Population [396]                    | 2022 | /        | /             | /          | DEM,Sentinel-2             | 10m              | /        |
| Pose                   | Satellite Pose Estimation [397]            | 2019 | 15303    | 1920x1200     | /          | Grayscale                  | /                | 4.6      |
| Poverty                | Poverty in Africa [398]                    | 2020 | 32823    | 256           | /          | RGB                        | /                | 5.58     |
| Soil Parameter         | Hyperview Challenge [350]                  | 2022 | 2,886    | 11~250        | /          | Hyperspectral              | 2m               | 1.85     |
| Super Resolution       | ALSAT-2B [399]                             | 2021 | 5518     | 256           | /          | RGB-NIR                    | 2.5m/10m         | 0.044    |
|                        | The WorldStrat [400]                       | 2022 | 3449     | 1054          | 8          | MS,Sentinel-2,RGB          | 1.5~60m          | 109.5    |
|                        | SEN2VENmuS [401]                           | 2022 | 132955   | 256           | /          | Sentinel-1,Sentinel-2      | 10m~20m          | 87       |
|                        | Proba-V Super Resolution [402]             | 2018 | 1160     | 384           | /          | RNIR                       | 100~300m         | 0.71     |
| Unmixing               | DLR HySU [403]                             | 2021 | 1        | 86x123        | /          | Hyperspectral              | 0.3m~1m          | 0.005    |
| Urban 3D Point Cloud   | CORE3D [404]                               | 2018 | /        | /             | /          | Panchromatic,MS,PointCloud | /                | /        |
|                        | benchmark_ISPRS2021 [405]                  | 2021 | 20       | 1024          | /          | RGB                        | 0.08m            | 3.22     |
|                        | SemanticKITTI [406]                        | 2019 | 4549M    | 39.2 km2      | 25         | PointCloud                 | /                | 80.2     |
|                        | Toronto3D [407]                            | 2020 | 78.3M    | 1.0 km2       | 8          | PointCloud                 | /                | 1.1      |
|                        | Swiss3DCities [408], [409]                 | 2020 | 226M     | 2.7 km2       | 5          | PointCloud                 | /                | /        |
|                        | DALES [410]                                | 2020 | 505.3M   | 10.0 km2      | 8          | PointCloud                 | /                | /        |
|                        | LASDU [411]                                | 2020 | 3.12M    | 1.02 km2      | 5          | PointCloud                 | Aircraft @ 1200m | /        |
|                        | Campus3D [412]                             | 2020 | 937.1M   | 1.58 km2      | 14         | PointCloud                 | UAV              | /        |
|                        | SensatUrban [413]                          | 2020 | 2847.1M  | 6 km2         | 13         | PointCloud                 | UAV              | 20.6     |
|                        | Heisenheim3D [345]                         | 2021 | 125.7M   | 0.19 km2      | 11         | PointCloud                 | /                | 58.8     |
|                        | SUM-Helsinki [414]                         | 2021 | 19M      | 4 km2         | 6          | Mesh                       | 0.075m           | 8.35     |
|                        | Oakland 3-D PointCloud [415]               | 2009 | 1.6 M    | 1.5 km        | 5          | PointCloud                 | /                | 0.033    |
|                        | District of Columbia LiDAR 2015 [109]      | 2015 | /        | /             | 8          | PointCloud                 | /                | 34.4     |
|                        | Semantic3D.net [416]                       | 2017 | 4000 M   | /             | 8          | PointCloud                 | /                | 24.5     |
|                        | District of Columbia LiDAR 2018 [109]      | 2018 | /        | /             | 11         | PointCloud                 | /                | 279.8    |
|                        | Paris-Lille-3D [417]                       | 2017 | 143 M    | 1.94 km2      | 50         | PointCloud                 | /                | 19.9     |
| DublinCity [418]       | 2019                                       | 260M | 2.0 km2  | 13            | PointCloud | /                          | 166.8            |          |
| Paris-rue-Madame [419] | 2014                                       | 20 M | 1 km     | 26            | PointCloud | /                          | /                |          |
| Vehicles               | AM3D-Real [420]                            | 2022 | 1,012    | 720x480       | 2          | RGB,PointCloud             | 0.25m            | /        |
| VQA.Change Detection   | CDVQA [342]                                | 2022 | 2968     | 512           | 19         | RGB                        | 0.5-3m           | /        |
| Water Body             | Forel-Ule Index global inland waters [421] | 2021 | /        | /             | /          | MS                         | 500m             | 0.004    |
| Weather                | Historical Hourly Weather [422]            | 2017 | /        | /             | /          | Weather Attributes         | /                | 0.075    |
|                        | DeepWeather [349]                          | 2020 | 20       | /             | 9          | Weather Attributes         | /                | 2.965    |
|                        | ClimateNet [348]                           | 2020 | 459      | 16 (768,1152) | 9          | NC variables               | /                | 28       |
|                        | EarthNet2021 [423]                         | 2021 | 32000    | 128           | /          | Sentinel-2                 | 20m              | 614.4    |
| Climate                | Earth Surface Temperature [424]            | 2017 | 16       | /             | /          | Climate variables          | /                | 0.09     |
|                        | Greenhouse Gas [425]                       | 2017 | /        | /             | /          | Gas Emission               | /                | 0.0001   |
|                        | Hurricane Wind Speed[426]                  | 2020 | 114634   | 366           | /          | LWIR                       | /                | 2.24     |

CNN-based method, i.e., ResNet-50, works better than Swin-Transformer. Hence, an effective combination of these two architectures could yield better performance. In Table XII, Table XIII and Table XIV, we provide detailed experimental results for each semantic category.

For the image classification task on the FMoW dataset, we also show the confusion matrices to compare the performance of different network architectures in Fig. 10. From left to right, the figure displays the confusion matrix for the ResNet-50, ConvNext, and Swin-Transformer.

## REFERENCES

- [1] Charles Toth and Grzegorz Jóźków. Remote sensing platforms and sensors: A survey. *ISPRS J. Photogramm. Remote Sens.*, 115:22–36, 2016. 1
- [2] Xiao Xiang Zhu, Devis Tuia, Lichao Mou, Gui-Song Xia, Liangpei Zhang, Feng Xu, and Friedrich Fraundorfer. Deep learning in remote sensing: A comprehensive review and list of resources. *IEEE GRSM*, 5(4):8–36, 2017. 1
- [3] Ahmed Shaker, Wai Yeung Yan, and Paul E LaRoque. Automatic land-water classification using multispectral airborne lidar data for near-shore and river environments. *ISPRS J. Photogramm. Remote Sens.*, 152:94–108, 2019. 1

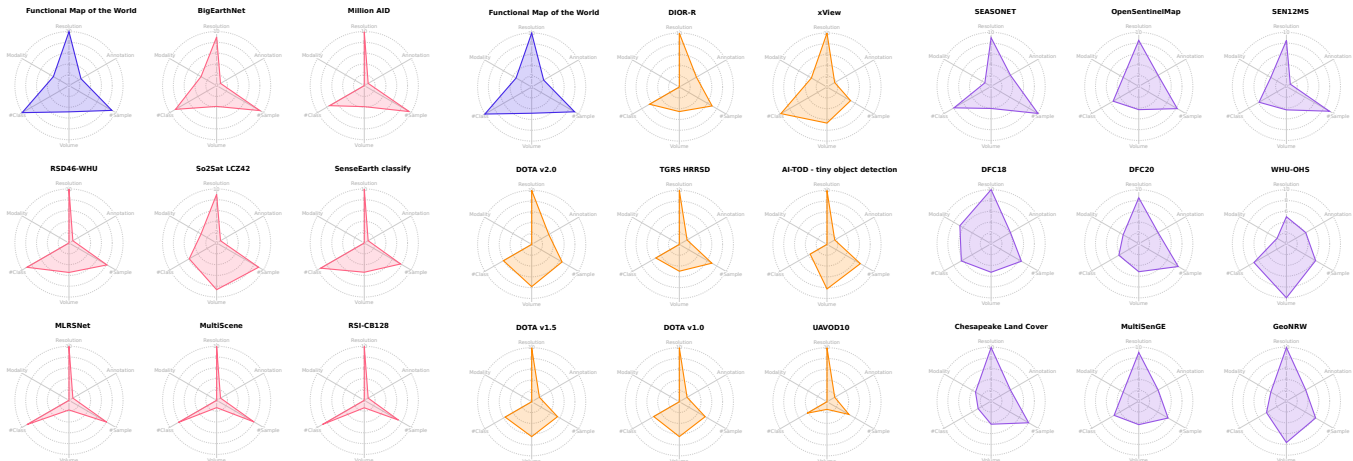


Fig. 8. Radar charts visualization of some top-ranked RS datasets for three different tasks. Six different attributes are compared and displayed in this figure. Note that all the attribute values are normalized to the range of 0 to 10.

TABLE XII  
DETAILED COMPARISON RESULTS ON THE GEONRW [263] DATASET

| Methods                           | DeepLabv3+/RN50 |       | DeepLabv3+/ConvNext-Tiny |       | DeepLabv3+/Swin-Tiny |       |
|-----------------------------------|-----------------|-------|--------------------------|-------|----------------------|-------|
|                                   | IoU             | Acc   | IoU                      | Acc   | IoU                  | Acc   |
| forest                            | 72.49           | 84.57 | 71.07                    | 84.93 | 72.22                | 83.97 |
| water                             | 90.14           | 92.91 | 91.4                     | 94.54 | 91.69                | 95.07 |
| agricultural                      | 86.66           | 92.33 | 86.2                     | 92.56 | 86.48                | 92.66 |
| residential,commercial,industrial | 69.67           | 85.5  | 67.96                    | 84.8  | 68.38                | 85.2  |
| grassland,swamp,shrubbery         | 38.92           | 58.25 | 35.72                    | 53.96 | 36.98                | 56.23 |
| railway,trainstation              | 59.03           | 73.76 | 56.66                    | 77.29 | 58.89                | 78.58 |
| highway,squares                   | 43.97           | 51.96 | 39.89                    | 46.17 | 41.31                | 48.79 |
| airport,shipyard                  | 55.37           | 79.18 | 59.35                    | 73.98 | 58.77                | 75.34 |
| roads                             | 43.05           | 53.14 | 39.32                    | 48.3  | 38.86                | 47.95 |
| buildings                         | 70.75           | 81.04 | 68.76                    | 79.54 | 68.24                | 78.97 |

TABLE XIII  
DETAILED COMPARISON RESULTS ON THE SEASONET [26] DATASET

| Methods                                    | DeepLabv3+/RN50 |       | DeepLabv3+/ConvNext-Tiny |       | DeepLabv3+/Swin-Tiny |       |
|--|-----------------|-------|--------------------------|-------|----------------------|-------|
|  | IoU             | Acc   | IoU                      | Acc   | IoU                  | Acc   |
| Continuous Urban Fabric                    | 36.38           | 44.72 | 33.28                    | 39.83 | 36.02                | 44.87 |
| Discontinuous Urban Fabric                 | 74.01           | 87.85 | 71.22                    | 86.83 | 73                   | 87.06 |
| Industrial or Commercial Units             | 53.94           | 67.27 | 47.52                    | 60.65 | 52.11                | 65.89 |
| Road and Rail Networks and Associated Land | 42.94           | 57.27 | 33.73                    | 44.09 | 39.06                | 53.54 |
| Port Areas                                 | 33.28           | 46.01 | 25.28                    | 29.79 | 30.77                | 38.1  |
| Airports                                   | 56.54           | 74.48 | 44.64                    | 55.86 | 56.74                | 68.67 |
| Mineral Extraction Sites                   | 59.36           | 76.3  | 52.06                    | 69.84 | 57.53                | 75.17 |
| Dump Sites                                 | 25.4            | 32.51 | 8.65                     | 9.79  | 22.39                | 28.24 |
| Construction Sites                         | 8.52            | 9.7   | 2.42                     | 2.53  | 7.12                 | 7.84  |
| Green Urban Areas                          | 30.58           | 43.06 | 23.23                    | 29.66 | 27.62                | 37.05 |
| Sport and Leisure Facilities               | 39.7            | 48.86 | 29.98                    | 36.82 | 36.18                | 44.6  |
| Non-irrigated Arable Land                  | 83.67           | 91.7  | 80.99                    | 90.23 | 82.65                | 91.87 |
| Vineyards                                  | 75.34           | 88.8  | 66.46                    | 82.52 | 73.73                | 85.66 |
| Fruit Trees and Berry Plantations          | 42.95           | 53.5  | 33.82                    | 43.59 | 40.44                | 51    |
| Pastures                                   | 64.1            | 78.73 | 59.46                    | 75.49 | 61.89                | 76.15 |
| Broad-leaved Forest                        | 65.09           | 80.71 | 62                       | 79.62 | 63.72                | 80.45 |
| Coniferous Forest                          | 76.01           | 89.41 | 74.02                    | 88.6  | 75.16                | 88.92 |
| Mixed Forest                               | 28.56           | 36.48 | 24.2                     | 30.31 | 26.54                | 33.45 |
| Natural Grasslands                         | 34.23           | 42.65 | 28.07                    | 34.97 | 32.66                | 40.26 |
| Moors and Heathland                        | 59.66           | 78.55 | 54.33                    | 73.16 | 58.86                | 76.18 |
| Transitional Woodland / Shrub              | 25.39           | 31.29 | 20.46                    | 25.17 | 23.03                | 28.03 |
| Beaches, Dunes, Sands                      | 38.39           | 67.53 | 40.91                    | 53.36 | 43.94                | 59.31 |
| Bare Rock                                  | 0               | 0     | 29.26                    | 36.52 | 34.67                | 50.25 |
| Sparsely Vegetated Areas                   | 10.13           | 18.06 | 7.24                     | 8.71  | 7.45                 | 9.57  |
| Inland Marshes                             | 31.86           | 44.94 | 23.77                    | 31.19 | 28.2                 | 38.27 |
| Peat Bogs                                  | 56.68           | 72.8  | 50.81                    | 63.44 | 54.5                 | 69.69 |
| Salt Marshes                               | 70.42           | 86.18 | 60.76                    | 77.6  | 66.55                | 80.6  |
| Intertidal Flats                           | 76.26           | 86.21 | 77.72                    | 89.63 | 80.02                | 90.66 |
| Water Courses                              | 64.86           | 77.79 | 54.93                    | 68.02 | 60.61                | 72.87 |
| Water Bodies                               | 77.94           | 86.09 | 73.38                    | 83.31 | 78.25                | 87.76 |
| Coastal Lagoons                            | 79.77           | 90.37 | 80.55                    | 89.6  | 83.7                 | 92.3  |
| Estuaries                                  | 59.04           | 80.07 | 60.1                     | 69.98 | 65.3                 | 77.48 |
| Sea and Ocean                              | 95.16           | 97.5  | 95.54                    | 97.52 | 96.19                | 97.75 |

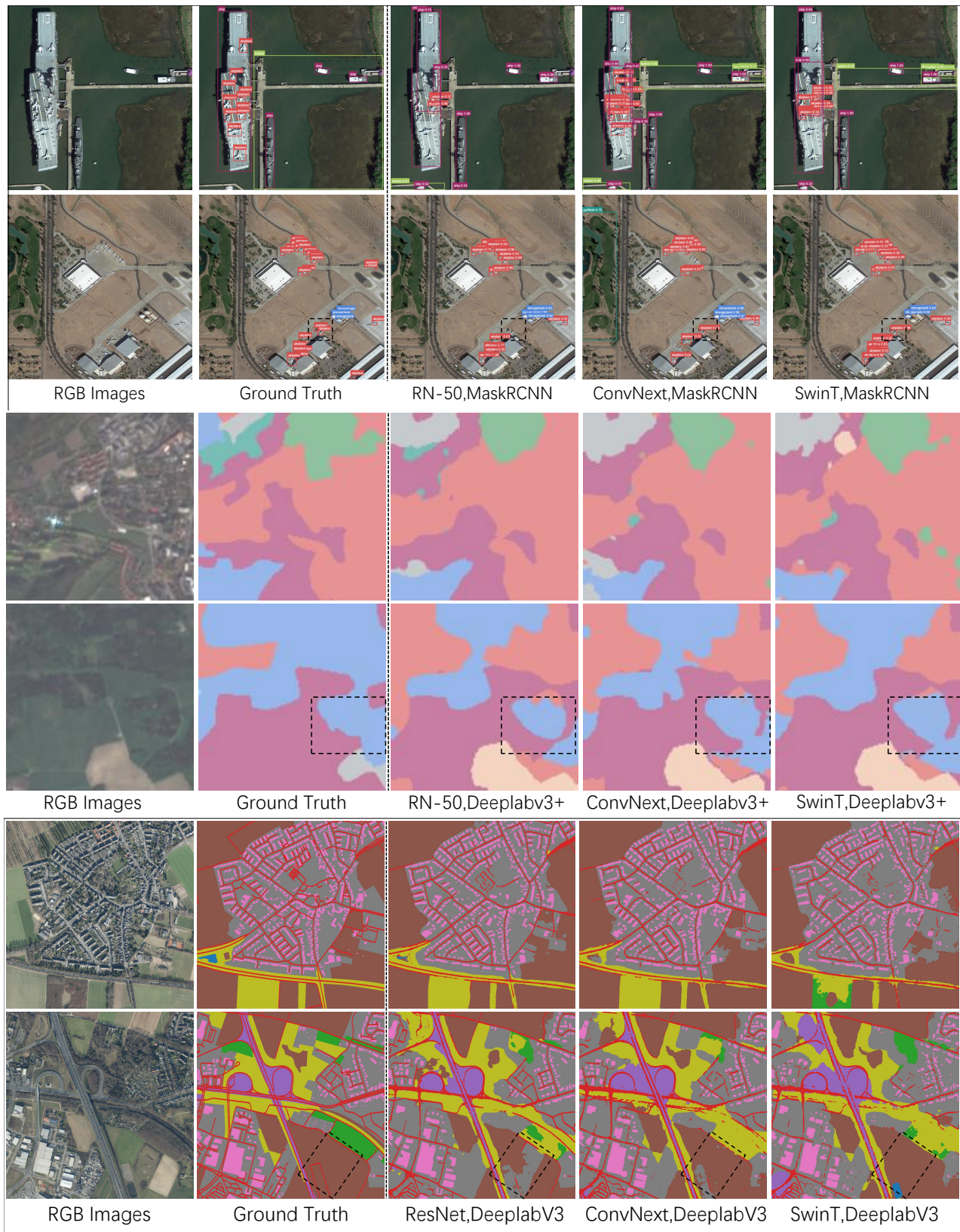


Fig. 9. Object detection and semantic segmentation results on three datasets. The first two rows present the object detection results on the DIOR dataset. The second two rows show the semantic segmentation results on the SEASONET dataset. The final two rows are the semantic segmentation results on the GeoNRW dataset.

TABLE XIV  
DETAILED COMPARISON RESULTS ON THE FMOW [134] DATASET

| Methods                       | RN50      |        |       | ConvNext-Tiny |        |       | Swin-Tiny |        |       |
|-------------------------------|-----------|--------|-------|---------------|--------|-------|-----------|--------|-------|
|                               | Precision | Recall |       | Precision     | Recall |       | Precision | Recall |       |
| Airport                       | 77.18     | 90.29  | 83.22 | 93.72         | 86.89  | 90.18 | 85.71     | 90.29  | 87.94 |
| Airport_hangar                | 58.25     | 57.82  | 58.03 | 66.50         | 58.55  | 62.27 | 67.71     | 66.81  | 67.26 |
| Airport_terminal              | 68.45     | 72.54  | 70.43 | 74.20         | 71.57  | 72.86 | 80.34     | 75.93  | 78.07 |
| Amusement_park                | 53.25     | 82.80  | 64.81 | 73.10         | 83.24  | 77.84 | 79.85     | 85.35  | 82.51 |
| Aquaculture                   | 76.71     | 81.28  | 78.93 | 80.08         | 85.53  | 82.72 | 82.92     | 84.68  | 83.79 |
| Archaeological_site           | 54.40     | 43.49  | 48.34 | 66.11         | 51.82  | 58.10 | 63.08     | 53.39  | 57.83 |
| Barn                          | 55.02     | 57.89  | 56.42 | 61.58         | 60.66  | 61.12 | 61.71     | 69.40  | 65.33 |
| Border_checkpoint             | 47.54     | 31.69  | 38.03 | 70.00         | 26.78  | 38.74 | 64.55     | 38.80  | 48.46 |
| Burial_site                   | 58.39     | 60.23  | 59.30 | 66.73         | 63.06  | 64.84 | 64.35     | 70.88  | 67.46 |
| Car_dealership                | 61.86     | 66.49  | 64.09 | 60.92         | 76.61  | 67.87 | 67.22     | 74.38  | 70.62 |
| Construction_site             | 27.70     | 16.78  | 20.90 | 32.13         | 15.47  | 20.88 | 29.34     | 22.44  | 25.43 |
| Crop_field                    | 80.07     | 89.51  | 84.53 | 79.63         | 92.35  | 85.52 | 86.96     | 91.98  | 89.40 |
| Dam                           | 75.58     | 74.31  | 74.94 | 81.38         | 75.54  | 78.35 | 79.02     | 83.49  | 81.19 |
| Debris_or_rubble              | 54.84     | 19.92  | 29.23 | 49.61         | 25.00  | 33.25 | 40.72     | 26.56  | 32.15 |
| Educational_institution       | 36.43     | 35.57  | 35.99 | 36.46         | 41.88  | 38.98 | 48.22     | 46.46  | 47.32 |
| Electric_substation           | 57.33     | 59.22  | 58.26 | 62.71         | 65.08  | 63.87 | 67.14     | 69.84  | 68.46 |
| Factory_or_powerplant         | 46.00     | 32.80  | 38.29 | 56.73         | 34.58  | 42.97 | 59.69     | 47.77  | 53.07 |
| Fire_station                  | 24.54     | 17.25  | 20.26 | 26.26         | 16.09  | 19.95 | 27.73     | 24.84  | 26.21 |
| Flooded_road                  | 56.28     | 40.12  | 46.85 | 57.64         | 40.74  | 47.74 | 69.83     | 50.00  | 58.27 |
| Fountain                      | 47.86     | 33.22  | 39.22 | 51.65         | 39.27  | 44.62 | 55.20     | 46.69  | 50.59 |
| Gas_station                   | 38.32     | 42.08  | 40.11 | 41.84         | 43.58  | 42.70 | 52.45     | 56.99  | 54.63 |
| Golf_course                   | 84.54     | 72.74  | 78.20 | 84.35         | 72.58  | 78.02 | 83.97     | 83.42  | 83.69 |
| Ground_transportation_station | 53.03     | 59.32  | 56.00 | 55.28         | 65.34  | 59.89 | 62.47     | 71.12  | 66.51 |
| Helipad                       | 45.77     | 37.36  | 41.14 | 65.27         | 31.87  | 42.83 | 56.98     | 46.15  | 51.00 |
| Hospital                      | 30.14     | 30.69  | 30.41 | 30.28         | 36.58  | 33.13 | 35.13     | 33.69  | 34.40 |
| Impoverished_settlement       | 69.20     | 83.17  | 75.55 | 77.46         | 90.87  | 83.63 | 84.07     | 91.35  | 87.56 |
| Interchange                   | 77.08     | 79.49  | 78.27 | 69.93         | 83.59  | 76.16 | 85.34     | 81.84  | 83.55 |
| Lake_or_pond                  | 30.14     | 16.67  | 21.46 | 43.56         | 33.33  | 37.77 | 45.28     | 36.36  | 40.34 |
| Lighthouse                    | 72.89     | 73.29  | 73.09 | 78.96         | 73.83  | 76.31 | 78.92     | 81.77  | 80.32 |
| Military_facility             | 57.71     | 51.35  | 54.35 | 58.67         | 60.65  | 59.65 | 61.80     | 59.62  | 60.69 |
| Multi-unit_residential        | 40.95     | 32.17  | 36.03 | 47.38         | 37.57  | 41.91 | 51.17     | 45.39  | 48.11 |
| Nuclear_powerplant            | 75.86     | 75.86  | 75.86 | 92.00         | 79.31  | 85.19 | 83.87     | 89.66  | 86.67 |
| Office_building               | 13.12     | 8.76   | 10.51 | 17.76         | 9.29   | 12.20 | 18.84     | 9.72   | 12.83 |
| Oil_or_gas_facility           | 73.04     | 76.55  | 74.75 | 79.38         | 83.07  | 81.18 | 77.78     | 81.52  | 79.61 |
| Park                          | 27.81     | 20.08  | 23.32 | 36.67         | 26.69  | 30.89 | 37.57     | 27.24  | 31.58 |
| Parking_lot_or_garage         | 28.77     | 35.33  | 31.71 | 35.28         | 41.92  | 38.31 | 46.46     | 47.19  | 46.82 |
| Place_of_worship              | 42.18     | 51.19  | 46.25 | 46.87         | 54.06  | 50.21 | 51.96     | 61.25  | 56.22 |
| Police_station                | 14.13     | 12.90  | 13.48 | 17.33         | 15.07  | 16.12 | 20.59     | 18.77  | 19.64 |
| Port                          | 73.44     | 79.72  | 76.45 | 73.53         | 88.97  | 80.52 | 78.66     | 87.90  | 83.03 |
| Prison                        | 65.23     | 46.52  | 54.31 | 61.42         | 54.32  | 57.65 | 71.61     | 53.76  | 61.42 |
| Race_track                    | 90.18     | 81.83  | 85.80 | 85.81         | 87.65  | 86.72 | 87.27     | 88.72  | 87.99 |
| Railway_bridge                | 58.35     | 50.15  | 53.94 | 59.11         | 57.56  | 58.33 | 64.69     | 63.89  | 64.29 |
| Recreational_facility         | 68.37     | 78.95  | 73.28 | 72.19         | 80.23  | 76.00 | 75.11     | 84.55  | 79.55 |
| Road_bridge                   | 54.50     | 69.25  | 61.00 | 62.75         | 63.15  | 62.95 | 72.13     | 74.33  | 73.22 |
| Runway                        | 74.15     | 86.05  | 79.66 | 86.35         | 86.58  | 86.47 | 90.49     | 92.63  | 91.55 |
| Shipyard                      | 56.86     | 52.73  | 54.72 | 64.71         | 40.00  | 49.44 | 66.28     | 51.82  | 58.16 |
| Shopping_mall                 | 50.89     | 49.30  | 50.08 | 53.69         | 57.28  | 55.43 | 62.32     | 60.30  | 61.29 |
| Single-unit_residential       | 58.07     | 64.63  | 61.17 | 57.34         | 73.22  | 64.31 | 65.39     | 69.23  | 67.25 |
| Smokestack                    | 56.40     | 43.56  | 49.16 | 53.53         | 60.08  | 56.62 | 58.82     | 64.63  | 61.59 |
| Solar_farm                    | 83.18     | 83.51  | 83.34 | 80.76         | 84.84  | 82.75 | 84.70     | 86.84  | 85.75 |
| Space_facility                | 89.13     | 93.18  | 91.11 | 88.64         | 88.64  | 88.64 | 87.76     | 97.73  | 92.47 |
| Stadium                       | 80.22     | 79.83  | 80.02 | 80.78         | 81.74  | 81.26 | 83.81     | 87.11  | 85.43 |
| Storage_tank                  | 75.00     | 79.95  | 77.40 | 77.59         | 79.95  | 78.75 | 80.77     | 85.28  | 82.96 |
| Surface_mine                  | 81.86     | 75.00  | 78.28 | 80.50         | 78.85  | 79.67 | 77.84     | 82.01  | 79.87 |
| Swimming_pool                 | 62.86     | 64.35  | 63.60 | 68.84         | 63.78  | 66.21 | 76.08     | 74.90  | 75.48 |
| Toll_booth                    | 84.85     | 88.33  | 86.56 | 87.37         | 94.87  | 90.96 | 89.46     | 95.77  | 92.51 |
| Tower                         | 47.76     | 32.20  | 38.47 | 64.29         | 36.54  | 46.60 | 55.32     | 43.72  | 48.84 |
| Tunnel_opening                | 82.05     | 82.05  | 82.05 | 83.20         | 86.75  | 84.94 | 86.95     | 89.00  | 87.96 |
| Waste_disposal                | 45.78     | 29.44  | 35.84 | 61.81         | 31.41  | 41.66 | 56.98     | 49.01  | 52.70 |
| Water_treatment_facility      | 68.49     | 69.04  | 68.77 | 73.69         | 75.77  | 74.72 | 74.12     | 79.41  | 76.67 |
| Wind_farm                     | 89.82     | 94.20  | 91.96 | 91.82         | 96.18  | 93.95 | 90.69     | 96.31  | 93.42 |
| Zoo                           | 51.40     | 37.86  | 43.60 | 61.18         | 42.80  | 50.36 | 59.26     | 46.09  | 51.85 |

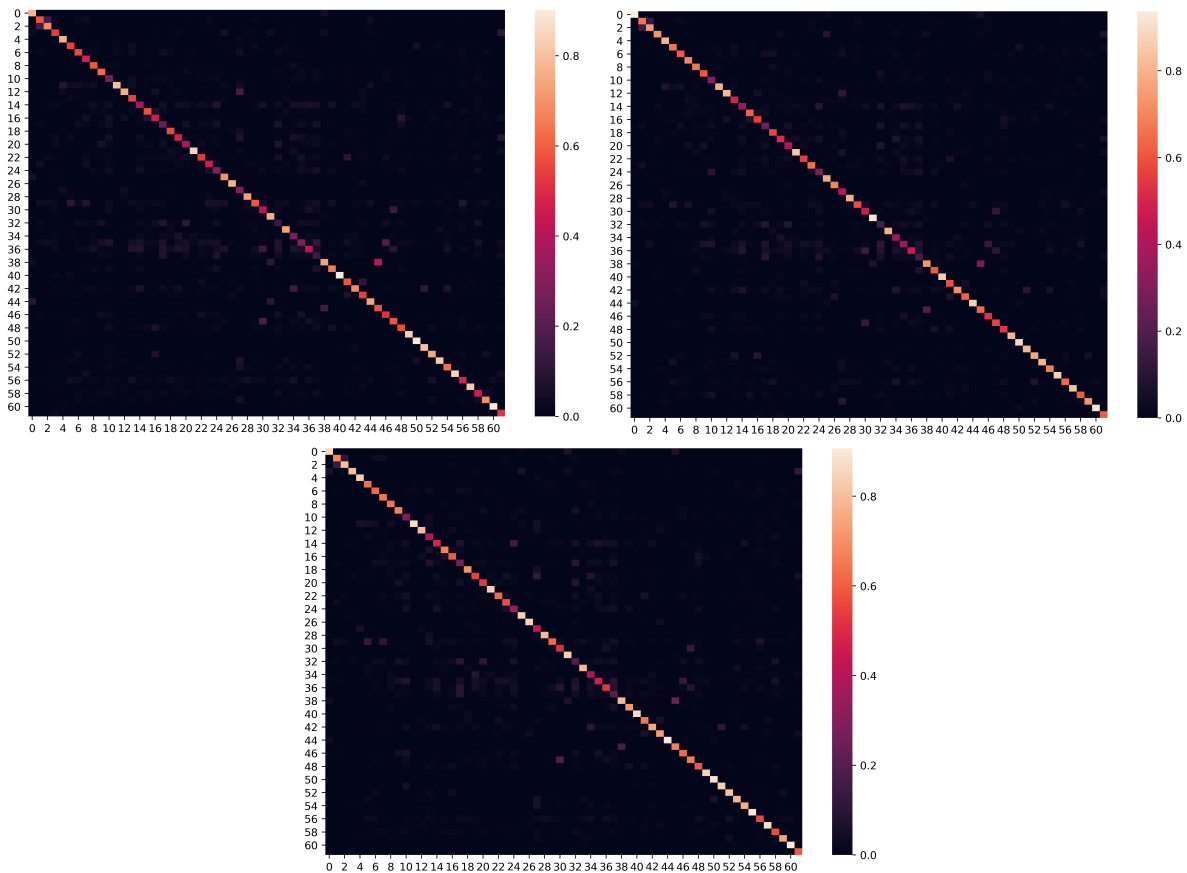


Fig. 10. Confusion matrices of different methods on the FMoW dataset [76]. From left to right are the confusion matrices for the ResNet-50, ConvNext, and Swin-Transformer models.

- [4] Marvin E Bauer. Remote sensing of environment: history, philosophy, approach and contributions, 1969–2019. *Remote Sens. Environ.*, 237:111522, 2020. 1
- [5] Marek Wójtowicz, Andrzej Wójtowicz, Jan Piekarczyk, et al. Application of remote sensing methods in agriculture. *Communications in Biometry and Crop Science*, 11(1):31–50, 2016. 1
- [6] L Karthikeyan, Ila Chawla, and Ashok K Mishra. A review of remote sensing applications in agriculture for food security: Crop growth and yield, irrigation, and crop losses. *Journal of Hydrology*, 586:124905, 2020. 1
- [7] Karen E Joyce, Kim C Wright, Sergey V Samsonov, and Vincent G Ambrosia. Remote sensing and the disaster management cycle. *Advances in geoscience and remote sensing*, 48:7, 2009. 1
- [8] CJ Van Westen. Remote sensing for natural disaster management. *ISPRS Archives*, 33(B7/4; PART 7):1609–1617, 2000. 1
- [9] Alex Krizhevsky, Ilya Sutskever, and Geoffrey E Hinton. Imagenet classification with deep convolutional neural networks. *Communications of the ACM*, 60(6):84–90, 2017. 1
- [10] Liangpei Zhang, Lefei Zhang, and Bo Du. Deep learning for remote sensing data: A technical tutorial on the state of the art. *IEEE GRSM*, 4(2):22–40, 2016. 1
- [11] Zhitong Xiong, Yuan Yuan, and Qi Wang. AI-NET: Attention inception neural networks for hyperspectral image classification. In *IGARSS*, pages 2647–2650. IEEE, 2018. 1
- [12] Giovanni Marchisio, Patrick Helber, Benjamin Bischke, Timothy Davis, Caglar Senaras, Daniele Zanaga, Ruben Van De Kerchove, and Annett Wania. Rapidai4eo: A corpus for higher spatial and temporal reasoning. In *2021 IEEE International Geoscience and Remote Sensing Symposium IGARSS*, pages 1161–1164. IEEE, 2021. 1, 8
- [13] Antje Hechelting, Frank Thonfeld, and Gunter Menz. Recent advances in remote sensing change detection—a review. *Land use and land cover mapping in Europe*, pages 145–178, 2014. 1
- [14] Maryam Rahneemoonfar, Tashnim Chowdhury, Argho Sarkar, Debvrat Varshney, Masoud Yari, and Robin Roberson Murphy. Floodnet: A high resolution aerial imagery dataset for post flood scene understanding. *IEEE Access*, 9:89644–89654, 2021. 1, 4
- [15] K Bakula, JP Mills, and F Remondino. A review of benchmarking in photogrammetry and remote sensing. *ISPRS Archives*, 2019. 1
- [16] Michael Schmitt, Seyed Ali Ahmadi, and Ronny Hänsch. There is no data like more data-current status of machine learning datasets in remote sensing. In *IGARSS*, pages 1206–1209. IEEE, 2021. 1
- [17] Michael Schmitt, Seyed Ali Ahmadi, Yonghao Xu, Gülşen Taşkın, Ujjwal Verma, Francesco Paolo Sica, and Ronny Hänsch. There are no data like more data: Datasets for deep learning in earth observation. *IEEE Geoscience and Remote Sensing Magazine*, 2023. 1
- [18] Yang Long, Gui-Song Xia, Shengyang Li, Wen Yang, Michael Ying Yang, Xiao Xiang Zhu, Liangpei Zhang, and Deren Li. On creating benchmark dataset for aerial image interpretation: Reviews, guidances, and million-aid. *IEEE J. Sel. Top. Appl. Earth Obs. Remote Sens.*, 14:4205–4230, 2021. 1, 2, 4, 11, 12
- [19] Ke Li, Gang Wan, Gong Cheng, Liqiu Meng, and Junwei Han. Object detection in optical remote sensing images: A survey and a new benchmark. *ISPRS J. Photogramm. Remote Sens.*, 159:296–307, 2020. 1, 6, 12, 14
- [20] Abolfazl Abdollahi, Biswajeet Pradhan, Nagesh Shukla, Subrata Chakraborty, and Abdullah Alamri. Deep learning approaches applied to remote sensing datasets for road extraction: A state-of-the-art review. *Remote Sensing*, 12(9):1444, 2020. 1, 5
- [21] Ivan Tomljenovic, Bernhard Höfle, Dirk Tiede, and Thomas Blaschke. Building extraction from airborne laser scanning data: An analysis of the state of the art. *Remote Sensing*, 7(4):3826–3862, 2015. 1
- [22] Michael Schmitt, Pedram Ghamisi, Naoto Yokoya, and Ronny Hänsch. Eod: The ieee grss earth observation database. In *IGARSS*, pages 5365–5368. IEEE, 2022. 1
- [23] Jia Deng, Wei Dong, Richard Socher, Li-Jia Li, Kai Li, and Li Fei-Fei. Imagenet: A large-scale hierarchical image database. In *CVPR*, pages 248–255. Ieee, 2009. 2, 16
- [24] Xiao Xiang Zhu, Jingliang Hu, Chunping Qiu, Yilei Shi, Jian Kang,

- Lichao Mou, Hossein Bagheri, Matthias Häberle, Yuansheng Hua, Rong Huang, et al. So2sat lcz42: A benchmark dataset for global local climate zones classification. *arXiv preprint arXiv:1912.12171*, 2019. 2, 3, 4, 12
- [25] Gordon Christie, Neil Fendley, James Wilson, and Ryan Mukherjee. Functional map of the world. In *CVPR*, pages 6172–6180, 2018. 2, 4
- [26] Dominik Kofmann, Viktor Brack, and Thorsten Wilhelm. Seasonet: A seasonal scene classification, segmentation and retrieval dataset for satellite imagery over germany. In *IGARSS*, pages 243–246. IEEE, 2022. 2, 5, 7, 12, 14, 18
- [27] Johannes Jakubik, Sujit Roy, CE Phillips, Paolo Fraccaro, Denys Godwin, Bianca Zadrozny, Daniela Szwarzman, Carlos Gomes, Gabby Nyirjesy, Blair Edwards, et al. Foundation models for generalist geospatial artificial intelligence. *arXiv preprint arXiv:2310.18660*, 2023. 2, 8, 9
- [28] Adam J Stewart, Caleb Robinson, Isaac A Corley, Anthony Ortiz, Juan M Lavista Ferres, and Arindam Banerjee. Torchgeo: deep learning with geospatial data. *arXiv preprint arXiv:2111.08872*, 2021. 2, 13
- [29] Otávio AB Penatti, Keiller Nogueira, and Jefersson A Dos Santos. Do deep features generalize from everyday objects to remote sensing and aerial scenes domains? In *CVPRW*, pages 44–51, 2015. 3, 4
- [30] Marion F Baumgardner, Larry L Biehl, and David A Landgrebe. 220 band aviris hyperspectral image data set: June 12, 1992 indian pine test site 3. *Purdue University Research Repository*, 10(7):991, 2015. 4
- [31] B. A. M Gra and Veganzons MA. Hyperspectral datasets, 2022. 3, 4
- [32] Rose M Rustowicz, Robin Cheong, Lijing Wang, Stefano Ermon, Marshall Burke, and David Lobell. Semantic segmentation of crop type in africa: A novel dataset and analysis of deep learning methods. In *CVPRW*, pages 75–82, 2019. 4
- [33] Hannah Kerner, Catherine Nakalembe, and Inbal Becker-Reshef. Field-level crop type classification with k nearest neighbors: a baseline for a new kenya smallholder dataset. *arXiv preprint arXiv:2004.03023*, 2020. 4
- [34] Marc Rußwurm, Charlotte Pelletier, Maximilian Zollner, Sébastien Lefèvre, and Marco Körner. Breizhcrops: A time series dataset for crop type mapping. *ISPRS (2020)*, 2020. 4
- [35] Shyamal Virnoddar, Vinod Pachghare, V. Patil, and Sunil Kumar Jha. Canesat, 2020. 4
- [36] Gabriel Tseng, Ivan Zvonkov, Catherine Lilian Nakalembe, and Hannah Kerner. CropHarvest: A global dataset for crop-type classification. In *NeurIPS Datasets and Benchmarks Track*, 2021. 4
- [37] Radiant Earth Foundation Western Cape Department of Agriculture. Crop type classification dataset for western cape, south africa, 2021. 4
- [38] Lukas Kondmann, Aysim Tokar, Marc Rußwurm, Andres Camero Unzueta, Devis Peressuti, Grega Milcinski, Nicolas Longépé, Pierre-Philippe Mathieu, Timothy Davis, Giovanni Marchisio, et al. DENETHOR: The DynamicEarthNET dataset for Harmonized, inter-Operable, analysis-Ready, daily crop monitoring from space. In *NeurIPS Datasets and Benchmarks Track*, 2021. 3, 4
- [39] Étienne Lord Amanda A. Boatswain Jacques, Abdoulaye Baniré Diallo. Towards the creation of a canadian land-use dataset for agricultural land classification. In *Canadian Symposium on Remote Sensing*, 2021. 3, 4
- [40] George Choumos, Alkiviadis Koukos, Vasileios Sitokonstantinou, and Charalampos Kontoes. Towards space-to-ground data availability for agriculture monitoring. In *IVMSP*, pages 1–5, 2022. 4
- [41] Dimitris Sykas, Ioannis Papoutsis, and Dimitrios Zografakis. Sen4grinet: A harmonized multi-country, multi-temporal benchmark dataset for agricultural earth observation machine learning applications. In *IGARSS*, pages 5830–5833. IEEE, 2021. 3, 4, 9
- [42] Xian Sun, Yixuan Lv, Zhirui Wang, and Kun Fu. Scan: Scattering characteristics analysis network for few-shot aircraft classification in high-resolution sar images. *IEEE TGRS*, 60:1–17, 2022. 3, 4, 5
- [43] YU Wenqi, CHENG Gong, WANG Meijun, YAO Yanqing, XIE Xingxing, YAO Xiwen, and HAN Junwei. Mar20: A benchmark for military aircraft recognition in remote sensing images. *National Remote Sensing Bulletin*, 27(12):2688–2696, 2024. 4, 6
- [44] M Joseph Hughes and Daniel J Hayes. Automated detection of cloud and cloud shadow in single-date landsat imagery using neural networks and spatial post-processing. *Remote Sensing*, 6(6):4907–4926, 2014. 4
- [45] Max Planck Institute for Meteorology. Understanding clouds from satellite images, 2019. 4
- [46] A. H. Nielsen, A. Iosifidis, and H. Karstoft. Cloudcast: A satellite-based dataset and baseline for forecasting clouds. *IEEE J. Sel. Top. Appl. Earth Obs. Remote Sens.*, 14:3485–3494, 2021. 4
- [47] Sentinel-2 cloud mask catalogue, 2020. 4
- [48] L. Mou, Y. Hua, P. Jin, and X. X. Zhu. ERA: A dataset and deep learning benchmark for event recognition in aerial videos. *IEEE GRSM*, in press. 4
- [49] Quoc Dung Cao and Youngjun Choe. Building damage annotation on post-hurricane satellite imagery based on convolutional neural networks. *Natural Hazards*, 103(3):3357–3376, 2020. 3, 4
- [50] Clément Rambour, Nicolas Audebert, E Koeniguer, Bertrand Le Saux, M Crucianu, and Mihai Datcu. Flood detection in time series of optical and sar images. *ISPRS Archives*, 43:1343–1346, 2020. 3, 4
- [51] Derrick Bonafilia, Beth Tellman, Tyler Anderson, and Erica Issenberg. Sen1floods11: A georeferenced dataset to train and test deep learning flood algorithms for sentinel-1. In *CVPRW*, pages 210–211, 2020. 3, 4
- [52] Georgios I Drakonakis, Grigorios Tsagkatakis, Konstantina Fotiadou, and Panagiotis Tsakalides. Ombrianet—supervised flood mapping via convolutional neural networks using multitemporal sentinel-1 and sentinel-2 data fusion. *IEEE J. Sel. Top. Appl. Earth Obs. Remote Sens.*, 15:2341–2356, 2022. 4
- [53] Shubham Chandak, Vamsi Chitters, and Sagar Honnunar. Understanding the amazon rainforest from space using cnns. 2017. 4
- [54] David Noever and Samantha E Miller Noever. Overhead mnist: A benchmark satellite dataset. *arXiv preprint arXiv:2102.04266*, 2021. 4
- [55] Yi Yang and Shawn Newsam. Bag-of-visual-words and spatial extensions for land-use classification. In *ACM SIGSPATIAL*, pages 270–279, 2010. 4
- [56] Gui-Song Xia, Wen Yang, Julie Delon, Yann Gousseau, Hong Sun, and Henri Maître. Structural high-resolution satellite image indexing. Vienna, Austria, 2010. 4
- [57] Qin Zou, Lihao Ni, Tong Zhang, and Qian Wang. Deep learning based feature selection for remote sensing scene classification. *IEEE Geosci. Remote Sens. Lett.*, 12(11):2321–2325, 2015. 4
- [58] Gong Cheng, Junwei Han, and Xiaoqiang Lu. Remote sensing image scene classification: Benchmark and state of the art. *Proceedings of the IEEE*, 105(10):1865–1883, 2017. 3, 4
- [59] Lijun Zhao, Ping Tang, and Lianzhi Huo. Feature significance-based multibag-of-visual-words model for remote sensing image scene classification. *Journal of Applied Remote Sensing*, 10(3):035004, 2016. 4
- [60] Gui-Song Xia, Jingwen Hu, Fan Hu, Baoguang Shi, Xiang Bai, Yanfei Zhong, Liangpei Zhang, and Xiaoqiang Lu. Aid: A benchmark data set for performance evaluation of aerial scene classification. *IEEE TGRS*, 55(7):3965–3981, 2017. 4
- [61] Zhifeng Xiao, Yang Long, Deren Li, Chunshan Wei, Gefu Tang, and Junyi Liu. High-resolution remote sensing image retrieval based on cnns from a dimensional perspective. *Remote Sensing*, 9(7):725, 2017. 3, 4, 12
- [62] Weixun Zhou, Shawn Newsam, Congmin Li, and Zhenfeng Shao. Patternnet: A benchmark dataset for performance evaluation of remote sensing image retrieval. *ISPRS J. Photogramm. Remote Sens.*, 145:197–209, 2018. 4
- [63] Qi Wang, Shaoteng Liu, Jocelyn Chanussot, and Xuelong Li. Scene classification with recurrent attention of vhr remote sensing images. *IEEE TGRS*, 57(2):1155–1167, 2018. 4
- [64] Xiaoman Qi, Panpan Zhu, Yuebin Wang, Liqiang Zhang, Junhuan Peng, Mengfan Wu, Jialong Chen, Xudong Zhao, Ning Zang, and P Takis Mathiopoulos. Mlrsnet: A multi-label high spatial resolution remote sensing dataset for semantic scene understanding. *ISPRS J. Photogramm. Remote Sens.*, 169:337–350, 2020. 3, 4
- [65] Haifeng Li, Hao Jiang, Xin Gu, Jian Peng, Wenbo Li, Liang Hong, and Chao Tao. Clrs: Continual learning benchmark for remote sensing image scene classification. *Sensors*, 20(4):1226, 2020. 4
- [66] Zhuang Zhou, Shengyang Li, Wei Wu, Weilong Guo, Xuan Li, Guisong Xia, and Zifei Zhao. Nasc-tg2: Natural scene classification with tiangong-2 remotely sensed imagery. *IEEE J. Sel. Top. Appl. Earth Obs. Remote Sens.*, 14:3228–3242, 2021. 4
- [67] Mahmoud Reda. Satellite image classification, 2021. 4
- [68] Yuansheng Hua, Lichao Mou, Pu Jin, and Xiao Xiang Zhu. Multiscene: A large-scale dataset and benchmark for multiscene recognition in single aerial images. *IEEE TGRS*, 60:1–13, 2021. 4
- [69] Nikolaos Ioannis Bountos, Ioannis Papoutsis, Dimitrios Michail, Andreas Karavias, Panagiotis Elias, and Isaak Parcharidis. Hephaestus: A large scale multitask dataset towards insar understanding. In *CVPR*, pages 1453–1462, 2022. 4
- [70] Kazuki Uehara, Hidenori Sakanashi, Hirokazu Nosato, Masahiro Murakawa, Hiroki Miyamoto, and Ryosuke Nakamura. Object detection of

- satellite images using multi-channel higher-order local autocorrelation. In *IEEE SMC*, pages 1339–1344. IEEE, 2017. 4
- [71] Statoil. Statoil/c-core iceberg classifier challenge, 2017. 4
- [72] Saikat Basu, Sangram Ganguly, Supratik Mukhopadhyay, Robert DiBiano, Manohar Karki, and Ramakrishna Nemani. DeepSAT: a learning framework for satellite imagery. In *ACM SIGSPATIAL*, pages 1–10, 2015. 4
- [73] Tiselac: Time series land cover classification challenge, 2017. 4
- [74] Xin-Yi Tong, Gui-Song Xia, Qikai Lu, Huanfeng Shen, Shengyang Li, Shucheng You, and Liangpei Zhang. Land-cover classification with high-resolution remote sensing images using transferable deep models. *Remote Sens. Environ.*, 237:111322, 2020. 4
- [75] Reza Bahmanyar, Daniela Espinoza-Molina, and Mihai Datcu. Multisensor earth observation image classification based on a multimodal latent dirichlet allocation model. *IEEE Geosci. Remote Sens. Lett.*, 15(3):459–463, 2018. 3, 4
- [76] Gencer Sumbul, Marcela Charfuelan, Begum Demir, and Volker Markl. Bigearthnet: A large-scale benchmark archive for remote sensing image understanding. In *IGARSS*, pages 5901–5904. IEEE, 2019. 3, 4, 12, 13, 21
- [77] Eopatches for slovenia 2019, 2019. 4
- [78] Tianggong1 high-resolution satellite scene classification, 2016. 4
- [79] Yanfei Zhong, Qiqi Zhu, and Liangpei Zhang. Scene classification based on the multifeature fusion probabilistic topic model for high spatial resolution remote sensing imagery. *IEEE TGRS*, 53(11):6207–6222, 2015. 3, 4
- [80] Haifeng Li, Xin Dou, Chao Tao, Zhixiang Wu, Jie Chen, Jian Peng, Min Deng, and Ling Zhao. Rsi-cb: A large-scale remote sensing image classification benchmark using crowdsourced data. *Sensors*, 20(6):1594, 2020. 3, 4
- [81] Austin zoning satellite images, 2017. 4
- [82] Rémi Ratajczak, Carlos F Crispim-Junior, Élodie Faure, Béatrice Fervers, and Laure Tougne. Automatic Land Cover Reconstruction From Historical Aerial Images: An Evaluation of Features Extraction and Classification Algorithms. *IEEE Trans. Image Process.*, January 2019. 4
- [83] Gabriel Machado, Edemir Ferreira, Keiller Nogueira, Hugo Oliveira, Matheus Brito, Pedro Henrique Targino Gama, and Jefersson Alex dos Santos. Airound and cv-brct: Novel multiview datasets for scene classification. *IEEE J. Sel. Top. Appl. Earth Obs. Remote Sens.*, 14:488–503, 2020. 3, 4
- [84] Patrick Helber, Benjamin Bischke, Andreas Dengel, and Damian Borth. EuroSAT: A novel dataset and deep learning benchmark for land use and land cover classification. *IEEE J. Sel. Top. Appl. Earth Obs. Remote Sens.*, 12(7):2217–2226, 2019. 3, 4
- [85] Sense earth satellite scene classification, 2020. 4
- [86] Shunping Ji, Dawen Yu, Chaoyong Shen, Weile Li, and Qiang Xu. Landslide detection from an open satellite imagery and digital elevation model dataset using attention boosted convolutional neural networks. *Landslides*, 17(6):1337–1352, 2020. 4
- [87] Uma S Ranjan and Akash Narayana. Classification of objects in sar images using scaling features. In *ICVGIP*, 2002. 4
- [88] Nikolaos Ioannis Bountos, Arthur Ouaknine, and David Rolnick. Fomo-bench: a multi-modal, multi-scale and multi-task forest monitoring benchmark for remote sensing foundation models, 2024. 4, 8, 9
- [89] Wids datathon 2019, 2019. 4
- [90] Sara Beery, Guanhang Wu, Trevor Edwards, Filip Pavetic, Bo Majewski, Shreyasee Mukherjee, Stanley Chan, John Morgan, Vivek Rathod, and Jonathan Huang. The auto arborist dataset: A large-scale benchmark for multiview urban forest monitoring under domain shift. In *CVPR*, pages 21294–21307, 2022. 4
- [91] Steve Ahlswede, Christian Schulz, Christiano Gava, Patrick Helber, Benjamin Bischke, Michael Förster, Florencia Arias, Jörn Hees, Begüm Demir, and Birgit Kleinschmit. Treesatai benchmark archive: A multi-sensor, multi-label dataset for tree species classification in remote sensing. *Earth System Science Data Discussions*, pages 1–22, 2022. 4
- [92] Swedish Forest Agency. Forest damages – larch casebearer 1.0. national forest data lab. dataset., 2021. 4
- [93] NOAA fisheries steller sea lion population count, 2017. 3, 4, 6
- [94] Ships in satellite imagery, 2018. 3, 4
- [95] Gallego Antonio-Javier, Pertusa Antonio, and Gil Pablo. Automatic ship classification from optical aerial images with convolutional neural networks. *Remote Sensing*, 10(4), 2018. 3, 4
- [96] Yanghua Di, Zhiguo Jiang, Haopeng Zhang, and Gang Meng. A public dataset for ship classification in remote sensing images. In *SPIE*, volume 11155, pages 515–521, 2019. 3, 4
- [97] Igor G Rizaev and Alin Achim. Synthwakesar: A synthetic sar dataset for deep learning classification of ships at sea. *Remote Sensing*, 14(16):3999, 2022. 3, 4
- [98] Rui Ba, Chen Chen, Jing Yuan, Weiguo Song, and Siuming Lo. Smokenet: Satellite smoke scene detection using convolutional neural network with spatial and channel-wise attention. *Remote Sensing*, 11(14):1702, 2019. 3, 4
- [99] Nevrez Imamoglu, Motoki Kimura, Hiroki Miyamoto, Aito Fujita, and Ryosuke Nakamura. Solar power plant detection on multi-spectral satellite imagery using weakly-supervised cnn with feedback features and m-pcnn fusion. *arXiv preprint arXiv:1704.06410*, 2017. 3, 4
- [100] Elijah Cole, Benjamin Deneu, Titouan Lorieul, Maximilien Servajean, Christophe Botella, Dan Morris, Nebojsa Jojic, Pierre Bonnet, and Alexis Joly. The geolifeclef 2020 dataset. *arXiv preprint arXiv:2004.04192*, 2020. 4
- [101] Edemir Ferreira, Matheus Brito, Remis Balaniuk, Mário S Alvim, and Jefersson A dos Santos. Brazildam: A benchmark dataset for tailings dam detection. In *LAGIRS*, pages 339–344. IEEE, 2020. 4
- [102] Boan Chen, Quanlong Feng, Bowen Niu, Fengqin Yan, Bingbo Gao, Jianyu Yang, Jianhua Gong, and Jiantao Liu. Multi-modal fusion of satellite and street-view images for urban village classification based on a dual-branch deep neural network. *Int. J. Appl. Earth Obs. Geoinf.*, 109:102794, 2022. 4
- [103] Kennedy space center, 2022. 4
- [104] Keiller Nogueira, Jefersson A Dos Santos, Tamires Fornazari, Thiago Sanna Freire Silva, Leonor Patricia Morellato, and Ricardo da S Torres. Towards vegetation species discrimination by using data-driven descriptors. In *PRRS*, pages 1–6. Ieee, 2016. 4
- [105] Burak Uz Kent, Aneesh Rangnekar, and Matthew J Hoffman. Tracking in aerial hyperspectral videos using deep kernelized correlation filters. *arXiv preprint arXiv:1711.07235*, 2017. 4
- [106] Find a car park, 2019. 4
- [107] Eran Dahan, Tzvi Diskin, Amit Amram, Amit Moryossef, and Omer Koren. Cofga: A dataset for fine grained classification of objects from aerial imagery. *arXiv preprint arXiv:2105.12786*, 2021. 4
- [108] Airbus wind turbines patches, 2018. 3, 4, 9
- [109] District of columbia – classified point cloud lidar, 2015. 3, 17
- [110] ISPRS-Contest. Isprs 2d semantic labeling contest,” accessed on oct. 9, 2022., 2022. 3, 5, 7
- [111] ISPRS-Contest. Isprs 2d semantic labeling contest,” accessed on oct. 9, 2022., 2022. 3, 5, 7
- [112] Shaoqing Ren, Kaiming He, Ross Girshick, and Jian Sun. Faster r-cnn: Towards real-time object detection with region proposal networks. *NeurIPS*, 28, 2015. 5, 14
- [113] Wei Liu, Dragomir Anguelov, Dumitru Erhan, Christian Szegedy, Scott Reed, Cheng-Yang Fu, and Alexander C Berg. SSD: Single shot multibox detector. In *ECCV*, pages 21–37. Springer, 2016. 5
- [114] Joseph Redmon, Santosh Divvala, Ross Girshick, and Ali Farhadi. You only look once: Unified, real-time object detection. In *CVPR*, pages 779–788, 2016. 5, 14, 16
- [115] Nicolas Carion, Francisco Massa, Gabriel Synnaeve, Nicolas Usunier, Alexander Kirillov, and Sergey Zagoruyko. End-to-end object detection with transformers. In *ECCV*, pages 213–229. Springer, 2020. 5
- [116] Shubhankar Rawat. Casia-aircraft, 2021. 5, 6
- [117] Ilke Demir, Krzysztof Koperski, David Lindenbaum, Guan Pang, Jing Huang, Saikat Basu, Forest Hughes, Devis Tuia, and Ramesh Raskar. Deepglobe 2018: A challenge to parse the earth through satellite images. In *CVPRW*, June 2018. 5, 6
- [118] Microsoft. US building footprints, 2019. 5, 6
- [119] Segmenting buildings in satellite images, 2018. 5, 7
- [120] Nicholas Weir, David Lindenbaum, Alexei Bastidas, Adam Van Etten, Sean McPherson, Jacob Shermeyer, Varun Kumar, and Hanlin Tang. Spacenet mvoi: A multi-view overhead imagery dataset. In *ICCV*, pages 992–1001, 2019. 5, 6
- [121] Lanqing Huang, Bin Liu, Boying Li, Weiwei Guo, Wenhao Yu, Zenghui Zhang, and Wenxian Yu. Opensarship: A dataset dedicated to sentinel-1 ship interpretation. *IEEE J. Sel. Top. Appl. Earth Obs. Remote Sens.*, 11(1):195–208, 2017. 5, 6
- [122] Jianwei Li, Changwen Qu, and Jiaqi Shao. Ship detection in sar images based on an improved faster r-cnn. In *BIGSDATA*, pages 1–6. IEEE, 2017. 5, 6
- [123] Airbus. Airbus ship detection challenge, 2018. 5, 6
- [124] pineda moreno adrian and Ardian Umam. Ships in google earth, 2018. 5, 6
- [125] Jeremy Heitz and Daphne Koller. Learning spatial context: Using stuff to find things. In *ECCV*, pages 30–43. Springer, 2008. 5, 6

- [126] Sebastien Razakarivony and Frederic Jurie. Vehicle detection in aerial imagery: A small target detection benchmark. *Journal of Visual Communication and Image Representation*, 34:187–203, 2016. 5, 6
- [127] T Nathan Mundhenk, Goran Konjevod, Wesam A Sakla, and Kofi Boakye. A large contextual dataset for classification, detection and counting of cars with deep learning. In *ECCV*, pages 785–800. Springer, 2016. 5, 6
- [128] DLR. Dir multi-class vehicle detection and orientation in aerial imagery, 2016. 5, 6
- [129] Michael Ying Yang, Wentong Liao, Xinbo Li, and Bodo Rosenhahn. Deep learning for vehicle detection in aerial images. In *ICIP*, 2018. 5, 6
- [130] Gong Cheng and Junwei Han. A survey on object detection in optical remote sensing images. *ISPRS J. Photogramm. Remote Sens.*, 117:11–28, 2016. 5, 6
- [131] Yang Long, Yiping Gong, Zhifeng Xiao, and Qing Liu. Accurate object localization in remote sensing images based on convolutional neural networks. *IEEE TGRS*, 55(5):2486–2498, 2017. 5, 6
- [132] Yuanlin Zhang, Yuan Yuan, Yachuang Feng, and Xiaoqiang Lu. Hierarchical and robust convolutional neural network for very high-resolution remote sensing object detection. *IEEE TGRS*, 57(8):5535–5548, 2019. 5, 6, 12
- [133] xView. xview 2018 object detection challenge, 2019. 5, 6, 12
- [134] Gordon Christie, Neil Fendley, James Wilson, and Ryan Mukherjee. Functional map of the world. In *CVPR*, 2018. 5, 6, 9, 12, 13, 20
- [135] Gui-Song Xia, Xiang Bai, Jian Ding, Zhen Zhu, Serge Belongie, Jiebo Luo, Mihai Datcu, Marcello Pelillo, and Liangpei Zhang. DOTA: A large-scale dataset for object detection in aerial images. In *CVPR*, June 2018. 5, 6
- [136] Han Wei, Li Jun, Wang Sheng, Wang Yi, Yan Jining, Fan Runyu, Zhang Xiaohan, and Wang Lizhe. A context-scale-aware detector and a new benchmark for remote sensing small weak object detection in unmanned aerial vehicle images. *Int. J. Appl. Earth Obs. Geoinformation*, 112:102966, 2022. 5, 6
- [137] Dstl satellite imagery feature detection, 2017. 5, 6
- [138] Airbus. Airbus oil storage detection, 2021. 5, 6
- [139] Tianwen Zhang. Large-scale sar ship detection dataset-v1.0, 2020. 5, 6
- [140] Shunjun Wei, Xiangfeng Zeng, Qizhe Qu, Mou Wang, Hao Su, and Jun Shi. Hrsid: A high-resolution sar images dataset for ship detection and instance segmentation. *Ieee Access*, 8:120234–120254, 2020. 5, 6
- [141] Jinwang Wang, Wen Yang, Haowen Guo, Ruixiang Zhang, and Gui-Song Xia. Tiny object detection in aerial images. pages 3791–3798, 2021. 5, 6
- [142] Gong Cheng, Xiang Yuan, Xiwen Yao, Kebin Yan, Qinghua Zeng, and Junwei Han. Towards large-scale small object detection: Survey and benchmarks. *arXiv preprint arXiv:2207.14096*, 2022. 5, 6
- [143] Hydice image of washington dc mall, 2022. 5
- [144] Ronald Kemker, Carl Salvaggio, and Christopher Kanan. Algorithms for semantic segmentation of multispectral remote sensing imagery using deep learning. *ISPRS J. Photogramm. Remote Sens.*, 2018. 5, 7
- [145] Adrian Boguszewski, Dominik Batorski, Natalia Ziemba-Jankowska, Tomasz Dzedzic, and Anna Zambrzycka. Landcover. ai: Dataset for automatic mapping of buildings, woodlands, water and roads from aerial imagery. In *CVPR*, pages 1102–1110, 2021. 5, 7
- [146] Michael Schmitt, Lloyd Haydn Hughes, Chunping Qiu, and Xiao Xiang Zhu. Sen12ms—a curated dataset of georeferenced multi-spectral sentinel-1/2 imagery for deep learning and data fusion. *arXiv preprint arXiv:1906.07789*, 2019. 5, 7, 12
- [147] Semantic segmentation of aerial imagery, 2019. 5, 7
- [148] Zhirui Wang, Xuan Zeng, Zhiyuan Yan, Jian Kang, and Xian Sun. Airpolsar-seg: A large-scale data set for terrain segmentation in complex-scene polsar images. *IEEE J. Sel. Top. Appl. Earth Obs. Remote Sens.*, 15:3830–3841, 2022. 5, 6, 7
- [149] Vivien Sainte Fare Garnot and Loic Landrieu. Panoptic segmentation of satellite image time series with convolutional temporal attention networks. *ICCV*, 2021. 5, 6
- [150] Zhize Wu. Multi-type aircraft of remote sensing images: Mtarsi, 2019. 6
- [151] Rareplanes, 2020. 6
- [152] Shubhankar Rawat. Cgi planes in satellite imagery w/ bboxes, 2021. 6
- [153] Berkay Alan Jeff Faudi. Airbus aircraft detection, 2021. 6
- [154] Peng Zhang, Hao Xu, Tian Tian, Peng Gao, Linfeng Li, Tianming Zhao, Nan Zhang, and Jinwen Tian. Sefepnet: Scale expansion and feature enhancement pyramid network for sar aircraft detection with small sample dataset. *IEEE J. Sel. Top. Appl. Earth Obs. Remote Sens.*, 15:3365–3375, 2022. 6
- [155] Keiller Nogueira, Caio da Silva, Pedro Gama, Gabriel Machado, and Jefferson Alex Dos Santos. A tool for bridge detection in major infrastructure works using satellite images. *WVC*, 2019. 6
- [156] Shunping Ji, Shiqing Wei, and Meng Lu. Fully convolutional networks for multisource building extraction from an open aerial and satellite imagery data set. *IEEE TGRS*, 57(1):574–586, 2018. 6, 8
- [157] Sharada Prasanna Mohanty, Jakub Czakon, Kamil A Kaczmarek, Andrzej Pyskir, Piotr Tarasiewicz, Saket Kunwar, Janick Rohrbach, Dave Luo, Manjunath Prasad, Sascha Fleer, et al. Deep learning for understanding satellite imagery: An experimental survey. *Frontiers in Artificial Intelligence*, 3, 2020. 5, 6
- [158] 2018 open ai tanzania building footprint segmentation challenge, 2018. 5, 6
- [159] Microsoft. Australia building footprints, 2019. 5, 6
- [160] Microsoft. Uganda tanzania building footprints public, 2019. 5, 6
- [161] Microsoft. Canadian building footprints, 2019. 5, 6
- [162] AICyberTeam. Urban building classification dataset, 2022. 5, 6
- [163] Jinwang Wang, Lingxuan Meng, Weijia Li, Wen Yang, Lei Yu, and Gui-Song Xia. Learning to extract building footprints from off-nadir aerial images. *IEEE Trans. Pattern Anal. Mach. Intell.*, pages 1–1, 2022. 6
- [164] Xiaoyu Zhu, Junwei Liang, and Alexander Hauptmann. Msnet: A multilevel instance segmentation network for natural disaster damage assessment in aerial videos. In *Proceedings of the IEEE/CVF winter conference on applications of computer vision*, pages 2023–2032, 2021. 6
- [165] Ding Jian, Xue Nan, Long Yang, Xia Gui-Song, and Lu Qikai. Learning roi transformer for detecting oriented objects in aerial images. In *CVPR*, June 2019. 6
- [166] Jian Ding, Nan Xue, Gui-Song Xia, Xiang Bai, Wen Yang, Michael Yang, Serge Belongie, Jiebo Luo, Mihai Datcu, Marcello Pelillo, and Liangpei Zhang. Object detection in aerial images: A large-scale benchmark and challenges. *IEEE Trans. Pattern Anal. Mach. Intell.*, pages 1–1, 2021. 6, 12
- [167] Syed Waqas Zamir, Aditya Arora, Akshita Gupta, Salman Khan, Guolei Sun, Fahad Shahbaz Khan, Fan Zhu, Ling Shao, Gui-Song Xia, and Xiang Bai. isaid: A large-scale dataset for instance segmentation in aerial images. In *CVPRW*, pages 28–37, 2019. 6
- [168] VALID. Virtual aerial image dataset, 2020. 6
- [169] Elizabeth Bondi, Raghav Jain, Palash Aggrawal, Saket Anand, Robert Hannaford, Ashish Kapoor, Jim Piavis, Shital Shah, Lucas Joppa, Bistra Dilkina, et al. Birdsai: A dataset for detection and tracking in aerial thermal infrared videos. In *WACV*, pages 1747–1756, 2020. 6
- [170] Guangshuai Gao, Qingjie Liu, and Yunhong Wang. Counting from sky: A large-scale data set for remote sensing object counting and a benchmark method. *IEEE TGRS*, 59(5):3642–3655, 2020. 6, 17
- [171] Jakaria Rabbi, Subir Chowdhury, and Dennis Chao. Oil and gas tank dataset, 2020. 6
- [172] Heyer Karl and Mubasir Md. Oil storage tanks, 2019. 6
- [173] Nikolaos Ioannis Bountos, Ioannis Papoutsis, Dimitrios Michail, Andreas Karavias, Panagiotis Elias, and Isaak Parcharidis. Hephaestus: A large scale multitask dataset towards insar understanding. In *CVPRW*, pages 1453–1462, June 2022. 6
- [174] Semantic drone dataset, 2019. 6, 7
- [175] A Robicquet, A Sadeghian, A Alahi, and S Savarese. Learning social etiquette: Human trajectory prediction in crowded scenes. In *ECCV*, volume 2, 2020. 6
- [176] Jacob Solawetz. Aerial maritime drone dataset, 2020. 6
- [177] Leon Amadeus Varga, Benjamin Kiefer, Martin Messmer, and Andreas Zell. Seadronesee: A maritime benchmark for detecting humans in open water. In *WACV*, pages 2260–2270, 2022. 6
- [178] Jan Gąsienica-Józkowy, Mateusz Knapik, and Bogusław Cyganek. An ensemble deep learning method with optimized weights for drone-based water rescue and surveillance. *Integrated Computer-Aided Engineering*, pages 1–15, 01 2021. 6
- [179] Michael Thoreau and Frazer Wilson. Sarnet: A dataset for deep learning assisted search and rescue with satellite imagery, 2021. 6
- [180] Zikun Liu, Liu Yuan, Lubin Weng, and Yiping Yang. A high resolution optical satellite image dataset for ship recognition and some new baselines. In *ICPRAM*, volume 2, pages 324–331. SciTePress, 2017. 6
- [181] Yuanyuan Wang, Chao Wang, Hong Zhang, Yingbo Dong, and Sisi Wei. A sar dataset of ship detection for deep learning under complex backgrounds. *Remote Sensing*, 11(7), 2019. 6



- [182] SUN Xian, WANG Zhirui, SUN Yuanrui, DIAO Wenhui, ZHANG Yue, and FU Kun. Air-sarship-1.0: High-resolution sar ship detection dataset. *Journal of Radars*, 8(6):852–863, 2019. 6
- [183] Fuduo Xue, Weiqi Jin, Su Qiu, and Jie Yang. Rethinking automatic ship wake detection: State-of-the-art cnn-based wake detection via optical images. *IEEE TGRS*, 60:1–22, 2021. 6
- [184] Casia-ship, 2020. 6
- [185] xview. xview3 competition, 2022. 6
- [186] Ilker Bozcan and Erdal Kayacan. Au-air: A multi-modal unmanned aerial vehicle dataset for low altitude traffic surveillance. In *ICRA*, pages 8504–8510. IEEE, 2020. 6
- [187] Robert Krajewski, Julian Bock, Laurent Kloeker, and Lutz Eckstein. The highd dataset: A drone dataset of naturalistic vehicle trajectories on german highways for validation of highly automated driving systems. In *ITSC*, pages 2118–2125, 2018. 6
- [188] Wei Zhan, Liting Sun, Di Wang, Haojie Shi, Aubrey Clausse, Maximilian Naumann, Julius Kümmerle, Hendrik Königshof, Christoph Stiller, Arnaud de La Fortelle, and Masayoshi Tomizuka. INTER-ACTION Dataset: An INTERNATIONAL, Adversarial and Cooperative moTION Dataset in Interactive Driving Scenarios with Semantic Maps. [arXiv:1910.03088 \[cs, eess\]](https://arxiv.org/abs/1910.03088), 2019. 6
- [189] Julian Bock, Robert Krajewski, Tobias Moers, Steffen Runde, Lennart Vater, and Lutz Eckstein. The ind dataset: A drone dataset of naturalistic road user trajectories at german intersections. In *IV*, pages 1929–1934, 2020. 6
- [190] Robert Krajewski, Tobias Moers, Julian Bock, Lennart Vater, and Lutz Eckstein. The round dataset: A drone dataset of road user trajectories at roundabouts in germany. In *ITSC*, pages 1–6, 2020. 6
- [191] Ben Weinstein, Sergio Marconi, Alina Zare, Stephanie Bohlman, Sarah Graves, Aditya Singh, and Ethan White. Neon tree crowns dataset, April 2020. Gordon and Betty Moore Foundation: GBMF4563. 6
- [192] Liu Emily, Logan Judy, kitushan, Lee Meredith, phoebeliuF8, QMirsharif, Roy Sam, Wang Sherrie, Valerie, Vani M, Venkatesh Varsha, and Datathon WiDS. Wids datathon 2019, 2019. 6
- [193] Swedish Forest Agency. Forest damages – larch casebearer 1.0, 2021. 6
- [194] Overhead imagery research data set, 2009. 6
- [195] Haigang Zhu, Xiaogang Chen, Weiqun Dai, Kun Fu, Qixiang Ye, and Jianbin Jiao. Orientation robust object detection in aerial images using deep convolutional neural network. In *ICIP*, pages 3735–3739. IEEE, 2015. 6
- [196] Paulo RL De Almeida, Luiz S Oliveira, Alceu S Britto Jr, Eunelson J Silva Jr, and Alessandro L Koerich. Pklot—a robust dataset for parking lot classification. *Expert Systems with Applications*, 42(11):4937–4949, 2015. 6
- [197] Meng-Ru Hsieh, Yen-Liang Lin, and Winston H Hsu. Drone-based object counting by spatially regularized regional proposal network. In *ICCV*, pages 4145–4153, 2017. 6
- [198] Pengfei Zhu, Longyin Wen, Dawei Du, Xiao Bian, Heng Fan, Qinghua Hu, and Haibin Ling. Detection and tracking meet drones challenge. *IEEE Trans. Pattern Anal. Mach. Intell.*, pages 1–1, 2021. 6, 17
- [199] M. Haroon, M. Shahzad, and M. M. Fraz. Multi-sized object detection using spaceborne optical imagery. *IEEE J. Sel. Top. Appl. Earth Obs. Remote Sens.*, 13:3032–3046, 2020. 6
- [200] Pengfei Zhu, Longyin Wen, Dawei Du, Xiao Bian, Heng Fan, Qinghua Hu, and Haibin Ling. Detection and tracking meet drones challenge. *IEEE Trans. Pattern Anal. Mach. Intell.*, 2021. 6
- [201] Seyed Majid Azimi, Reza Bahmanyar, Corentin Henry, and Franz Kurz. Eagle: Large-scale vehicle detection dataset in real-world scenarios using aerial imagery. In *ICPR*, pages 6920–6927, 2021. 6
- [202] Murari Mandal, Lav Kush Kumar, and Santosh Kumar Vipparthi. Mor-uav: A benchmark dataset and baselines for moving object recognition in uav videos. In *ACM Multimedia*, pages 2626–2635, 2020. 6
- [203] Yiming Sun, Bing Cao, Pengfei Zhu, and Qinghua Hu. Drone-based rgb-infrared cross-modality vehicle detection via uncertainty-aware learning. *IEEE TCSVT*, pages 1–1, 2022. 6
- [204] Ari, Masha Enxhi, and Khechine Elyes. Swimming pool and car detection, 2019. 6
- [205] Immanuel Weber, Jens Bongartz, and Ribana Roscher. Artifice-potsdam: A benchmark for learning with artificial objects for improved aerial vehicle detection. In *IGARSS*, pages 1214–1217. IEEE, 2021. 6
- [206] Yahui Liu, Jian Yao, Xiaohu Lu, Menghan Xia, Xingbo Wang, and Yuan Liu. Roadnet: Learning to comprehensively analyze road networks in complex urban scenes from high-resolution remotely sensed images. *IEEE TGRS*, 57(4):2043–2056, 2019. 5, 7
- [207] Emmanuel Maggiori, Yuliya Tarabalka, Guillaume Charpiat, and Pierre Alliez. Can semantic labeling methods generalize to any city? the inria aerial image labeling benchmark. In *IGARSS*, pages 3226–3229. IEEE, 2017. 5, 7
- [208] Gellért Mátyus, Shenlong Wang, Sanja Fidler, and Raquel Urtasun. Hd maps: Fine-grained road segmentation by parsing ground and aerial images. In *CVPR*, pages 3611–3619, 2016. 5, 7
- [209] Gellert Matyus, Shenlong Wang, Sanja Fidler, and Raquel Urtasun. Enhancing road maps by parsing aerial images around the world. In *ICCV*, pages 1689–1697, 2015. 5, 7
- [210] Favyen Bastani, Songtao He, Sofiane Abbar, Mohammad Alizadeh, Hari Balakrishnan, Sanjay Chawla, Sam Madden, and David DeWitt. Roadtracer: Automatic extraction of road networks from aerial images. In *CVPR*, pages 4720–4728, 2018. 5, 7
- [211] Microsoft road-detections, 2020. 5, 7
- [212] Steve Foga, Pat L Scaramuzza, Song Guo, Zhe Zhu, Ronald D Dilley Jr, Tim Beckmann, Gail L Schmidt, John L Dwyer, M Joseph Hughes, and Brady Laue. Cloud detection algorithm comparison and validation for operational landsat data products. *Remote Sens. Environ.*, 194:379–390, 2017. 5, 7
- [213] S. Mohajerani and P. Saedi. Cloud-net: An end-to-end cloud detection algorithm for landsat 8 imagery. In *IGARSS*, pages 1029–1032, July 2019. 5, 7
- [214] S. Mohajerani and P. Saedi. Cloud-Net+: A Cloud Segmentation CNN for Landsat 8 Remote Sensing Imagery Optimized with Filtered Jaccard Loss Function. volume 2001.08768, 2020. 5, 7
- [215] Zhiwei Li, Huanfeng Shen, Qing Cheng, Yuhao Liu, Shucheng You, and Zongyi He. Deep learning based cloud detection for remote sensing images by the fusion of multi-scale convolutional features. [arXiv preprint arXiv:1810.05801](https://arxiv.org/abs/1810.05801), 2018. 5, 7
- [216] Jun Li, Zhaocong Wu, Zhongwen Hu, Canliang Jian, Shaojie Luo, Lichao Mou, Xiao Xiang Zhu, and Matthieu Molinier. A lightweight deep learning-based cloud detection method for sentinel-2a imagery fusing multiscale spectral and spatial features. *IEEE TGRS*, 60:1–19, 2021. 5, 7
- [217] Julia A Barsi, Kenton Lee, Geir Kvaran, Brian L Markham, and Jeffrey A Pedely. The spectral response of the landsat-8 operational land imager. *Remote sensing*, 6(10):10232–10251, 2014. 5, 7
- [218] Shunping Ji, Zhili Zhang, Chi Zhang, Shiqing Wei, Meng Lu, and Yulin Duan. Learning discriminative spatiotemporal features for precise crop classification from multi-temporal satellite images. *Int. J. Remote Sens.*, 41(8):3162–3174, 2020. 5, 7
- [219] Giulio Weikmann, Claudia Paris, and Lorenzo Bruzzone. Time-sen2crop: A million labeled samples dataset of sentinel 2 image time series for crop-type classification. *IEEE J. Sel. Top. Appl. Earth Obs. Remote Sens.*, 14:4699–4708, 2021. 5, 7
- [220] Mang Tik Chiu, Xingqian Xu, Yunchao Wei, Zilong Huang, Alexander G Schwing, Robert Brunner, Hrant Khachatryan, Hovnatán Karapetyan, Ivan Dozier, Greg Rose, et al. Agriculture-vision: A large aerial image database for agricultural pattern analysis. In *CVPR*, pages 2828–2838, 2020. 5, 7
- [221] Yanfei Zhong, Xin Hu, Chang Luo, Xinyu Wang, Ji Zhao, and Liangpei Zhang. Whu-hi: Uav-borne hyperspectral with high spatial resolution (h2) benchmark datasets and classifier for precise crop identification based on deep convolutional neural network with crf. *Remote Sens. Environ.*, 250:112012, 2020. 7
- [222] Mehmet Ozgur Turkoglu, Stefano D’Aronco, Gregor Perich, Frank Liebisch, Constantin Streit, Konrad Schindler, and Jan Dirk Wegner. Crop mapping from image time series: Deep learning with multi-scale label hierarchies. *Remote Sens. Environ.*, 264:112603, 2021. 7
- [223] Maja Schneider, Amelie Broszeit, and Marco Körner. EuroCrops: A pan-european dataset for time series crop type classification. In Pierre Soille, Sveinung Loekken, and Sergio Albani, editors, *BiDS*. 7
- [224] Yi-Ran Wang and Xiao-Ming Li. Arctic sea ice cover data from spaceborne synthetic aperture radar by deep learning. *Earth System Science Data*, 13(6):2723–2742, 2021. 7
- [225] Adam Van Etten, Dave Lindenbaum, and Todd M Bacastow. Spacenet: A remote sensing dataset and challenge series. [arXiv preprint arXiv:1807.01232](https://arxiv.org/abs/1807.01232), 2018. 7
- [226] Anza Shakeel, Waqas Sultani, and Mohsen Ali. Deep built-structure counting in satellite imagery using attention based re-weighting. *ISPRS J. Photogramm. Remote Sens.*, 151:313–321, 2019. 7
- [227] Jacob Shermeyer, Daniel Hogan, Jason Brown, Adam Van Etten, Nicholas Weir, Fabio Pacifici, Ronny Hansch, Alexei Bastidas, Scott Soenen, Todd Bacastow, et al. Spacenet 6: Multi-sensor all weather mapping dataset. In *CVPRW*, pages 196–197, 2020. 7

- [228] Adam Van Etten, Daniel Hogan, Jesus Martinez Manso, Jacob Shermeyer, Nicholas Weir, and Ryan Lewis. The multi-temporal urban development spacenet dataset. In *CVPR*, pages 6398–6407, 2021. 7
- [229] Fanjie Kong, Bohao Huang, Kyle Bradbury, and Jordan Malof. The synthinel-1 dataset: A collection of high resolution synthetic overhead imagery for building segmentation. In *WACV*, pages 1814–1823, 2020. 7
- [230] Volodymyr Mnih. *Machine Learning for Aerial Image Labeling*. PhD thesis, University of Toronto, 2013. 7
- [231] GFDRR Labs. Open cities ai challenge dataset, version 1.0, radiant mlhub, 2018. 7
- [232] GitHub repository. Segmenting buildings in satellite images, 2018. 7
- [233] Pascal Kaiser, Jan Dirk Wegner, Aurélien Lucchi, Martin Jaggi, Thomas Hofmann, and Konrad Schindler. Learning aerial image segmentation from online maps. *IEEE TGRS*, 55(11):6054–6068, 2017. 7
- [234] Louis Baetens, Camille Desjardins, and Olivier Hagolle. Validation of copernicus sentinel-2 cloud masks obtained from maja, sen2cor, and fmask processors using reference cloud masks generated with a supervised active learning procedure. *Remote Sensing*, 11(4):433, 2019. 7
- [235] Shunping Ji, Peiyu Dai, Meng Lu, and Yongjun Zhang. Simultaneous cloud detection and removal from bimodal remote sensing images using cascade convolutional neural networks. *IEEE TGRS*, 59(1):732–748, 2020. 7, 16
- [236] Q. He, X. Sun, Z. Yan, and K. Fu. Dabnet: Deformable contextual and boundary-weighted network for cloud detection in remote sensing images. *IEEE TGRS*, pages 1–16, 2021. 7
- [237] GitHub repository. The azavea cloud dataset, 2018. 7
- [238] Radiant Earth Foundation. Sentinel-2 cloud cover segmentation dataset (version 1). radiant mlhub., 2022. 7
- [239] Zhenfeng Shao, Ke Yang, and Weixun Zhou. Performance evaluation of single-label and multi-label remote sensing image retrieval using a dense labeling dataset. *Remote Sensing*, 10(6):964, 2018. 7
- [240] Jiangye Yuan, Shaun S Gleason, and Anil M Cheriyyad. Systematic benchmarking of aerial image segmentation. *IEEE Geosci. Remote Sens. Lett.*, 10(6):1527–1531, 2013. 7
- [241] Gabriele Moser, Devis Tuia, and Michal Shimoni. 2015 ieee grss data fusion contest: Extremely high resolution lidar and optical data [technical committees]. *IEEE GRSM*, 3(1):40–41, 2015. 7
- [242] Michele Volpi and Vittorio Ferrari. Semantic segmentation of urban scenes by learning local class interactions. In *CVPRW*, pages 1–9, 2015. 7
- [243] Mirko Paolo Barbato, Flavio Piccoli, and Paolo Napoletano. Ticino: A multi-modal remote sensing dataset for semantic segmentation. *Expert Systems with Applications*, page 123600, 2024. 7
- [244] Mi Zhang, Xiangyun Hu, Like Zhao, Ye Lv, Min Luo, and Shiyang Pang. Learning dual multi-scale manifold ranking for semantic segmentation of high-resolution images. *Remote Sensing*, 9(5):500, 2017. 7
- [245] Maria Scanlon. *Semantic Annotation of Aerial Images using Deep Learning, Transfer Learning, and Synthetic Training Data*. PhD thesis, 09 2018. 7
- [246] Ishan Nigam, Chen Huang, and Deva Ramanan. Ensemble knowledge transfer for semantic segmentation. In *WACV*, pages 1499–1508. IEEE, 2018. 7
- [247] Yu Chen, Yao Wang, Peng Lu, Yisong Chen, and Guoping Wang. Large-scale structure from motion with semantic constraints of aerial images. In *PRCV*, pages 347–359. Springer, 2018. 7
- [248] Drone deploy medium dataset, 2019. 7
- [249] Michael Fonder and Marc Van Droogenbroeck. Mid-air: A multi-modal dataset for extremely low altitude drone flights. In *CVPRW*, pages 0–0, 2019. 7
- [250] Aneesh Rangnekar, Nilay Mokashi, Emmett J Ientilucci, Christopher Kanan, and Matthew J Hoffman. Aerorit: A new scene for hyperspectral image analysis. *IEEE TGRS*, 58(11):8116–8124, 2020. 7
- [251] Ribana Roscher, Michele Volpi, Clément Mallet, Lukas Drees, and Jan Dirk Wegner. Semicity Toulouse: A benchmark for building instance segmentation in satellite images. In *ISPRS Annals*, volume 5, pages 109–116, 2020. 7
- [252] Ye Lyu, George Vosselman, Gui-Song Xia, Alper Yilmaz, and Michael Ying Yang. Uavid: A semantic segmentation dataset for uav imagery. *ISPRS J. Photogramm. Remote Sens.*, 165:108 – 119, 2020. 7
- [253] 2021 ieee grss data fusion contest track dse, 2021. 7, 8
- [254] Ilke Demir, Krzysztof Koperski, David Lindenbaum, Guan Pang, Jing Huang, Saikat Basu, Forest Hughes, Devis Tuia, and Ramesh Raskar. Deepglobe 2018: A challenge to parse the earth through satellite images. In *CVPRW*, pages 172–181, 2018. 7
- [255] K. Karantzalos, C. Karakizi, Z. Kandalakis, and G. Antoniou. Hyrank hyperspectral satellite dataset i (version v001). In *I.W.III/4; ISPRS: Hannover, Germany*, 2018. 7
- [256] Bertrand Le Saux, Naoto Yokoya, Ronny Hänsch, and Myron Brown. 2019 ieee grss data fusion contest: large-scale semantic 3d reconstruction. *IEEE GRSM*, 7(4):33–36, 2019. 7
- [257] Caleb Robinson, Le Hou, Kolya Malkin, Bistra Dilkina, and Nebojsa Jojic. Large scale high-resolution land cover mapping with multi-resolution data. In *CVPR*, pages 12726–12735, 2019. 7
- [258] Naoto Yokoya, Pedram Ghamisi, Ronny Hänsch, and Michael Schmitt. 2020 IEEE GRSS data fusion contest: Global land cover mapping with weak supervision [technical committees]. *IEEE GRSM*, 8(1):154–157, 2020. 7
- [259] Ccf big data & computing intelligence contest 2020, 2019. 7
- [260] Yue Xu, Jianya Gong, Xin Huang, Xiangyun Hu, Jiayi Li, Qiang Li, and Min Peng. LuoJia-hsr: A high spatial-spectral resolution remote sensing dataset for land-cover classification with a new 3d-hrnet. *Geo-Spatial Information Science*, 26(3):289–301, 2023. 7
- [261] Junjue Wang, Zhuo Zheng, Ailong Ma, Xiaoyan Lu, and Yanfei Zhong. Loveda: A remote sensing land-cover dataset for domain adaptive semantic segmentation. *arXiv preprint arXiv:2110.08733*, 2021. 7
- [262] Javiera Castillo-Navarro, Bertrand Le Saux, Alexandre Boulch, Nicolas Audebert, and Sébastien Lefèvre. Semi-supervised semantic segmentation in earth observation: The minifrance suite, dataset analysis and multi-task network study. *Machine Learning*, pages 1–36, 2021. 7
- [263] Gerald Baier, Antonin Deschamps, Michael Schmitt, and Naoto Yokoya. Synthesizing optical and sar imagery from land cover maps and auxiliary raster data. *IEEE TGRS*, 60:1–12, 2021. 7, 12, 14, 18
- [264] Rohaifa Khaldi, Domingo Alcaraz-Segura, Emilio Guirado, Yassir Benhammou, Abdellatif El Afia, Francisco Herrera, and Siham Tabik. Timespec4lulc: a global multispectral time series database for training lulc mapping models with machine learning. *Earth System Science*, 14(3):1377–1411, 2022. 7
- [265] Xin-Yi Tong, Gui-Song Xia, and Xiao Xiang Zhu. Enabling country-scale land cover mapping with meter-resolution satellite imagery. *arXiv preprint arXiv:2209.00727*, 2022. 7, 12
- [266] Zhitong Xiong, Sining Chen, Yi Wang, Lichao Mou, and Xiao Xiang Zhu. Gamus: A geometry-aware multi-modal semantic segmentation benchmark for remote sensing data, 2023. 7
- [267] Jiayi Li, Xin Huang, and Lilin Tu. Whu-ohs: A benchmark dataset for large-scale hyperspectral image classification. *Int. J. Appl. Earth Obs. Geoinf.*, 113:103022, 2022. 7
- [268] Noah Johnson, Wayne Treible, and Daniel Crispell. Opensentinelmap: A large-scale land use dataset using openstreetmap and sentinel-2 imagery. In *CVPR*, pages 1333–1341, 2022. 7, 12
- [269] Bertrand Le Saux, Naoto Yokoya, Ronny Hänsch, and Saurabh Prasad. 2018 ieee grss data fusion contest: Multimodal land use classification [technical committees]. *IEEE GRSM*, 6(1):52–54, 2018. 7
- [270] Romain Wenger, A Puissant, J Weber, L Idoumghar, and G Forestier. Multisenge: A multimodal and multimodal benchmark dataset for land use/land cover remote sensing applications. *ISPRS Annals*, pages 635–640, 2022. 7
- [271] Nisim Hurst-Tarrab, Leonardo Chang, Miguel Gonzalez-Mendoza, and Neil Hernandez-Gress. Robust parking block segmentation from a surveillance camera perspective. *Applied Sciences*, 10(15):5364, 2020. 7
- [272] Rabab Abdelfattah, Xiaofeng Wang, and Song Wang. Ttpla: An aerial-image dataset for detection and segmentation of transmission towers and power lines. In *ACCV*, 2020. 7
- [273] Songtao He and Hari Balakrishnan. Lane-level street map extraction from aerial imagery. In *WACV*, pages 2080–2089, 2022. 7
- [274] Ronny Hänsch, Jacob Arndt, Dalton Lunga, Matthew Gibb, Tyler Pedelose, Arnold Boedihardjo, Desiree Petrie, and Todd M Bacastow. Spacenet 8-the detection of flooded roads and buildings. In *CVPR*, pages 1472–1480, 2022. 7
- [275] Qi Chen, Lei Wang, Yifan Wu, Guangming Wu, Zhiling Guo, and Steven L Waslander. Aerial imagery for roof segmentation: A large-scale dataset towards automatic mapping of buildings. *ISPRS J. Photogramm. Remote Sens.*, 147:42–55, 2019. 7
- [276] Drivendata. Open AI caribbean challenge:mapping disaster risk from aerial imagery, 2019. 7
- [277] Sebastian Krapf, Lukas Bogenrieder, Fabian Netzler, Georg Balke, and Markus Lienkamp. Rid—roof information dataset for computer vision-based photovoltaic potential assessment. *Remote Sensing*, 14(10):2299, 2022. 7

- [278] Qijian Zhang, Runmin Cong, Chongyi Li, Ming-Ming Cheng, Yuming Fang, Xiaochun Cao, Yao Zhao, and Sam Kwong. Dense attention fluid network for salient object detection in optical remote sensing images. *IEEE Trans. Image Process.*, 30:1305–1317, 2020. 7
- [279] Shuang Luo, Huifang Li, and Huanfeng Shen. Deeply supervised convolutional neural network for shadow detection based on a novel aerial shadow imagery dataset. *ISPRS J. Photogramm. Remote Sens.*, 167:443–457, 2020. 7
- [280] Seyed Majid Azimi, Corentin Henry, Lars Sommer, Arne Schumann, and Eleonora Vig. Skyscapes fine-grained semantic understanding of aerial scenes. In *CVPR*, pages 7393–7403, 2019. 7
- [281] Satellite images of water bodies, 2020. 7
- [282] Li Shen, Yao Lu, Hao Chen, Hao Wei, Donghai Xie, Jiabao Yue, Rui Chen, Shouye Lv, and Bitao Jiang. S2looking: A satellite side-looking dataset for building change detection. *Remote Sensing*, 13(24):5094, 2021. 5, 8
- [283] Luigi T Luppino, Filippo M Bianchi, Gabriele Moser, and Stian N Anfinsen. Unsupervised image regression for heterogeneous change detection. *arXiv preprint arXiv:1909.05948*, 2019. 5, 8
- [284] Mengxi Liu, Zhuoqun Chai, Haojun Deng, and Rong Liu. A cnn-transformer network with multi-scale context aggregation for fine-grained cropland change detection. *IEEE J. Sel. Top. Appl. Earth Obs. Remote Sens.*, 2022. 5, 8
- [285] Iris de Gélis, Sébastien Lefèvre, and Thomas Corpetti. Change detection in urban point clouds: An experimental comparison with simulated 3d datasets. *Remote Sensing*, 13(13):2629, 2021. 5, 8
- [286] Kunping Yang, Gui-Song Xia, Zicheng Liu, Bo Du, Wen Yang, Marcello Pelillo, and Liangpei Zhang. Asymmetric siamese networks for semantic change detection in aerial images. *IEEE TGRS*, 60:1–18, 2021. 5, 8
- [287] Christopher F Brown, Steven P Brumby, Brookie Guzder-Williams, Tanya Birch, Samantha Brooks Hyde, Joseph Mazzariello, Wanda Czerwinski, Valerie J Pasquarella, Robert Haertel, Simon Ilyushchenko, et al. Dynamic world, near real-time global 10 m land use land cover mapping. *Scientific Data*, 9(1):1–17, 2022. 5, 8
- [288] Valerio Marsocci, Virginia Coletta, Roberta Ravanelli, Simone Scardapane, and Mattia Crespi. Inferring 3d change detection from bitemporal optical images. *ISPRS Journal of Photogrammetry and Remote Sensing*, 196:325–339, 2023. 8
- [289] Aito Fujita, Ken Sakurada, Tomoyuki Imaizumi, Riho Ito, Shuhei Hikosaka, and Ryosuke Nakamura. Damage detection from aerial images via convolutional neural networks. In *IAPR MVA*, pages 5–8. IEEE, 2017. 8
- [290] Hao Chen and Zhenwei Shi. A spatial-temporal attention-based method and a new dataset for remote sensing image change detection. *Remote Sensing*, 12(10), 2020. 8
- [291] Ritwik Gupta, Richard Hosfelt, Sandra Sajeev, Nirav Patel, Bryce Goodman, Jigar Doshi, Eric Heim, Howie Choset, and Matthew Gaston. xBD: A dataset for assessing building damage from satellite imagery. *arXiv preprint arXiv:1911.09296*, 2019. 8
- [292] Csaba Benedek and Tamás Szirányi. Change detection in optical aerial images by a multilayer conditional mixed markov model. *IEEE TGRS*, 47(10):3416–3430, 2009. 8
- [293] Michele Volpi, Gustau Camps-Valls, and Devis Tuia. Spectral alignment of multi-temporal cross-sensor images with automated kernel canonical correlation analysis. *ISPRS J. Photogramm. Remote Sens.*, 107:50–63, 2015. 8
- [294] Qi Wang, Zhenghang Yuan, Qian Du, and Xuelong Li. GETNET: A general end-to-end 2-d cnn framework for hyperspectral image change detection. *IEEE TGRS*, 57(1):3–13, 2018. 8
- [295] Rodrigo Caye Daudt, Bertr Le Saux, Alexandre Boulch, and Yann Gousseau. Urban change detection for multispectral earth observation using convolutional neural networks. In *IGARSS*, pages 2115–2118. Ieee, 2018. 8
- [296] MA Lebedev, Yu V Vizilter, OV Vygolov, VA Knyaz, and A Yu Rubis. Change detection in remote sensing images using conditional adversarial networks. *ISPRS Archives*, 42(2), 2018. 8
- [297] Multitemporal hyperspectral change detection, 2016. 8
- [298] Chen Wu, Lefei Zhang, and Liangpei Zhang. A scene change detection framework for multi-temporal very high resolution remote sensing images. *Signal Processing*, 124:184–197, 2016. 8
- [299] Min Zhang and Wenzhong Shi. A feature difference convolutional neural network-based change detection method. *IEEE TGRS*, 2020. 8
- [300] Chenxiao Zhang, Peng Yue, Deodato Tapete, Liangcun Jiang, Boyi Shanguan, Li Huang, and Guangchao Liu. A deeply supervised image fusion network for change detection in high resolution bi-temporal remote sensing images. *ISPRS J. Photogramm. Remote Sens.*, 166:183–200, 2020. 8
- [301] Javier López-Fandiño, Alberto S Garea, Dora B Heras, and Francisco Argüello. Stacked autoencoders for multiclass change detection in hyperspectral images. In *IGARSS*, pages 1906–1909. IEEE, 2018. 8
- [302] Shiqi Tian, Ailong Ma, Zhuo Zheng, and Yanfei Zhong. Hi-ucd: A large-scale dataset for urban semantic change detection in remote sensing imagery. *arXiv preprint arXiv:2011.03247*, 2020. 8
- [303] Daifeng Peng, Lorenzo Bruzzone, Yongjun Zhang, Haiyan Guan, Haiyong Ding, and Xu Huang. Semicdnet: A semisupervised convolutional neural network for change detection in high resolution remote-sensing images. *IEEE TGRS*, 59(7):5891–5906, 2020. 8
- [304] Armin Moghimi, Ali Mohammadzadeh, Turgay Celik, and Meisam Amani. A novel radiometric control set sample selection strategy for relative radiometric normalization of multitemporal satellite images. *IEEE TGRS*, 59(3):2503–2519, 2020. 8
- [305] Ruizhe Shao, Chun Du, Hao Chen, and Jun Li. Sunet: Change detection for heterogeneous remote sensing images from satellite and uav using a dual-channel fully convolution network. *Remote Sensing*, 13(18):3750, 2021. 8
- [306] Qian Shi, Mengxi Liu, Shengchen Li, Xiaoping Liu, Fei Wang, and Liangpei Zhang. A deeply supervised attention metric-based network and an open aerial image dataset for remote sensing change detection. *IEEE TGRS*, 60:1–16, 2021. 8
- [307] Jingwen Yuan, Lixiang Ru, Shugen Wang, and Chen Wu. Wh-mavs: A novel dataset and deep learning benchmark for multiple land use and land cover applications. *IEEE J. Sel. Top. Appl. Earth Obs. Remote Sens.*, 15:1575–1590, 2022. 8
- [308] Marrit Leenstra, Diego Marcos, Francesca Bovolo, and Devis Tuia. Self-supervised pre-training enhances change detection in sentinel-2 imagery. In *ICPR*, pages 578–590. Springer, 2021. 8
- [309] Aysim Toker, Lukas Kondmann, Mark Weber, Marvin Eisenberger, Andrés Camero, Jingliang Hu, Ariadna Pregel Hoderlein, Caglar Senaras, Timothy Davis, Daniel Cremers, Giovanni Marchisio, Xiao Xiang Zhu, and Laura Leal-Taié. DynamicEarthNet: Daily Multi-Spectral Satellite Dataset for Semantic Change Segmentation. In *CVPR*, 2022. 8
- [310] Haoyang Li, Fangjie Zhu, Xiaoyu Zheng, Mengxi Liu, and Guangzhao Chen. Mscdunet: A deep learning framework for built-up area change detection integrating multispectral, sar and vhr data. *IEEE J. Sel. Top. Appl. Earth Obs. Remote Sens.*, 2022. 8
- [311] Deyi Ji, Siqi Gao, Mingyuan Tao, Hongtao Lu, and Feng Zhao. Changenet: Multi-temporal asymmetric change detection dataset. In *ICASSP 2024-2024 IEEE International Conference on Acoustics, Speech and Signal Processing (ICASSP)*, pages 2725–2729. IEEE, 2024. 8
- [312] Chao Pang, Jiang Wu, Jian Ding, Can Song, and Gui-Song Xia. Detecting building changes with off-nadir aerial images. *Science China Information Sciences*, 66(4):1–15, 2023. 8
- [313] Gustau Camps-Valls, Devis Tuia, Xiao Xiang Zhu, and Markus Reichstein. Deep learning for the Earth sciences: A comprehensive approach to remote sensing, climate science and geosciences. 2021. 5
- [314] Rishi Bommasani, Drew A Hudson, Ehsan Adeli, Russ Altman, Simran Arora, Sydney von Arx, Michael S Bernstein, Jeannette Bohg, Antoine Bosselut, Emma Brunskill, et al. On the opportunities and risks of foundation models. *arXiv preprint arXiv:2108.07258*, 2021. 5
- [315] Favven Bastani, Piper Wolters, Ritwik Gupta, Joe Ferdinando, and Aniruddha Kembhavi. Satlaspretrain: A large-scale dataset for remote sensing image understanding. In *Proceedings of the IEEE/CVF International Conference on Computer Vision*, pages 16772–16782, 2023. 5, 9
- [316] Zhitong Xiong, Yi Wang, Fahong Zhang, Adam J Stewart, Joëlle Hanna, Damian Borth, Ioannis Papoutsis, Bertrand Le Saux, Gustau Camps-Valls, and Xiao Xiang Zhu. Neural plasticity-inspired foundation model for observing the earth crossing modalities. *arXiv preprint arXiv:2403.15356*, 2024. 5, 9
- [317] Matias Mendieta, Boran Han, Xingjian Shi, Yi Zhu, Chen Chen, and Mu Li Gfm. Building geospatial foundation models via continual pretraining. *arXiv preprint arXiv:2302.04476*, 6(7), 2023. 8, 9
- [318] Alexandre Lacoste, Nils Lehmann, Pau Rodriguez, Evan Sherwin, Hannah Kerner, Björn Lütjens, Jeremy Irvin, David Dao, Hamed Alemohammad, Alexandre Drouin, et al. Geo-bench: Toward foundation models for earth monitoring. *Advances in Neural Information Processing Systems*, 36, 2024. 8, 9
- [319] Jonathan Roberts, Kai Han, and Samuel Albanie. Satin: A multi-task metadataset for classifying satellite imagery using vision-language models. *arXiv preprint arXiv:2304.11619*, 2023. 8, 9

- [320] Casper Fibaek, Luke Camilleri, Andreas Luyts, Nikolaos Dionelis, and Bertrand Le Saux. Phileo bench: Evaluating geo-spatial foundation models. *arXiv preprint arXiv:2401.04464*, 2024. 9
- [321] Christopher Yeh, Chenlin Meng, Sherrie Wang, Anne Driscoll, Erik Rozi, Patrick Liu, Jiyeon Lee, Marshall Burke, David B Lobell, and Stefano Ermon. Sustainbench: Benchmarks for monitoring the sustainable development goals with machine learning. *arXiv preprint arXiv:2111.04724*, 2021. 9
- [322] Adam Stewart, Nils Lehmann, Isaac Corley, Yi Wang, Yi-Chia Chang, Nassim Ait Ali Braham, Shradha Sehgal, Caleb Robinson, and Arindam Banerjee. Ssl4eo-l: Datasets and foundation models for landsat imagery. *Advances in Neural Information Processing Systems*, 36, 2024. 9
- [323] Utkarsh Mall, Bharath Hariharan, and Kavita Bala. Change-aware sampling and contrastive learning for satellite images. In *Proceedings of the IEEE/CVF Conference on Computer Vision and Pattern Recognition*, pages 5261–5270, 2023. 9
- [324] Chao Tao, Ji Qi, Guo Zhang, Qing Zhu, Weipeng Lu, and Haifeng Li. Tov: The original vision model for optical remote sensing image understanding via self-supervised learning. *IEEE Journal of Selected Topics in Applied Earth Observations and Remote Sensing*, 2023. 9
- [325] Utkarsh Mall, Cheng Peng Phoo, Meilin Kelsey Liu, Carl Vondrick, Bharath Hariharan, and Kavita Bala. Remote sensing vision-language foundation models without annotations via ground remote alignment. *arXiv preprint arXiv:2312.06960*, 2023. 9
- [326] Di Wang, Jing Zhang, Bo Du, Minqiang Xu, Lin Liu, Dacheng Tao, and Liangpei Zhang. Samrs: Scaling-up remote sensing segmentation dataset with segment anything model. *Advances in Neural Information Processing Systems*, 36, 2024. 9
- [327] Xin Guo, Jiangwei Lao, Bo Dang, Yingying Zhang, Lei Yu, Lixiang Ru, Liheng Zhong, Ziyuan Huang, Kang Wu, Dingxiang Hu, et al. Skysense: A multi-modal remote sensing foundation model towards universal interpretation for earth observation imagery. *arXiv preprint arXiv:2312.10115*, 2023. 9
- [328] Yuanxin Zhao, Mi Zhang, Bingnan Yang, Zhan Zhang, Jiaju Kang, and Jianya Gong. Luojiangohg: A hierarchy oriented geo-aware image caption dataset for remote sensing image-text retrieval. *arXiv preprint arXiv:2403.10887*, 2024. 8, 9
- [329] Yang Zhan, Zhitong Xiong, and Yuan Yuan. Rsvg: Exploring data and models for visual grounding on remote sensing data. *IEEE Transactions on Geoscience and Remote Sensing*, 61:1–13, 2023. 8, 9
- [330] Sylvain Lobry, Diego Marcos, Jesse Murray, and Devis Tuia. Rsvqa: Visual question answering for remote sensing data. *IEEE TGRS*, 58(12):8555–8566, 2020. 8, 9
- [331] Sylvain Lobry, Jesse Murray, Diego Marcos, and Devis Tuia. Visual question answering from remote sensing images. In *IGARSS*, pages 4951–4954. IEEE, 2019. 9
- [332] Zilun Zhang, Tiancheng Zhao, Yulong Guo, and Jianwei Yin. Rs5m: A large scale vision-language dataset for remote sensing vision-language foundation model. *arXiv preprint arXiv:2306.11300*, 2023. 8, 9
- [333] Xiaoqiang Lu, Binqiang Wang, Xiangtao Zheng, and Xuelong Li. Exploring models and data for remote sensing image caption generation. *IEEE TGRS*, 56(4):2183–2195. 8, 9
- [334] Qimin Cheng, Haiyan Huang, Yuan Xu, Yuzhuo Zhou, Huanying Li, and Zhongyuan Wang. Nwpu-captions dataset and mlca-net for remote sensing image captioning. *IEEE Transactions on Geoscience and Remote Sensing*, 60:1–19, 2022. 9
- [335] Zhiqiang Yuan, Wenkai Zhang, Kun Fu, Xuan Li, Chubo Deng, Hongqi Wang, and Xian Sun. Exploring a fine-grained multiscale method for cross-modal remote sensing image retrieval. *arXiv preprint arXiv:2204.09868*, 2022. 9
- [336] Yuan Hu, Jianlong Yuan, Congcong Wen, Xiaonan Lu, and Xiang Li. Rsgpt: A remote sensing vision language model and benchmark. *arXiv preprint arXiv:2307.15266*, 2023. 9
- [337] Zhecheng Wang, Rajanie Prabha, Tianyuan Huang, Jiajun Wu, and Ram Rajagopal. Skyscript: A large and semantically diverse vision-language dataset for remote sensing. In *Proceedings of the AAAI Conference on Artificial Intelligence*, volume 38, pages 5805–5813, 2024. 8, 9
- [338] Zhenghang Yuan, Zhitong Xiong, Lichao Mou, and Xiao Xiang Zhu. Chatearthnet: A global-scale, high-quality image-text dataset for remote sensing. *arXiv preprint arXiv:2402.11325*, 2024. 8, 9
- [339] Dilxat Muhtar, Zhenshi Li, Feng Gu, Xueliang Zhang, and Pengfeng Xiao. Lhrs-bot: Empowering remote sensing with vgi-enhanced large multimodal language model. *arXiv preprint arXiv:2402.02544*, 2024. 9
- [340] Mikolaj Czerkawski and Alistair Francis. From laion-5b to laion-eo: Filtering billions of images using anchor datasets for satellite image extraction. *arXiv preprint arXiv:2309.15535*, 2023. 9
- [341] Chen-Yang-Liu. Remote sensing image change captioning (rsicc), 2022. 8
- [342] Zhenghang Yuan, Lichao Mou, Zhitong Xiong, and Xiao Xiang Zhu. Change detection meets visual question answering. *IEEE TGRS*, 2022. 8, 17
- [343] Patil Sonali, Comandur Bharath, Prakash Tanmay, and C. Kak Avinash. A New Stereo Benchmarking Dataset for Satellite Images. *arXiv:1907.04404*, 2019. 9, 16, 17
- [344] Jin Liu and Shunping Ji. A novel recurrent encoder-decoder structure for large-scale multi-view stereo reconstruction from an open aerial dataset. In *CVPR*, pages 6050–6059, 2020. 9, 16, 17
- [345] Michael Kölle, Dominik Laupheimer, Stefan Schmohl, Norbert Haala, Franz Rottensteiner, Jan Dirk Wegner, and Hugo Ledoux. The hessigheim 3d (h3d) benchmark on semantic segmentation of high-resolution 3d point clouds and textured meshes from uav lidar and multi-view-stereo. *ISPRS Open Journal of Photogrammetry and Remote Sensing*, 1:100001, 2021. 9, 17
- [346] Scott Workman, Richard Souvenir, and Nathan Jacobs. Wide-area image geolocalization with aerial reference imagery. In *ICCV*, pages 3961–3969, 2015. 9, 16, 17
- [347] Zhedong Zheng, Yunchao Wei, and Yi Yang. University-1652: A multi-view multi-source benchmark for drone-based geo-localization. *ACM Multimedia*, 2020. 9, 16, 17
- [348] Karthik Kashinath, Mayur Mudigonda, Sol Kim, Lukas Kapp-Schworer, Andre Graubner, Ege Karaismailoglu, Leo Von Kleist, Thorsten Kurth, Annette Greiner, Ankur Mahesh, et al. Climateset: an expert-labeled open dataset and deep learning architecture for enabling high-precision analyses of extreme weather. *Geoscientific Model Development*, 14(1):107–124, 2021. 9, 16, 17
- [349] Peter Grönquist, Chengyuan Yao, Tal Ben-Nun, Nikoli Dryden, Peter Dueben, Shigang Li, and Torsten Hoefler. Deep learning for post-processing ensemble weather forecasts. 2020. 9, 16, 17
- [350] Hyperview challenge, 2022. 9, 16, 17
- [351] Radiant Earth Foundation. Tropical cyclone wind estimation competition dataset, version 1.0, radiant mlhub, 2022. 9
- [352] Tomas Mikolov, Kai Chen, Greg Corrado, and Jeffrey Dean. Efficient estimation of word representations in vector space. *arXiv preprint arXiv:1301.3781*, 2013. 10
- [353] Ivica Dimitrovski, Ivan Kitanovski, Panče Panov, Nikola Simidjievski, and Dragi Koccev. Aitlas: Artificial intelligence toolbox for earth observation. *arXiv preprint arXiv:2201.08789*, 2022. 11, 13
- [354] Adam Paszke, Sam Gross, Francisco Massa, Adam Lerer, James Bradbury, Gregory Chanan, Trevor Killeen, Zeming Lin, Natalia Gimelshein, Luca Antiga, et al. Pytorch: An imperative style, high-performance deep learning library. *NeurIPS*, 32, 2019. 13
- [355] Oscar Mañas, Alexandre Lacoste, Xavier Giro-i Nieto, David Vazquez, and Pau Rodriguez. Seasonal contrast: Unsupervised pre-training from uncurated remote sensing data. *arXiv preprint arXiv:2103.16607*, 2021. 13, 14
- [356] Min Lu, Jiayin Liu, Feng Wang, and Yuming Xiang. Multi-task learning of relative height estimation and semantic segmentation from single airborne rgb images. *Remote Sensing*, 14(14):3450, 2022. 14
- [357] Ze Liu, Yutong Lin, Yue Cao, Han Hu, Yixuan Wei, Zheng Zhang, Stephen Lin, and Baining Guo. Swin transformer: Hierarchical vision transformer using shifted windows. In *ICCV*, pages 10012–10022, 2021. 13, 16
- [358] Zhuang Liu, Hanzi Mao, Chao-Yuan Wu, Christoph Feichtenhofer, Trevor Darrell, and Saining Xie. A convnet for the 2020s. In *CVPR*, pages 11976–11986, 2022. 13, 16
- [359] Gencer Sumbul, Jian Kang, Tristan Kreuziger, Filipe Marcelino, Hugo Costa, Pedro Benevides, Mario Caetano, and Begüm Demir. Bigearthnet dataset with a new class-nomenclature for remote sensing image understanding. *arXiv preprint arXiv:2001.06372*, 2020. 14
- [360] Ilya O Tolstikhin, Neil Houlsby, Alexander Kolesnikov, Lucas Beyer, Xiaohua Zhai, Thomas Unterthiner, Jessica Yung, Andreas Steiner, Daniel Keysers, Jakob Uszkoreit, et al. Mlp-mixer: An all-mlp architecture for vision. *NeurIPS*, 34:24261–24272, 2021. 14, 16
- [361] Xinle Chen, Haoqi Fan, Ross Girshick, and Kaiming He. Improved baselines with momentum contrastive learning. *arXiv preprint arXiv:2003.04297*, 2020. 14
- [362] Kaiming He, Georgia Gkioxari, Piotr Dollár, and Ross Girshick. Mask r-cnn. In *ICCV*, pages 2961–2969, 2017. 14

- [363] Liang-Chieh Chen, George Papandreou, Florian Schroff, and Hartwig Adam. Rethinking atrous convolution for semantic image segmentation. *arXiv preprint arXiv:1706.05587*, 2017. 14, 16
- [364] Enze Xie, Wenhai Wang, Zhiding Yu, Anima Anandkumar, Jose M Alvarez, and Ping Luo. Segformer: Simple and efficient design for semantic segmentation with transformers. *NeurIPS*, 34:12077–12090, 2021. 14, 16
- [365] Jonathan Long, Evan Shelhamer, and Trevor Darrell. Fully convolutional networks for semantic segmentation. In *CVPR*, pages 3431–3440, 2015. 14
- [366] Liang-Chieh Chen, Yukun Zhu, George Papandreou, Florian Schroff, and Hartwig Adam. Encoder-decoder with atrous separable convolution for semantic image segmentation. In *ECCV*, pages 801–818, 2018. 14
- [367] Hengshuang Zhao, Jianping Shi, Xiaojuan Qi, Xiaogang Wang, and Jiaya Jia. Pyramid scene parsing network. In *CVPR*, pages 2881–2890, 2017. 14
- [368] Tete Xiao, Yingcheng Liu, Bolei Zhou, Yuning Jiang, and Jian Sun. Unified perceptual parsing for scene understanding. In *ECCV*, pages 418–434, 2018. 14, 16
- [369] Mohammadamin Barekatin, Miquel Martí, Hsueh-Fu Shih, Samuel Murray, Kotaro Nakayama, Yutaka Matsuo, and Helmut Prendinger. Okutama-action: An aerial view video dataset for concurrent human action detection. In *CVPRW*, pages 28–35, 2017. 17
- [370] Hyun-Woo Jo and Woo-Kyun Lee. Paddy rice maps south korea (2017–2021), January 2022. 17
- [371] Kim Chanwoo, Jo Hyun-Woo, Lee Sujong, Kim Whijin, Yan Yan, Kim Joon, Song Minju, and Woo-Kyun Lee. Paddy rice labeling sites in south korea (2018), January 2022. 17
- [372] European Environment Agency. Air quality e-reporting (aq e-reporting), 2021. 16, 17
- [373] Pu Jin, Lichao Mou, Gui-Song Xia, and Xiao Xiang Zhu. Anomaly detection in aerial videos with transformers. *IEEE TGRS*, 60:1–13, 2022. 17
- [374] Hirsh Goldberg, Myron Brown, and Sean Wang. A benchmark for building footprint classification using orthorectified rgb imagery and digital surface models from commercial satellites. In *AIPRW*, 2017. 17
- [375] Draper satellite image chronology, 2016. 17
- [376] Vishnu Sarukkai, Anirudh Jain, Burak Uzcent, and Stefano Ermon. Dataset From: Cloud Removal from Satellite Images using Spatiotemporal Generator Networks, 2019. 16, 17
- [377] Patrick Ebel, Andrea Meraner, Michael Schmitt, and Xiao Xiang Zhu. Multisensor data fusion for cloud removal in global and all-season sentinel-2 imagery. *IEEE TGRS*, 59(7):5866–5878, 2020. 16, 17
- [378] Reza Bahmanyar, Elenora Vig, and Peter Reinartz. Mrcnet: Crowd counting and density map estimation in aerial and ground imagery. *arXiv preprint arXiv:1909.12743*, 2019. 17
- [379] Michael Schmitt, Lloyd Haydn Hughes, and Xiao Xiang Zhu. The sen1-2 dataset for deep learning in sar-optical data fusion. *arXiv preprint arXiv:1807.01569*, 2018. 16, 17
- [380] Meiyu Huang, Yao Xu, Lixin Qian, Weili Shi, Yaqin Zhang, Wei Bao, Nan Wang, Xuejiao Liu, and Xueshuang Xiang. The qxs-saropt dataset for deep learning in sar-optical data fusion. *arXiv preprint arXiv:2103.08259*, 2021. 16, 17
- [381] Binghui Huang, Li Zhi, Chao Yang, Fuchun Sun, and Yixu Song. Single satellite optical imagery dehazing using sar image prior based on conditional generative adversarial networks. In *WACV*, pages 1806–1813, 2020. 16, 17
- [382] Juan Miguel Requena Mullor. jmmrcode/Lidar-Landsat-data-fusion: lidar-landsat- data-fusion, October 2019. 16, 17
- [383] Yicong Tian, Chen Chen, and Mubarak Shah. Cross-view image matching for geo-localization in urban environments. In *CVPR*, pages 3608–3616, 2017. 16, 17
- [384] Liu Liu and Hongdong Li. Lending orientation to neural networks for cross-view geo-localization. In *CVPR*, June 2019. 17
- [385] Sijie Zhu, Taojiannan Yang, and Chen Chen. Vigor: Cross-view image geo-localization beyond one-to-one retrieval. In *CVPR*, pages 3640–3649, 2021. 17
- [386] Chen Wang, Alexis Mouche, Pierre Tandeo, Justin E Stopa, Nicolas Longépé, Guillaume Erhard, Ralph C Foster, Douglas Vandemark, and Bertrand Chapron. A labelled ocean sar imagery dataset of ten geophysical phenomena from sentinel-1 wave mode. *Geoscience Data Journal*, 6(2):105–115, 2019. 16, 17
- [387] Stefan Cavegn, Norbert Haala, Stephan Nebiker, Mathias Rothermel, and Patrick Tutzauer. Benchmarking high density image matching for oblique airborne imagery. *ISPRS Archives*, 40(3):45, 2014. 17
- [388] Lina García, Jean Díaz, Humberto Loaiza, and Andrés Restrepo. Thermal and visible aerial imagery, 2019. 17
- [389] Phillip Isola, Jun-Yan Zhu, Tinghui Zhou, and Alexei A Efros. Image-to-image translation with conditional adversarial networks. *CVPR*, 2017. 17
- [390] WHU. Whu-sen-city, 2019. 17
- [391] Gabriele Facciolo, Carlo De Franchis, and Enric Meinhardt-Llopis. Automatic 3d reconstruction from multi-date satellite images. In *CVPRW*, pages 57–66, 2017. 17
- [392] Jian Gao, Jin Liu, and Shunping Ji. Rational polynomial camera model warping for deep learning based satellite multi-view stereo matching. In *ICCV*, pages 6148–6157, October 2021. 16, 17
- [393] Efrén López-Jiménez, Juan Irving Vasquez-Gomez, Miguel Angel Sanchez-Acevedo, Juan Carlos Herrera-Lozada, and Abril Valeria Uriarte-Arcia. Columnar cactus recognition in aerial images using a deep learning approach. *Ecological Informatics*, 52:131–138, 2019. 16, 17
- [394] Gyri Reiersen, David Dao, Björn Lütjens, Konstantin Klemmer, Kenza Amara, Attila Steinegger, Ce Zhang, and Xiaoxiang Zhu. Reforestree: A dataset for estimating tropical forest carbon stock with deep learning and aerial imagery. *arXiv preprint arXiv:2201.11192*, 2022. 16, 17
- [395] Jonathan Ventura, Milo Honsberger, Cameron Gonsalves, Julian Rice, Camille Pawlak, Natalie LR Love, Sklyer Han, Viet Nguyen, Keilana Sugano, Jacqueline Doremus, et al. Individual tree detection in large-scale urban environments using high-resolution multispectral imagery. *arXiv preprint arXiv:2208.10607*, 2022. 16, 17
- [396] Sugandha Doda, Yuanyuan Wang, Matthias Kahl, Eike Jens Hoffmann, Hannes Taubenböck, and Xiao Xiang Zhu. So2sat pop—a curated benchmark data set for population estimation from space on a continental scale. *arXiv preprint arXiv:2204.08524*, 2022. 16, 17
- [397] Tae Ha Park, Marcus Märtens, Gurvan Lecuyer, Dario Izzo, and Simone D’Amico. Speed+: Next-generation dataset for spacecraft pose estimation across domain gap. In *AERO*, pages 1–15. IEEE, 2022. 17
- [398] Satellite images to predict poverty, 2020. 17
- [399] Achraf Djerida, Khelifa Djerriri, Moussa Sofiane Karoui, et al. A new public alsat-2b dataset for single-image super-resolution. In *IGARSS*, pages 8095–8098. IEEE, 2021. 16, 17
- [400] Julien Cornebise, Ivan Oršolić, and Freddie Kalaitzis. The WorldStrat Dataset: Open High-Resolution Satellite Imagery With Paired Multi-Temporal Low- Resolution, July 2022. 16, 17
- [401] Julien Michel, Juan Vinasco-Salinas, Jordi Inglada, and Olivier Hagolle. SEN2VENuS, a dataset for the training of Sentinel-2 super-resolution algorithms, May 2022. 16, 17
- [402] Marcus Märtens, Dario Izzo, Andrej Krzic, and Daniel Cox. Proba-v super-resolution dataset, November 2018. 16, 17
- [403] Daniele Cerra, Miguel Pato, Kevin Alonso, Claas Köhler, Mathias Schneider, Raquel de los Reyes, Emiliano Carmona, Rudolf Richter, Franz Kurz, Peter Reinartz, et al. Dlr hysu—a benchmark dataset for spectral unmixing. *Remote Sensing*, 13(13):2559, 2021. 17
- [404] Myron Brown, Hirsh Goldberg, Kevin Foster, Andrea Leichtman, Sean Wang, Shea Hagstrom, Marc Bosch, and Scott Almes. Large-scale public lidar and satellite image data set for urban semantic labeling. In *Laser Radar Technology and Applications*, volume 10636, pages 154–167. SPIE, 2018. 17
- [405] T Wu, B Vallet, M Pierrot-Deseilligny, and E Rupnik. A new stereo dense matching benchmark dataset for deep learning. *ISPRS Archives*, 43:405–412, 2021. 17
- [406] J. Behley, M. Garbade, A. Milioto, J. Quenzel, S. Behnke, C. Stachniss, and J. Gall. SemanticKITTI: A Dataset for Semantic Scene Understanding of LiDAR Sequences. In *ICCV*, 2019. 17
- [407] Weikai Tan, Nannan Qin, Lingfei Ma, Ying Li, Jing Du, Guorong Cai, Ke Yang, and Jonathan Li. Toronto-3d: A large-scale mobile lidar dataset for semantic segmentation of urban roadways. In *CVPRW*, pages 202–203, 2020. 16, 17
- [408] Gülcan Can, Dario Mantegazza, Gabriele Abbate, Sébastien Chappuis, and Alessandro Giusti. Swiss3dcities: Aerial photogrammetric 3d pointcloud dataset with semantic labels, December 2020. 16, 17
- [409] Gülcan Can, Dario Mantegazza, Gabriele Abbate, Sébastien Chappuis, and Alessandro Giusti. Semantic segmentation on swiss3dcities: a benchmark study on aerial photogrammetric 3d pointcloud dataset. *Pattern Recognition Letters*, 2021. 16, 17
- [410] Nina Varney, Vijayan K Asari, and Quinn Graehling. Dales: A large-scale aerial lidar data set for semantic segmentation. In *CVPRW*, pages 186–187, 2020. 17
- [411] Xin Li, Guodong Cheng, Shaomin Liu, Qing Xiao, Mingguo Ma, Rui Jin, Tao Che, Qinhuo Liu, Weizhen Wang, Yuan Qi, et al. Heihe

- watershed allied telemetry experimental research (hiwater): Scientific objectives and experimental design. *Bulletin of the American Meteorological Society*, 94(8):1145–1160, 2013. 17
- [412] Xinke Li, Chongshou Li, Zekun Tong, Andrew Lim, Junsong Yuan, Yuwei Wu, Jing Tang, and Raymond Huang. Campus3d: A photogrammetry point cloud benchmark for hierarchical understanding of outdoor scene. In *ACM Multimedia*, pages 238–246, 2020. 16, 17
- [413] Qingyong Hu, Bo Yang, Sheikh Khalid, Wen Xiao, Niki Trigoni, and Andrew Markham. Sensurban: Learning semantics from urban-scale photogrammetric point clouds. *International Journal of Computer Vision*, 130(2):316–343, 2022. 17
- [414] Weixiao Gao, Liangliang Nan, Bas Boom, and Hugo Ledoux. Sum: A benchmark dataset of semantic urban meshes. *ISPRS J. Photogramm. Remote Sens.*, 179:108–120, 2021. 17
- [415] Daniel Muñoz, J Andrew Bagnell, Nicolas Vandapel, and Martial Hebert. Contextual classification with functional max-margin markov networks. In *CVPR*, pages 975–982. IEEE, 2009. 17
- [416] Timo Hackel, N. Savinov, L. Ladicky, Jan D. Wegner, K. Schindler, and M. Pollefeys. SEMANTIC3D.NET: A new large-scale point cloud classification benchmark. In *ISPRS Annals*, volume IV-1-W1, pages 91–98, 2017. 17
- [417] Xavier Roynard, Jean-Emmanuel Deschaud, and François Goulette. Paris-lille-3d: A large and high-quality ground-truth urban point cloud dataset for automatic segmentation and classification. *The International Journal of Robotics Research*, 37(6):545–557, 2018. 17
- [418] SM Zolanvari, Susana Ruano, Aakanksha Rana, Alan Cummins, Rogério Eduardo da Silva, Morteza Rahbar, and Aljosa Smolic. Dublincity: Annotated lidar point cloud and its applications. *arXiv preprint arXiv:1909.03613*, 2019. 17
- [419] Andrés Serna, Beatriz Marcotegui, François Goulette, and Jean-Emmanuel Deschaud. Paris-rue-madame database: a 3d mobile laser scanner dataset for benchmarking urban detection, segmentation and classification methods. In *ICPRAM*, 2014. 17
- [420] Aerial monocular 3d object detection dataset, 2022. 17
- [421] Shenglei Wang, Junsheng Li, Wenzhi Zhang, Chang Cao, Fangfang Zhang, Qian Shen, Xianfeng Zhang, and Bing Zhang. A dataset of remote-sensed Forel-Ule Index for global inland waters during 2000–2018. 12 2020. 17
- [422] Siddharth Yadav, Chun Fu, and Andrich van Wyk. Historical hourly weather data 2012–2017, 2017. 17
- [423] Christian Requena-Mesa, Vitus Benson, Markus Reichstein, Jakob Runge, and Joachim Denzler. Earthnet2021: A large-scale dataset and challenge for earth surface forecasting as a guided video prediction task. In *CVPR*, pages 1132–1142, 2021. 17
- [424] Climate change: Earth surface temperature data, 2017. 17
- [425] International greenhouse gas emissions, 2017. 17
- [426] Manil Maskey, Rahul Ramachandran, Muthukumar Ramasubramanian, Iksha Gurung, Brian Freitag, Aaron Kaulfus, Drew Bollinger, Daniel J Cecil, and Jeffrey Miller. Deepti: Deep-learning-based tropical cyclone intensity estimation system. *IEEE J. Sel. Top. Appl. Earth Obs. Remote Sens.*, 13:4271–4281, 2020. 17
- [427] Kai Chen, Jiaqi Wang, Jiangmiao Pang, Yuhang Cao, Yu Xiong, Xiaoxiao Li, Shuyang Sun, Wansen Feng, Ziwei Liu, Jiarui Xu, et al. Mmdetection: Open mmlab detection toolbox and benchmark. *arXiv preprint arXiv:1906.07155*, 2019. 16
- [428] Kaiming He, Xiangyu Zhang, Shaoqing Ren, and Jian Sun. Deep residual learning for image recognition. In *CVPR*, pages 770–778, 2016. 16
- [429] Mingxing Tan and Quoc Le. Efficientnet: Rethinking model scaling for convolutional neural networks. In *ICML*, pages 6105–6114. PMLR, 2019. 16
- [430] Alexey Dosovitskiy, Lucas Beyer, Alexander Kolesnikov, Dirk Weissenborn, Xiaohua Zhai, Thomas Unterthiner, Mostafa Dehghani, Matthias Minderer, Georg Heigold, Sylvain Gelly, et al. An image is worth 16x16 words: Transformers for image recognition at scale. *arXiv preprint arXiv:2010.11929*, 2020. 16
- [431] Tsung-Yi Lin, Priya Goyal, Ross Girshick, Kaiming He, and Piotr Dollár. Focal loss for dense object detection. In *CVPR*, pages 2980–2988, 2017. 16
- [432] Olaf Ronneberger, Philipp Fischer, and Thomas Brox. U-net: Convolutional networks for biomedical image segmentation. In *MICCAI*, pages 234–241. Springer, 2015. 16
- [433] Ilya Loshchilov and Frank Hutter. Decoupled weight decay regularization. *arXiv preprint arXiv:1711.05101*, 2017. 16